Taylor & Francis
Taylor & Francis Group

Stabilization of Nanoscale Quasi-Liquid Interfacial Films in Inorganic Materials: A Review and Critical Assessment

Jian Luo*

School of Materials Science and Engineering, 201 Olin Hall, Clemson University, Clemson, South Carolina 29634, USA

Recent observations of three classes of nanometer-thick, disordered, interfacial films in multi-component inorganic materials are reviewed and critically assessed. The three classes of films are equilibrium-thickness intergranular films (IGFs) in ceramics, their free-surface counter-parts, that is, surficial amorphous films (SAFs), and their metallic counterparts. Also briefly reviewed are several related wetting and adsorption phenomena in simpler systems, including premelting in unary systems, prewetting in binary liquids or vapor adsorption on inert walls, and frustrated-complete wetting. Analogous diffuse-interface and force-balance models are discussed with the goal of exploring a unifying thermodynamic framework. In general, the stability of these nanometer-thick interfacial films does not follow bulk phase diagrams. Stabilization of quasi-liquid interfacial films at subeutectic or undersaturation conditions in multicomponent materials can be understood from coupled interfacial premelting and prewetting transitions. More realistic models should include additional interfacial interactions, for example, dispersion and electrostatic forces, and consider the possibility for metastable equilibration. It is suggested that quasi-liquid grain boundary films in binary metallic systems can be used to validate a basic thermodynamic model. These nanoscale interfacial films are technologically important. For example, the short-circuit diffusion that occurs in interface-stabilized, subeutectic, quasi-liquid films explains the long-standing mystery of the solid-state activated sintering mechanism in ceramics, refractory metals, and ice.

Keywords intergranular films, surficial amorphous films, equilibrium thickness, prewetting, premelting, activated sintering

Table of Contents

*E-mail: jianluo@clemson.edu or jluo@alum.mit.edu

LIST OF ACRONYMS

  AES: Auger Electron Spectroscopy; BET: Brunauer-Emmett-Teller (Model); DLVO: Derjaguin-Landau-Verwey-Overbeek
  (Theory); EELS: Electron Energy-Loss Spectroscopy; ELNES: (Electron) Energy-Loss Near-Edge Structures;
  GB: Grain Boundary; HAADF: High-Angle Annular Dark-Field; HRTEM: High-Resolution Transmission Electron
  Microscopy; IGF: Intergranular (Glassy) Film; KWC: Kobayashi-Warren-Carter (Model); SAF: Surficial Amorphous Film;
  STEM: Scanning Transmission Electron Microscopy; TEM: Transmission Electron Microscopy.

1. INTRODUCTION

Impurity-based intergranular films (IGFs) have been widely observed in ceramic materials.[1,2] These interface-stabilized disordered films exhibit "equilibrium thicknesses" of 0.5–5 nanometers.[1–5] Despite the existence of partial order within the films, they are often termed "glassy" or "amorphous" films. For decades, it has been widely accepted that such nanoscale films could be stabilized only at internal interfaces between two crystalline grains in ceramic materials and in the solid-liquid (or solid-glass) coexisting regimes of the bulk phase equilibria. However, this theory has been revisited due to several intriguing discoveries. First, free-surface counterparts to these IGFs, known as surficial amorphous films (SAFs), have been observed.[6–11] Second, nanometer-thick grain boundary (GB) films of similar character have been directly observed in a binary metal system.[12,13] Finally, a series of studies[8,10,12,14–18] revealed the stabilization of disordered or "quasi-liquid" interfacial films well below the bulk eutectic temperatures (referred to as "subeutectic conditions" in this article) or in the single-phase region containing dopant concentrations below the bulk solid-solubility limits (referred to as "undersaturation conditions" in this article), indicating a clear analogue to the well-known phenomena of premelting[19–24] and prewetting.[25–27] Given these discoveries, generalized thermodynamic models for a broad range of nanoscale interfacial films are envisioned.

This review critically assesses a variety of analogous interfacial phenomena in metals, ceramics, and molecular substances with the goal of formulating a unifying thermodynamic framework to understand the stability of the quasi-liquid interfacial films, particularly at subsolidus (subeutectic or undersaturation) conditions. An overview of several classes of interfacial films is presented in this article, and the relationships between them are shown in Figure 1. Related wetting and adsorption phenomena are briefly discussed in §2. The key experimental observations and thermodynamic models for these disordered interfacial films in multicomponent inorganic materials are critically reviewed and assessed in §3 and §4, respectively. Efforts were made to extend the fundamental physical principles from well-established theories for relatively simple systems, for example, premelting in unary materials and prewetting in binary liquids, to understand interfacial films in more complex multicomponent inorganic materials within a unifying thermodynamic framework. The author's subjective opinions and original insights are also offered, particularly in §4 and §6. In discussions of the thermodynamic models, the emphases are placed on the underlying physical principles and justifications for the models rather than on rigorous mathematical derivations. The technological importance of these nanoscale interfacial films is discussed in §5.

2. BACKGROUND: RELATED PHENOMENA

2.1 Wetting

Stabilization of nanoscale interfacial films can be considered as a particular case of a broad class of wetting phenomena. A comprehensive review of wetting phenomena is given by de Gennes.[28] Basic wetting theories that are relevant to the subject of this article are briefly summarized in this section. In particular, effort is made to clarify several concepts and definitions that are sometimes confusing in the literature.

As shown in Figure 2, when a small liquid drop is placed on a flat surface, two distinct equilibrium configurations may be found: partial wetting (also known as non-wetting) versus complete (or perfect) wetting. In case of partial wetting of a surface, the contact angle is given by the Young equation:

$$\gamma_{cv} = \gamma_{lv} \cdot \cos\theta + \gamma_{cl} \qquad [1]$$

Similarly, when a small amount of liquid is present inside a polycrystalline material at high temperatures, the dihedral angle for partial wetting of a GB where it meets a liquid pocket at a triple-grain or four-grain junction is given by:

$$\gamma_{gb} = 2\gamma_{cl} \cdot \cos\frac{\phi}{2}. \qquad [2]$$

Here γ_{cl}, γ_{lv}, γ_{cv}, and γ_{gb} are the excess free energies for crystal-liquid, liquid-vapor, and crystal-vapor interfaces and a GB, respectively. Unless otherwise noted, it is assumed in this article (for simplicity) that γ_{cl} is independent of grain orientation and that the GBs are high-angle, random boundaries with a constant γ_{gb}. In a real material, the wetting configuration can be different for each individual GB, because both γ_{gb} and γ_{cl} depend on boundary crystallography.

Some adsorption of the liquid species on the surface or at the GB is generally expected. Assuming that the surface or GB excess (Γ) is positive, γ_{sv} and γ_{gb} are reduced according to the Gibbs isothermal equation ($d\gamma = -\Gamma \cdot d\mu$):

$$\gamma_{cv} < \gamma_{cv}^{(0)} \qquad [3]$$

and

$$\gamma_{gb} < \gamma_{gb}^{(0)}, \qquad [4]$$

where $\gamma_{cv}^{(0)}$ or $\gamma_{gb}^{(0)}$ is the excess free energy of a "completely dry" surface or GB without any adsorption (i.e., $\Gamma = 0$). In principle, surfaces in equilibrium with a secondary liquid phase always have some adsorbates due to an entropic effect. However, the adsorption effect can be negligible in some cases.

For a surface, complete wetting occurs when

$$\Delta\gamma \equiv \gamma_{lv} + \gamma_{cl} - \gamma_{cv}^{(0)} < 0. \qquad [5]$$

For a GB, complete wetting occurs when

$$\Delta\gamma \equiv 2 \cdot \gamma_{cl} - \gamma_{gb}^{(0)} < 0. \qquad [6]$$

It is important to note that $\gamma_{cv}^{(0)}$ and $\gamma_{gb}^{(0)}$ should be used here. By definition, the excess surface and GB free energies for the case of complete wetting are given by[29]

$$\gamma_{cv} = \gamma_{lv} + \gamma_{cl} \qquad [7]$$

and

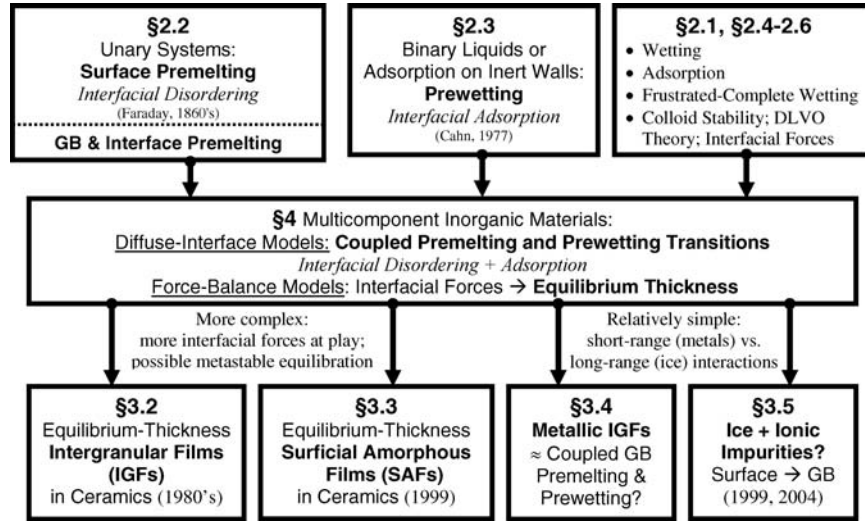$$\gamma_{gb} = 2 \cdot \gamma_{cl}, \qquad [8]$$

FIG. 1. Overview of several classes of nanoscale interfacial films.

which represent the thermodynamic equilibrium configurations, that is, surfaces and GBs with wetting films of macroscopic thickness (Figure 2). It should be noted that γ_{cl} and γ_{lv} can be rigorously defined for thick films (where the two interfaces are independent) in Eqs. 5 and 6 (and other equations used later) and no superscripts $^{(0)}$ are needed.

There is some confusion regarding Eqs. 1–8 in the literature, because the differences between the excess free energies of the interfaces with equilibrium adsorbates or wetting films (γ_{cv} and γ_{gb}) and those without any adsorption ($\gamma_{cv}^{(0)}$ and $\gamma_{gb}^{(0)}$) are often not noted. For example, it is common practice to compute contact and dihedral angles (Figure 2) based on $\gamma_{cv}^{(0)}$ or $\gamma_{gb}^{(0)}$, which are reasonable approximations only if the adsorption is negligible. $\gamma_{cv}^{(0)}$ or $\gamma_{gb}^{(0)}$ represents a non-

equilibrium configuration when a surface or GB coexists with a liquid.

2.2   Premelting in Unary Systems

Surface melting or premelting refers to the stabilization of thin surface quasi-liquid layers below the bulk melting temperature in unary (one-component) materials.[19-24] (This definition can be conveniently extended to compounds that melt congruently.) It occurs when the excess crystal-vapor interfacial energy is reduced when a "completely dry" crystalline surface is replaced with a crystal-liquid interface and a liquid surface. Convincing experimental evidence for surface premelting has been obtained in ice,[20,21] lead,[30,31] adsorbed Ar films,[32] and other one-component materials. The theories and experiments of
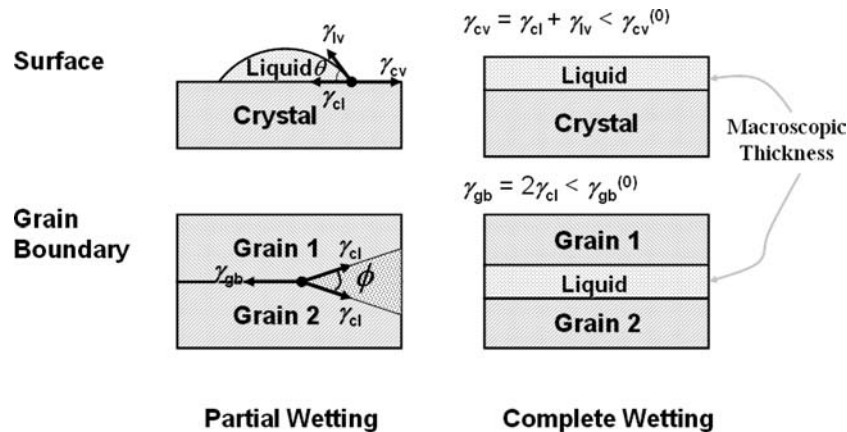

FIG. 2. Partial and complete wetting configurations for surfaces and GBs.

premelting have been reviewed.[19−24] Premelting of ice is a major reason that ice is slippery.[33] Furthermore, premelting plays a key role in the sintering, adhesion, and creep of snow and ice, and it has major environmental consequences, for example, in the phenomena of frost heave, glacier motion, and electrical charging in thunderstorms.[20,21]

Premelting can be either complete or incomplete. In "complete premelting," as the temperature rises and approaches the bulk melting temperature, the thickness of the surface quasi-liquid layer increases continuously (to infinity) until a bulk wetting liquid results. For ice, however, "incomplete premelting" has been predicted where a surface premelting layer of microscopic thickness form at the solid-liquid-vapor triple point, in equilibrium with a water drop on the surface with a non-zero contact angle ($\theta > 0$).[20,21] This unique wetting configuration is analogous to the phenomenon of frustrated-complete wetting discussed in §2.5.

Surface premelting does not occur in all systems.[23,24] Furthermore, premelting can occur anisotropically on surfaces of specific orientations (e.g., in Pb).[34,35] Whether a material exhibits premelting on a specific orientation can be roughly predicted by comparing the relative interfacial energies (§2.4). In an alternative (and equivalent) view, surface premelting occurs rather ubiquitously because the entropies of atoms or molecules at the free surface are in general greater than entropies of those inside the bulk phase due to the reduced coordination number. On the other hand, the opposite effect, "surface freezing," the occurrence of ordered surface layers for liquid phases, is rare but has been observed, for example, for a Si-Au alloy.[36]

Driven by a reduction of interfacial energies, nanoscale quasi-liquid films can also be stabilized at GBs below the bulk melting temperature, known as GB premelting. Numerous atomistic simulations have indicated the occurrence of GB disordering in metals[37−39] and silicon.[40−42] GB premelting has also been studied by diffuse-interface models, suggesting the existence of continuous[43] and first-order premelting transitions.[44,45] Theoretical investigation of GB premelting in ice (a molecular substance with long-range dispersion forces) has also been conducted.[46] Premelting behaviors of GBs should depend on the orientations of the two abutting grains,[44] but some universal characteristics may be expected for large-angle, random GBs.[37,38,41]

In parallel, researchers have made great efforts to confirm the existence of GB premelting experimentally. In 1989, Hsieh and Balluffi reported[47] an *in situ* hot-stage transmission electron microscopy (TEM) experiment that led them to conclude that GB premelting likely occurs for pure Al, but only at a temperature value above $0.999T_{melting}$. Subsequently, exploration in this area was greatly discouraged. Tang, Carter, and Cannon noted[44] that there is a bias toward special GBs with high symmetry and toward materials that do not easily form glass in experimental studies of GBs; these low-energy special GBs in non-glass-forming materials are less likely to exhibit premelting. Such a bias might contribute to the scarcity of convincing evidence for GB premelting. In 2005, direct evidence was reported for the occurrence of GB premelting in colloidal crystals of submicron-size particles (as a model for real materials).[48]

Most recently, premelting at ice-Si[49] and Pd-Al[50] heterophase interfaces has also been directly confirmed by *in situ* X-ray reflectivity measurements and hot-stage high-resolution transmission electron microscopy (HRTEM) experiments, respectively, demonstrating the ubiquitous existence of analogous interfacial phenomena with different configurations.

2.3 Prewetting: Binary Immiscible Liquids versus Vapor Adsorption on Inert Walls

Prewetting and wetting transitions were initially predicted in Cahn's critical point wetting model[25] for a binary liquid mixture exhibiting a miscibility gap (Figure 3). A schematic phase diagram of the system studied by Cahn is depicted in Figure 3c. The diffuse-interface theory that Cahn used is briefly discussed in §4.2, and the rigorous mathematical derivation can be found in Cahn's original article[25] or in recent reviews.[28,29] Some key predictions from Cahn's model are outlined here. Cahn's model predicted a first-order wetting transition in the two-phase region within the miscibility gap and a prewetting transition line in the single-phase region (Figure 3c). The prewetting line represents first-order (prewetting) transitions from thin to thick adsorption films, occurring when the phase that does the wetting is not yet stable. The prewetting line terminates at a surface critical point, where the difference between thin and thick adsorption films vanishes. The basic predictions of the critical point wetting models have been confirmed in organic systems[51,52] and the Pb-Ga liquid metal system.[53,54] Prior studies have primarily been focused on organic/aqueous systems and liquid metals.

Although Cahn's model was initially developed for a demixed binary fluid system, this model can be extended to model the vapor adsorption on chemically inert solid walls near the liquid-vapor critical point (commonly known as solid-liquid-vapor systems) in which the order parameter is the number density $[c_B(x) \rightarrow n(x)]$ (Figure 3a versus Figure 3b) or an Ising spin system in which the order parameter is the magnetization $[c_B(x) \rightarrow m(x)]$.[29] In the case of adsorption on inert walls, the "terminating surface" is taken to be the adsorbates-wall interface and the "bulk" is the vapor phase (Figure 3b). Prewetting and critical point wetting in both binary de-mixed liquids and vapor adsorption on inert walls can be represented by the same generic phase diagram in the $T-(\mu-\mu_0)$ space (Figure 3d).

Wetting transitions were predicted independently by Ebner and Saam[27] for thin argon films. Nakanishi and Fisher[26] systematically examined the wetting and prewetting transitions and summarized them in generic, global phase diagrams in the space
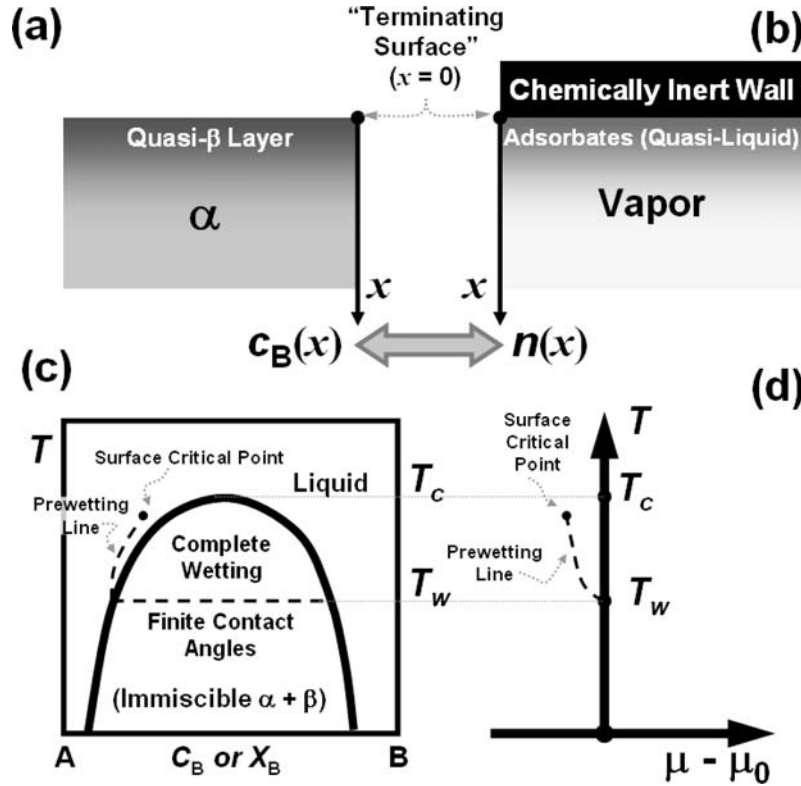
FIG. 3. Schematic illustration of prewetting in (a) a binary de-mixed liquid and (b) vapor adsorption on a chemically inert wall. The prewetting theory for vapor adsorption on an inert wall near the liquid-vapor critical point becomes isomorphic to Cahn's theory if the concentration field ($c_B(x)$) is replaced with a number density field ($n(x)$) and the wall-adsorbates interface is set as the "terminating surface." (c) The phase diagram depicts the major results of Cahn's critical point wetting model for binary de-mixed liquids. Dashed lines represent first-order wetting or prewetting transitions. (d) Representation of the prewetting and critical point wetting phase diagram in the T-($\mu - \mu_0$) space. This diagram represents both binary de-mixed liquids and vapor adsorption on inert walls.

of temperature, chemical potential, surface enhancement, and bulk and surface fields. Cahn's model has also been extended to systems with long-range (e.g., van der Waals) interactions[55] and ionic solutions.[56] Comprehensive reviews of wetting, prewetting, and related phenomena have been written by de Gennes[28] and Bonn and Ross.[29]

2.4 Prewetting/Premelting as Wetting and Adsorption Phenomena

Premelting and prewetting can be understood in the context of wetting and adsorption theories. Premelting is wetting of a crystalline solid by its own melt liquid.[24] Both prewetting and premelting (first-order or continuous) transitions are special wetting transitions, occurring when the phase that does the wetting is not yet a stable bulk phase.[29] Formation of premelting and prewetting layers at undercooled or undersaturation conditions can be considered in a unifying view as stabilization of a thin layer of a metastable β phase at an $\alpha - \gamma$ interface (Figure 4),
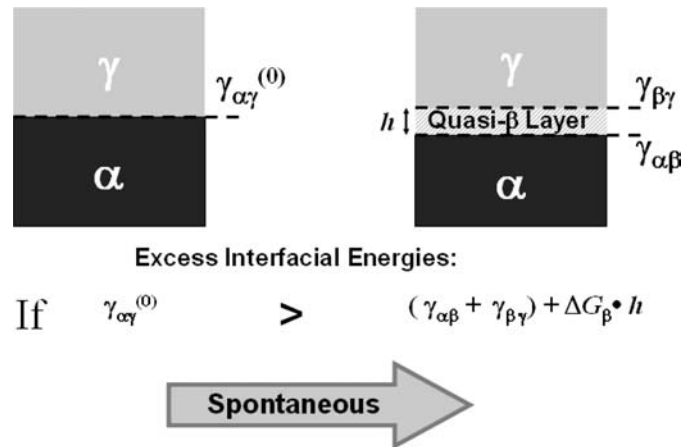
FIG. 4. A thin layer of a metastable β phase can be stabilized on the α-γ interface if the increased volumetric free energy to form a thin metastable β layer is over-compensated by the reduction in the interfacial energy. In the present case, the (equilibrium) thickness of quasi-β layer (h) is microscopic.
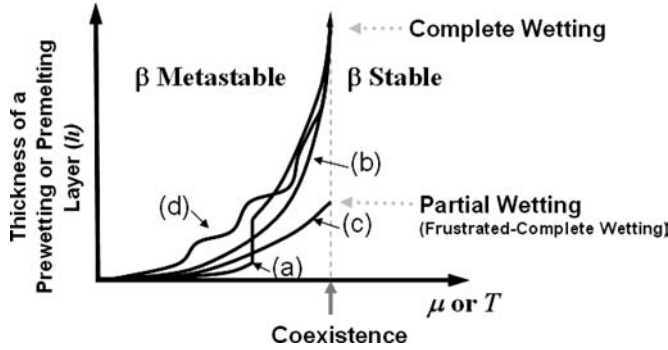
FIG. 5. Thickness of a premelting or prewetting layer versus temperature or chemical potential: the prewetting/premelting transitions can be (a) first-order, (b) continuous, (c) incomplete, or (d) with layering transitions.

which is thermodynamically favored if

$$-\Delta\gamma \equiv \gamma_{\alpha\gamma}^{(0)} - (\gamma_{\alpha\beta} + \gamma_{\beta\gamma}) > \Delta G_\beta \cdot h, \qquad [9]$$

where ΔG_β is the extra volumetric free energy for forming the metastable β phase and h is the thickness of the β phase layer. $\gamma_{\beta\gamma}$ and $\gamma_{\alpha\beta}$ are the excess free energies for the α-γ and β-γ interfaces, respectively. $\gamma_{\alpha\gamma}^{(0)}$ is the interfacial energy for a "completely dry" α-γ interface. For example, surface premelting is a case wherein the α, β, and γ phases in Figure 4 are the crystal, liquid, and vapor phases, respectively, of a one-component material.

In this regard, both premelting and prewetting layers are interface-stabilized films, and a necessary condition for their

occurrence is given by

$$\Delta\gamma < 0. \qquad [10]$$

In general, the structure and composition of nanometer-thick interfacial films should differ from those of the associated bulk phase. Thus, the term "quasi-β" (or "β-like") is often used. Furthermore, through-thickness gradients in composition or structure generally exist.

Premelting and prewetting transitions are wetting transitions, which can be either first-order (Figure 5a) or continuous (Figure 5b). Premelting or prewetting can be incomplete, which means that the layer thickness remains microscopic at the coexistence, in equilibrium with a partial-wetting β phase (Figure 5c; Figure 6; §2. 5). In principle, layering transitions can occur (Figure 5d).

Adsorption in the prewetting regime typically has a multilayer character. In this regard, the prewetting films in binary de-mixed liquids can be considered as multiple adsorbed layers with dilute concentration of the enriched solute and through-thickness compositional gradients. Multilayer gas adsorption occurs widely at free surfaces. In the classical Brunauer-Emmett-Teller (BET) model, only the first adsorbed layer is chemisorbed, subsequent layers are physically adsorbed, and chemical mixing of the adsorbed gas and the substrate is not expected. Multilayer adsorption phenomena on chemically inert, attractive substrates have been systematically investigated.[57] As discussed in §2.3, prewetting transitions are expected for vapor adsorption on inert substrates near the liquid-vapor critical point from a diffuse-interface theory that is isomorphic to Cahn's critical point wetting model[29]; prewetting transitions are indeed observed from lattice-gas models of multilayer adsorption.[57]
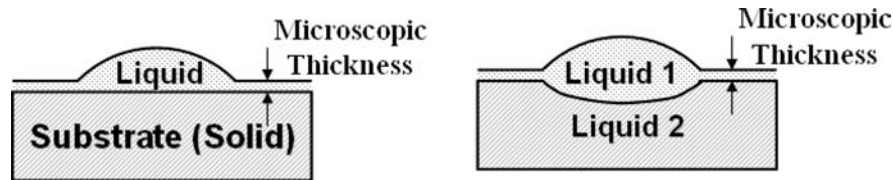
(a)
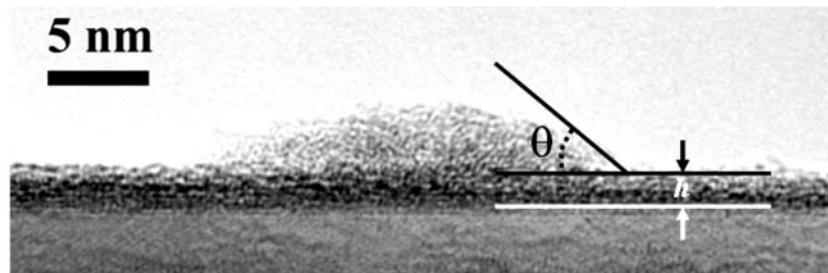
(b)

FIG. 6. (a) Schematic illustration of frustrated-complete (or pseudo-partial or autophobic) wetting. (b) HRTEM image of a nanometer-thick surficial amorphous film coexisting with a partial-wetting nano-droplet in the Bi_2O_3 on ZnO system. Panel (b) is reprinted from Ref. 10 with permission from the American Chemical Society.

Furthermore, equilibrium solute segregation of multilayer character at GBs is also known to occur[58,59]; for multilayer adsorption at GBs within the crystalline lattice, a "truncated BET" model was proposed for metals,[60] and the effect of space charges were considered for ionic materials.[58] Gibbs adsorption theory is always applicable for prewetting and all other types of multilayer adsorption.

2.5 Frustrated-Complete Wetting

The simple premelting or prewetting phenomenon refers to the formation of a quasi-β interfacial film when the bulk β phase is not yet stable. Approaching the phase boundary across which the β phase becomes stable, it is generally expected that the film thickness is divergent ($h \to +\infty$), resulting in a macroscopically-thick, complete wetting film. However, in some instances, the divergence in films thickness is constrained (by an attractive interfacial force); thus a microscopically-thick, interfacial quasi-β film can form in equilibrium with a partial-wetting bulk β phase. This is the case for incomplete premelting of ice at the triple point.[20,21]

Somewhat similar regions of nanoscale surficial films in equilibrium with a partial-wetting droplet have been observed in organic or aqueous liquid-liquid systems and described as frustrated-complete wetting.[61] These regions exist at a range of chemical potentials between those giving submonolayer surface coverage and complete wetting. A similar condition of a finite droplet with a non-zero contact (wetting) angle surrounded by a microscopic pure liquid film with thickness limited by dispersion forces has been termed pseudo-partial wetting[62] or autophobic wetting.[63] This unique wetting configuration is schematically shown in Figure 6a. A HRTEM image of a somewhat similar wetting configuration observed in a binary oxide system is shown in Figure 6b, which is discussed in §3.3.1 in the context of equilibrium SAFs.

An analogous dynamic wetting configuration has also been found for immiscible metal systems,[64–66] wherein a droplet of liquid metal with a finite contact angle coexists with monolayer/submonolayer adsorbates during the spreading process (termed "precursor films," which are kinetically limited in general). The formation of a precursor film during dynamic spreading is also well-known for aqueous, organic, and polymeric systems.[28] While the formation of precursor films during spreading does not typically represent an equilibrium wetting configuration, these precursor films can represent metastable minima in excess free energy versus thickness.

2.6 Colloid Stability, DLVO Theory, and Interfacial Forces

The famous Derjaguin-Landau-Verwey-Overbeek (DLVO) theory was developed to explain the stability of colloidal systems. The theory explained the equilibrium separation between two colloidal particles from a balance of an attractive London dispersion force and a repulsive electrical double-layer interaction. The DLVO theory has been confirmed for numerous colloidal dispersions and was extended by addition of new components of interfacial forces, for example, steric forces. Interested readers can find a detailed description of the DLVO theory and interfacial forces in the textbook written by Israelachvili.[63] Interfacial forces in thin wetting films have recently been reviewed.[67]

The generalized DLVO theory and interfacial forces are important for understanding the stability of nanoscale interfacial films in inorganic material systems. Although the inter-atomic forces in inorganic materials are not the same as those in the traditional colloidal systems, similar interfacial forces are often present. Clarke initially explained the "equilibrium thickness" of silicate-based IGFs in Si_3N_4 ceramics from a balance of attractive dispersion force and repulsive steric or electrical double-layer force,[3,4] which is essentially an extension of colloid theory to high-temperature, silicate-glass-based ceramic systems. In general, the stability of nanoscale interfacial films can be explained from a balance among multiple attractive and repulsive interfacial forces in force-balance models that are extended (and modified) from the generalized colloid stability theory, although the specific details of interfacial forces in inorganic material systems can be somewhat different. See §4.3 and §4.4 for elaboration.

3. NANOSCALE DISORDERED INTERFACIAL FILMS IN MULTICOMPONENT INORGANIC MATERIALS

3.1 Widespread Existence

Equilibrium-thickness intergranular films or IGFs were initially observed at GBs in Si_3N_4-based structural ceramics containing native oxide and various sintering aids or impurities (e.g., MgO, CaO, Y_2O_3, La_2O_3, Sm_2O_3, Er_2O_3, Gd_2O_3, Yb_2O_3, Lu_2O_3, F, Cl).[68–105] Furthermore, IGFs of similar character have also been observed at GBs in a variety of other nitrides,[106,107] carbides,[92,108–117] and oxides,[16–18,118–136] as well as at heterophase interfaces between dissimilar ceramics.[14,16,120,137,138] Key observations of these IGFs in ceramics are reviewed in §3.2.

Recently, nanometer-thick interfacial films of similar character have been found in an increasing number of other multicomponent inorganic materials (Figure 7). SiO_2-enriched films have been observed at metal-oxide interfaces with silicate doping to promote the formation of glassy films.[139–145] Metallic[12,13] and free-surface[6–11,146,147] counterparts to IGFs in ceramics, which are reviewed in §3.3 and §3.4, respectively, have also been discovered. Recent studies demonstrated that minor ionic impurities can further stabilize and thicken the premelting (quasi-liquid) layers at ice surfaces, GBs, or interfaces with inert walls.[46,148] This is yet another class of impurity-based, disordered, interfacial films in molecular substances, which is briefly discussed in §3.5. These discoveries suggest that similar interfacial phenomena occur more frequently than previously believed. Consequently, the existence of analogous underlying formation mechanisms and a unifying thermodynamic framework is envisioned. Materials systems in which such nanoscale interfacial films have been found or predicted are summarized in Table 1.
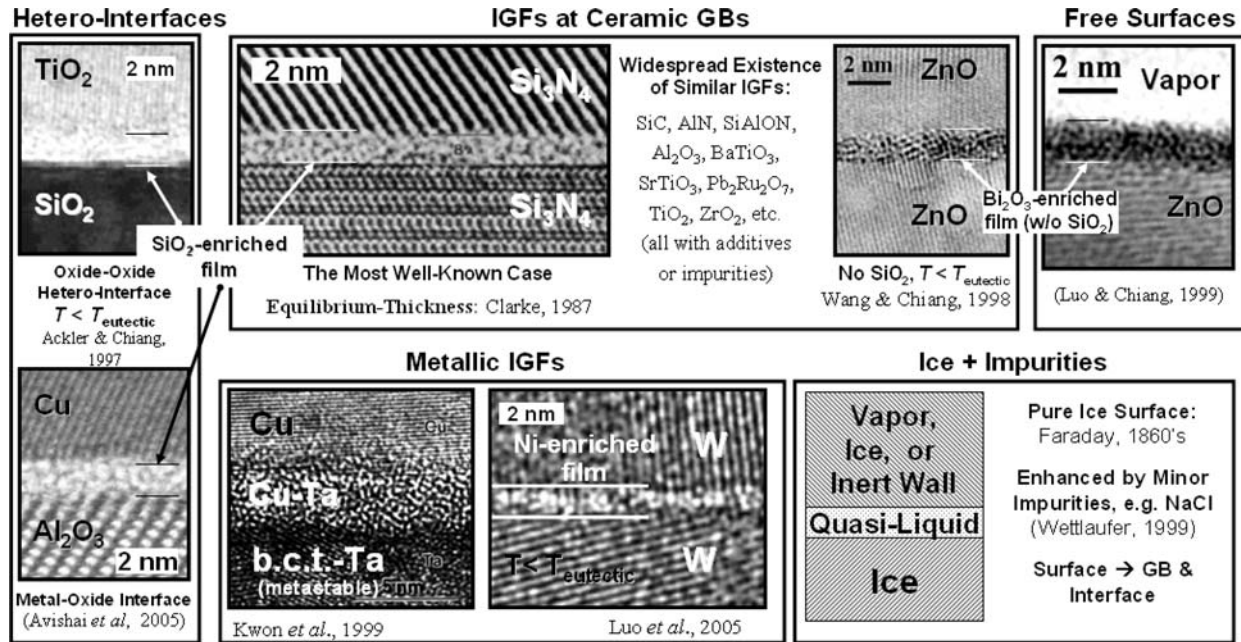
FIG. 7. Representative impurity-based, nanoscale, disordered, interfacial films in multicomponent inorganic materials. HRTEM images are reprinted from Refs. 9, 12, 14, 72, 219 with permissions from The American Ceramic Society, American Institute of Physics, and Elsevier.

3.2 Intergranular Films in Ceramics

Ceramic systems where nanometer-thick IGFs have been observed at GBs include: Si_3N_4,[68−105] SiC,[92,108−117] SiAlON,[149,150] Al_2O_3,[15,118,119,131−134] $Pb_2Ru_2O_7$-based thick-film resistors,[120] TiO_2,[121] ZrO_2,[122,135] high T_c superconductors,[123] AlN,[106,107] synroc,[124] mullite,[125] $BaTiO_3$,[126−128,130] ZnO,[16−18,136] and $SrTiO_3$,[128,129] in which IGFs always contain a significant amount of additives and impurities. IGFs have also been observed at the heterophase interfaces in Si_3N_4-Yb_2SiO_5,[85] ZnO-Bi_2O_3,[16] TiO_2-SiO_2,[14] Al_2O_3-TiN,[137] and BN-SiC.[138] Among these systems, IGFs in ZnO-Bi_2O_3[16,17] and $SrTiO_3$-TiO_2[128,129] (the primary phases are underlined), where silicate additive is not involved, and in Al_2O_3-(CaO+SiO_2)[118,132−134] where SiO_2 is present but partitions into the liquid pockets instead of into the films, are particularly interesting from a theoretical point of view because these IGFs are not based on polymeric oxides.[2,5] A recently published overview article provides a comprehensive summary of the observations, experimental techniques, models, and outstanding issues in the field for a "non-specialist audience."[1] In two important papers, Cannon et al. critically assessed the behaviors of IGFs in ten systems.[2,5] Key observations of the stability and character of these IGFs in ceramics are reviewed in this section.

3.2.1 Equilibrium Thickness

Perhaps the most important and interesting characteristic of these IGFs is their constant thickness on the order of one nanometer. In Si_3N_4-based ceramics, the film thickness is nearly constant along a given GB, and varies little from one GB to another for high-angle, random GBs in a given sample. A statistical study[72] revealed a narrow, Gaussian-like, distribution of film thickness in Si_3N_4 ceramics, where the measured standard deviations are on the order of 0.1 nm, approximately one-tenth of the corresponding mean values. In addition, the mean thicknesses measured for different specimens that have been prepared under the same conditions (including those reported by different researchers) are virtually identical. For example, Figure 8a represents three sets of film thickness measurements reported in the literature, which fall well within the range of experimental errors.[75,78,88]

The film thickness is independent of the fraction of excess secondary phase as long as the chemical potentials are kept the same. For example, the reported IGF thickness in high-purity Si_3N_4-SiO_2 materials stays at 1.0 ± 0.1 nm for specimens containing from ~4 to ~16 vol% secondary amorphous SiO_2 phase (in the Si_3N_4 and amorphous SiO_2 two-phase coexistence region), but the thickness is thinner for a specimen containing only nominal 0.55 vol% SiO_2 (which may be within the single-phase region with lower oxygen activity).[2,74,75,78,88,151] As another neat example, the measured mean thicknesses of IGFs in polycrystalline Si_3N_4 containing 5–12 vol% liquid and IGFs between Si_3N_4 particles that are dilutely suspended in a large amount of liquid/glass are identical within the range of experimental errors in two sets of specimens containing Y_2O_3 plus four lanthanide oxide dopants (Figure 8b).[79]

TABLE 1
Summary of material systems exhibiting nanoscale interfacial films

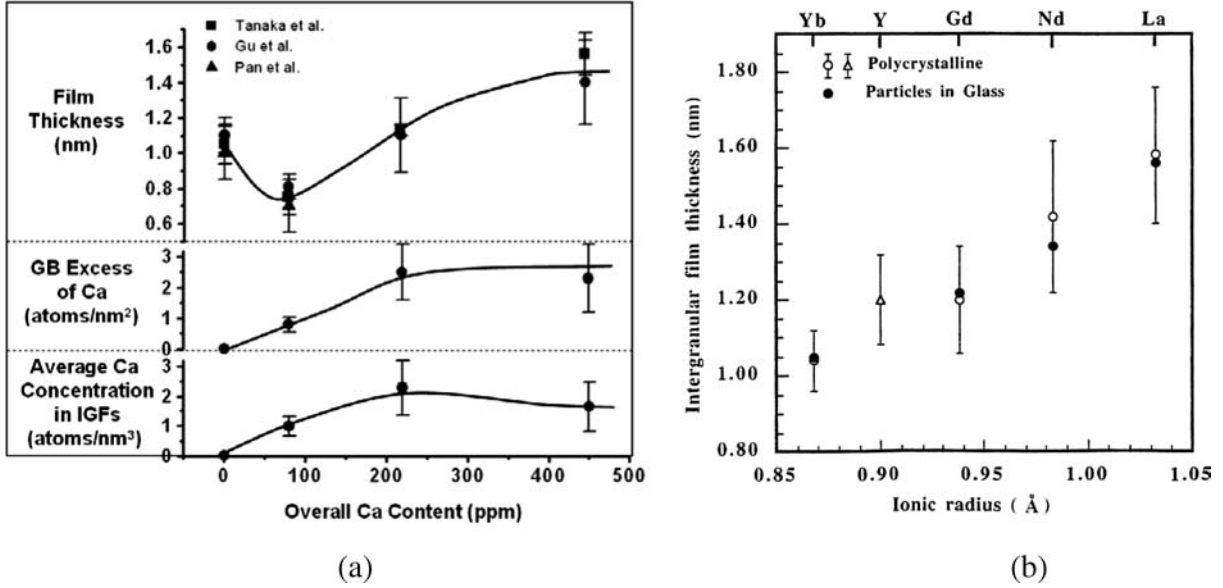|		Material Systems (Notes)
Premelting (unary systems)	Surface	Ice[20,21]
		Metals, e.g., Pb[34,35,233]
		Adsorbed Ar films[32]
	GB	Colloidal crystals[48]
		Ice (mainly predictions)[46]
	Hetero-interface	Pd at Pd-Al interface[50]
		Ice at ice-SiO_2 interface[49]
Prewetting (binary de-mixed liquids or adsorption on inert walls)	Surface	Organic systems[29,51,52]
		Liquid metals, e.g., Pd-Ga[53,54]
		Adsorption of vapor on chemically-inert walls[29,57]
Frustrated-complete wetting		E.g., alkanes on water[61]
IGFs in multicomponent ceramics	GB	**Silicate-based IGFs:**
		Primary materials: Si_3N_4,[69−72,74−91,93−97,99,101,105] SiC,[92,109−112,115−117] SiAlON,[149,150] Al_2O_3[15,131] $Pb_2Ru_2O_7$-based thick-film resistors,[120] TiO_2,[121] ZrO_2,[122,135] $BaTiO_3$,[126−128,130] high T_c superconductor,[123] AlN,[106,107] synroc,[124] and mullite[125]
		Dopants: SiO_2 + other additives or impurities
		IGFs free of SiO_2: $SrTiO_3$-TiO_2[128,129] and ZnO-Bi_2O_3[16−18] Al_2O_3-$(CaO+SiO_2)$ (Si/Ca partition is lower in IGFs than that in the liquid pockets; thus IGFs are not silicate-based.)[118,132−134]
	Hetero-interface	Si_3N_4-Yb_2SiO_5,[85] Al_2O_3-TiN[137] and BN-SiC[138] ZnO-Bi_2O_3[16] and TiO_2-SiO_2[14] (no other impurity; $T < T_{eutectic}$)
Silicate-based IGFs at metal-ceramic interfaces		Al_2O_3-Cu,[140,141] Al_2O_3-Ni,[140] Si_3N_4-Al,[145] and Al_2O_3-Au[144]
SAFs		Bi_2O_3 on ZnO (systematically characterized)[6−11]
		Bi_2O_3 on Fe_2O_3 and WO_3 on TiO_2($T < T_{eutectic}$; repulsive dispersion forces)[6,8]
		MoO_3 on Al_2O_3[6,10] and V_2O_5 on TiO_2(supported oxide catalysts)[147,185−187]
		Si_xO_y on Si[146]
		SAFs on nanowires and nanoparticles grown from vapor phase or solution[189−192,265]
IGFs in multicomponent metals	GB	Cu-Bi (discontinuities and anomalies in GB diffusivities, energies and other macroscopic properties; AES: ∼2-monolayer-thick Bi at GBs)[59,194,197−202]
		Fe-(Si, Zn) (abnormal GB diffusion)[204−207]
		Al-Ga (abnormal GB mobility; liquid metal embrittlement experiments)[194,214]
		WC-Co (∼ 1-nm-thick Co layer observed at ∼1/3 of GBs in liquid-phase sintered WC-Co)[211]
		Mo-Ni (∼2-nm-thick ordered δ-MoNi compound layer observed in activated sintered Mo-Ni)[210]
		Ni-Bi and Cu-Bi (nanometer-thick Bi films formed during GB liquid metal penetration/embrittlement experiments)[203,212,213]
		W-Ni (disordered IGFs identified by HRTEM + AES)[12,13]
	Hetero-interface	Cu-Ta (not solid-state amorphization)[219]
Ice-impurity systems	Surface, GB, hetero-interfaces	Premelting layers in ice are stabilized and thickened by minor ionic impurities, e.g., NaCl (controlled by long-range dispersion forces + electrical double-layer forces)[46,148]

FIG. 8. (a) IGF thickness, GB Ca excess, and the average Ca concentration in IGFs versus the overall (nominal) Ca content in high-purity $\underline{Si_3N_4}$-SiO_2 specimens with controlled Ca doping. (b) Thickness of IGFs in two sets of Si_3N_4 specimens involving an R-Si-Al-O-N (R = Y, Yb, Gd, Nd, and La) glass: IGFs in polycrystalline Si_3N_4 with a small fraction liquid/glass phase versus IGFs between Si_3N_4 particles embedded in a large amount of liquid/glass. Panel (a) is re-plotted from the data in Refs. 75, 78, 88 and panel (b) is reprinted from Ref. 79 with permission from Elsevier.

The film thickness depends on chemical potentials, temperature, and other intensive variables of the equilibrated system. Kleebe et al. showed a systematic dependence of IGF thickness on secondary phase chemistry for Si_3N_4 with various sintering aids.[85] A systematic variation in film thickness (as well as GB excess and average film concentration) with overall CaO content was revealed for high-purity $\underline{Si_3N_4}$-SiO_2-CaO specimens (Figure 8a).[75,78,88] In Si_3N_4 that sintered with rare-earth oxides, the IGF thickness appears to scale with the ionic radius of the rare-earth elements (Figure 8b).[79] Chemistry effects on film thickness were also observed in $Pb_2Ru_2O_7$-based thick-film resistors, where the film thickness increases from 0.8–1.1 nm to 1.2–1.6 nm upon adding 8.44% TiO_2.[120] Dependences of film thickness on processing/annealing temperature[86,101] and capillary pressures[17] were also evident.

In summary, the thickness of these nanometer-thick IGFs in ceramics

- is nearly constant along a given GB and varies little from one GB to another for high-angle, random GBs in a given specimen;
- is (virtually) identical for different specimens prepared under the same conditions;
- is independent of the fraction of excess secondary phase (but depends on the nature of the secondary phase, e.g., devitrification will affect IGF thickness, because of an associated change in chemical potentials);

- can be altered by changing bulk chemical potentials or the firing temperature; and
- decreases with increasing capillary pressure.

Therefore, these IGFs in ceramics appear to have an equilibrium thickness.

3.2.2 Film Energy and Stability

Historically, IGFs were believed to be kinetically limited remnants of processing. However, such films exist after long annealing and extensive grain growth. Thus, they likely represent equilibrium or near-equilibrium interfacial configurations. Additionally, dihedral angles are found to be nonzero where IGFs interact with glass or liquid pockets at triple-grain or four-grain junctions,[1,2,5] indicating that the excess free energy of an IGF (γ_{IGF}) is lower than the sum of two crystal-liquid (or crystal-glass) interfacial energies ($2\gamma_{cl}$). If γ_{cl} is isotropic, the following relation can be derived:

$$\gamma_{IGF} = 2\gamma_{cl} \cos \frac{\phi}{2} \qquad [11]$$

or

$$\Delta\gamma^* \equiv 2\gamma_{cl} - \gamma_{IGF} = 2\gamma_{cl} \cdot \left(1 - \cos\frac{\phi}{2}\right)$$
$$= \int_{h(eq.)}^{+\infty} \left(\sum_i \Pi_i(h)\right) dh > 0. \qquad [12]$$

Theoretically, $\Delta\gamma^*$ should be equal to an integral of the sum of all interfacial pressures (§4.3 and §4.4) from the equilibrium thickness (h_{eq}) to infinity.
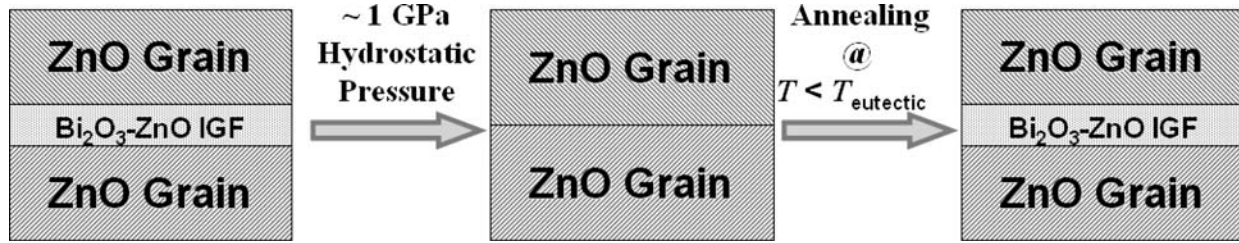
FIG. 9. Schematic illustration of a model experiment demonstrating that subeutectic IGFs represent a thermodynamic equilibrium GB configuration in Bi$_2$O$_3$-doped ZnO.[16,17]

The equilibrium thickness of IGFs can represent either a global or metastable minimum in excess film free energy.[14,121] In a model experiment using SiO$_2$-doped TiO$_2$, equilibration has been approached from two directions.[121] Nanometer-thick IGFs form in the specimen where TiO$_2$ particles are pre-coated with SiO$_2$ but not in the specimen where TiO$_2$ grains are initially in contact. This result was explained in terms of primary and metastable minima in film energy versus thickness, where IGFs may represent a metastable equilibration for this system. In other systems, IGFs appear to represent true thermodynamic equilibrium configurations. For example, IGFs in Pb$_2$Ru$_2$O$_7$-based thick-film resistors likely represent a global energy minimum because the observed increasing electrical conductivity during heating suggests that additional IGFs form at initially touching particles.[5,120] Furthermore, a model experiment showed that IGFs form at true thermodynamic equilibria at GBs in Bi$_2$O$_3$-doped ZnO (Figure 9),[16,17] which are discussed further in §3.2.3. If an IGF forms at a thermodynamic equilibrium, γ_{IGF} represents the equilibrium γ_{gb}.

3.2.3   Subsolidus Films

Disordered (quasi-liquid) IGFs have been found to form at subsolidus (subeutectic or undersaturation) conditions at heterophase interfaces in SiO$_2$-TiO$_2$[14] and Bi$_2$O$_3$-ZnO,[16,17] and GBs in Bi$_2$O$_3$-doped ZnO[16,17] and (Y$_2$O$_3$+ SiO$_2$)-doped Al$_2$O$_3$,[15] when the bulk liquid phase is no longer stable. In a model experiment, a highly pure silica film was deposited on a single crystal of rutile. A film of a constant thickness of ~1.5 nm retained at the heterophase interface of SiO$_2$-TiO$_2$ after annealing this assembly below the bulk eutectic temperature. This configuration is free of kinetic limitations to complete crystallization, thereby showing unequivocally that the amorphous film is not a kinetically limited remnant. This IGF at the SiO$_2$-TiO$_2$ heterointerface likely represents a true thermodynamic equilibrium.

In another model experiment (Figure 9),[16,17] the formation of IGFs in Bi$_2$O$_3$-doped ZnO was completely suppressed upon the application of a hydrostatic pressure of ~1 GPa (presumably because the molar volume of Bi is higher in IGFs than in crystalline phases). After re-annealing the pressure-desegregated samples in solid-state, IGFs are restored at virtually all GBs. It was then concluded that amorphous films are an energetically favored interfacial configuration, even below the bulk eutectic temperature. In this system, nanometer-thick IGFs also persist above the bulk eutectic temperature (740°C) into the solid–liquid co-existence regime (where dihedral angles remain nonzero) until complete wetting occurs at ~950°C.

Subeutectic IGFs have also been observed at Bi$_2$O$_3$-ZnO hetero-interfaces. Furthermore, disordered IGFs have been observed to form at undersaturation conditions (in the single-phase region containing dopant concentrations below the bulk solid-solubility limit) in Bi$_2$O$_3$-doped ZnO[16,17] and (Y$_2$O$_3$+ SiO$_2$)-doped Al$_2$O$_3$.[15] The stabilization of IGFs at subeutectic and undersaturation conditions are presumably driven by the reduction of interfacial energies (Figure 4), where an analogy can be made to the phenomena of premelting and/or prewetting.

3.2.4   Complete Wetting and Drying

If IGFs are considered as multilayer adsorbates in a prewetting region, a complete wetting transition may occur at a higher temperature. Cannon et al. assessed a few systems where IGFs have been observed to form and complete GB wetting transitions appeared to occur at higher temperatures.[2,5] Penetration of Bi$_2$O$_3$-ZnO liquid (pre-equilibrated with ZnO) into ZnO GBs have been observed at ~950°C.[2,152] In addition, earlier studies of quenched samples of less pure ZnO-Bi$_2$O$_3$[153] and SrTiO$_3$-TiO$_2$[154] revealed wetting transitions at about 1150°C and 1450 °C, respectively, and the wetting temperatures depends on the presence of other impurities. Cannon *et al.* also emphasized that cautious interpretation of the results of disruptive penetration of GBs is needed because transient, non-equilibrium wetting may occur.[2]

On the other hand, IGFs may vanish or fully crystallize at a lower "drying" temperature. In a SiC material with Al + B + C sintering additives, 1–2 nm-thick IGFs have been found to form at virtually all GBs after sintering above 1900°C. After long annealing at 1200–1400 °C, most GBs become ordered where IGFs vanish, but they still contain a significant amount of Al and O segregation.[115,155] Furthermore, the amorphous-to-crystalline transformation for IGFs in SiC has been observed directly by hot-stage HRTEM, where crystallization of IGFs was found to start from nucleation and local growth of short-range order structure.[116] Somewhat similarly, a study found that GBs in some

cooled ($Y_2O_3 + SiO_2$)-doped ZrO_2 samples are ordered but have significant Y and Si segregation.[156,157] Cannon et al. pointed out that this could be an indication that IGFs formed at high temperatures but crystallized during cooling.[2] Recently, evidence for formation and dewetting of IGFs in ($Y_2O_3 + SiO_2$)-doped ZrO_2 has been found by analyzing samples with different cooling rates.[135] In both cases, the segregation of the ordered GBs might be metastable, and diffusion into the secondary phases would occur if kinetic conditions permit.[2] On the other hand, equilibrium Langmuir-McLean type submonolayer segregation can certainly persist below the drying temperature where IGFs have vanished.

3.2.5 Distinct Film Composition and Structure

The average film compositions can be obtained by combining the GB solute excesses measured by a scanning transmission electron microscopy (STEM) area scanning method[158] and the film thickness measured by HRTEM. Alternatively, IGF compositions can be measured by electron energy-loss spectroscopy (EELS) and, particularly, via analysis of electron energy-loss near-edge structures (ELNES).[74] Using these methods, IGF compositions have been found to be distinctly different from those of the coexisting bulk secondary glass/liquid phases in a growing number of materials (see Cannon et al.[2,5] and references therein). For example, in high-purity $\underline{Si_3N_4}$-SiO_2 specimens, the N/O ratio was measured to be ~0.7 by the STEM/HRTEM method and ~0.5 by an ELNES analysis. These IGF compositions are within the bulk miscibility gap (Figure 10a); the maximum N/O ratio in bulk SiO_2 liquid/glass phase is only 1–4% at firing temperatures.[159] In another example, IGFs in Bi_2O_3-doped

ZnO are distinctly more enriched in ZnO than the associated bulk liquid phases (Figure 10b).[16,17]

In a critical assessment, Cannon *et al.* summarized a few other systems where experiments found that the average composition of IGFs is different from that of the bulk glass/liquid phase, including: Ti concentration in $\underline{Pb_2RuO_7}$+ (Ti-Pb-Al-silicate); Ca/O and N/(N+O) ratios in $\underline{Si_3N_4}$ + (SiO_2-CaO); R/Si ratio in $\underline{Si_3N_4}$+ (Si-Al-Re-O) where R = Y, Yb, Gd, Nd, and La; Ca/Si ratio in $\underline{Al_2O_3}$ + (SiO_2-CaO); Ti concentration in $\underline{SrTiO_3}$+ (TiO_2-FeO); and Al concentration in $\underline{SiC}$ + (Al-B-C-O) (See Cannon *et al.*[2,5] and references therein). Furthermore, Gu *et al.* carefully mapped the Ca/O and N/(N+O) ratios in IGFs and liquid pockets in $\underline{Si_3N_4}$+ (SiO_2-CaO) specimens, showing constant (average) film composition along IGFs (which is significantly different from that of the liquid phase) and diffuse character at the tips of the liquid pockets and grain–liquid interfaces.[69,75]

The atomic structure of IGFs is also expected to be different from that of bulk liquid or glass phase. Although IGFs appear to be largely disordered in HRTEM, the existence of partial order has been suggested by molecular dynamics simulations[160−164] and diffuse-interface models.[44,165−167] In this regard, IGFs can be viewed as "confined liquid films" where the abutting grains impose some partial order into the films. Structural order in liquids induced by interfaces with crystals has been recently reviewed.[168] The ordered segregation structures of rare-earth elements in IGFs in $\underline{Si_3N_4}$-SiO_2 have been confirmed experimentally using (aberration-corrected) high-angle annular dark-field (HAADF) STEM.[80,81,83,84] A recent assessment showed that the results of interfacial structures in Si_3N_4-based ceramics sintered with six different lanthanide oxides (La_2O_3, Sm_2O_3,
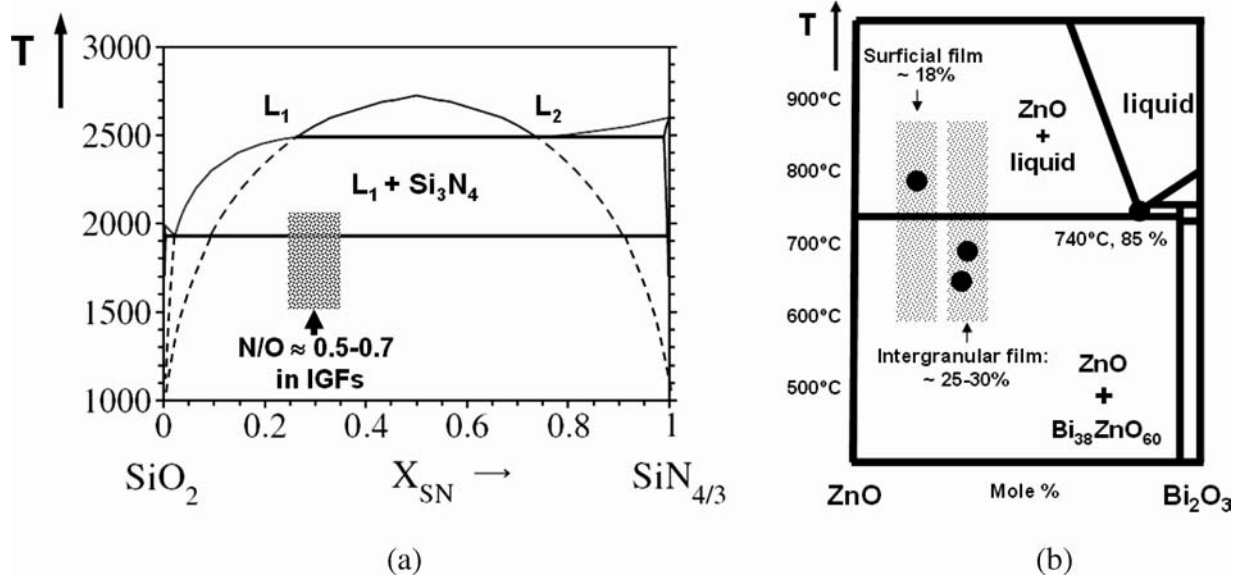

FIG. 10. Schematic illustrations of measured compositions of IGFs and SAFs in the phase regions of the corresponding bulk phase diagrams. The measured film compositions are markedly different from the associated bulk liquid phases (within the bulk miscibility gap in (a)). Panel (a) is a courtesy of R. M. Cannon. Panel (b) is reprinted from Ref. 10 with permission from Elsevier.

Er_2O_3, Gd_2O_3, Yb_2O_3, and Lu_2O_3) obtained by three independent research groups at Lawrence Berkeley National Laboratory, Oak ridge National Laboratory, and Oxford University exhibit good reproducibility.[169] Short-range order has also been detected in IGFs at SiC GBs by autocorrelation processing of HRTEM images.[116]

On the other hand, IGFs are not fully ordered films. The two abutting grains impose different order to the film, leading to frustration of ordering at the middle of the films. Through-thickness gradients in composition and structures are also expected from molecular dynamics simulations[160–164] and diffuse-interface models.[44,121,165–167,170]

Significant recent progress has been made by combining HAADF-STEM with first-principle quantum-mechanical calculations to understand the structures of IGFs (or grain-glass interfaces[171]) in Si_3N_4 based ceramics (e.g., partial order in IGFs) and to further relate them to processing and mechanical properties.[83,172] Recently, several other advanced TEM-based techniques (e.g., special electron diffraction techniques, measurement of electrostatic potential profiles, numerical nanodiffraction, ELNES) have been developed/used to characterize the structure and chemistry of IGFs.[173–177]

3.2.6 Influence of Boundary Crystallography

Dependence of IGF thickness and composition on the boundary crystallography deserves further discussion. In general IGFs do not form at small-angle or special-orientation GBs because these GBs have low excess free energy, which makes them stable against forming disordered IGFs.[1,5] At least in Si_3N_4, the equilibrium thickness showed little dependence on the boundary crystallography for large-angle, random GBs. This observation appears to be consistent with molecular dynamics simulations, which suggested that the random GBs exhibit universal charac-teristics in disordering when the misorientation is significantly great.[38]

On the other hand, some influences of the boundary crystallography on the equilibrium thickness are predicted by diffuse-interface models.[44,167] Because the standard deviations of IGF thicknesses are typically about 10% of the mean values in Si_3N_4-based materials, 95% confidence intervals represent as much as 40% variation.[1,72] The variations are even greater in other materials. The extent to which crystallographic anisotropy leads to observed GB-to-GB variation is an open question.[5] Gu and co-workers recent reported several studies showing that the GB crystallography can have measurable influence on IGF thickness and composition.[131,178,179]

3.3 Surficial Amorphous Films

Free-surface counterparts to equilibrium-thickness IGFs have been observed in several binary oxide systems.[6–11] These films are termed surficial amorphous films or SAFs despite indications of some local or partial order existing within them (Figure 11a). Key observations are reviewed in this section.

3.3.1 Bi_2O_3-Enriched Surficial Films on ZnO

Among all oxide systems studied, the Bi_2O_3-doped ZnO system has been the most extensively characterized. The observed SAFs in ZnO-Bi_2O_3 form preferentially on the $\{11\bar{2}0\}$ surfaces (Figure 11) and the anisotropic film formation has been attributed to induced order between the ZnO $\{11\bar{2}0\}$ surface and bismuth oxide structural units that constitute the film.[8]

SAFs with similar character were observed in Bi_2O_3-saturated samples equilibrated above and below the bulk eutectic temperature and in single-phase samples containing concentrations of Bi_2O_3 below the bulk solid-solubility limits.[6–8,10] The experimental observations are summarized in Figure 12. In the
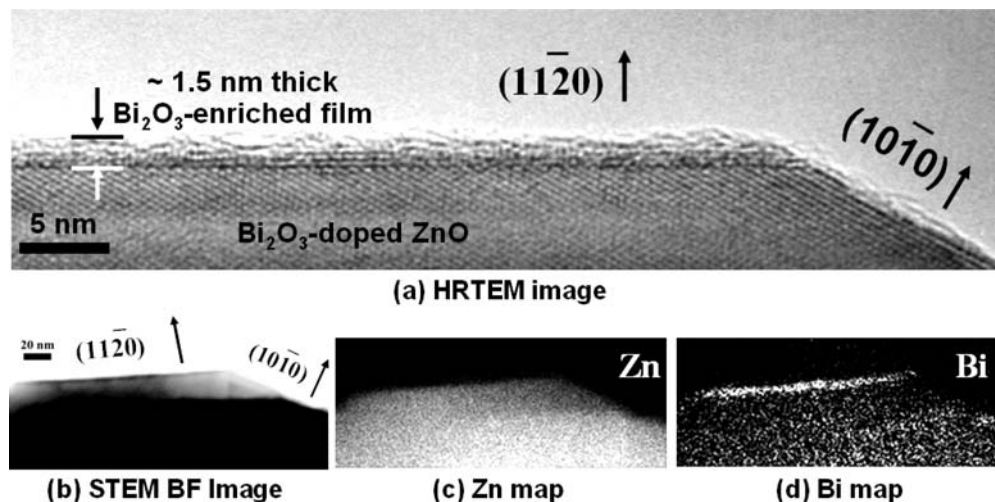

FIG. 11. (a) HRTEM image, (b) STEM bright-field image, (c) Zn map, and (d) Bi map demonstrating the anisotropic SAF formation in Bi_2O_3-doped ZnO. Adapted from Ref. 8 with permission from Elsevier.
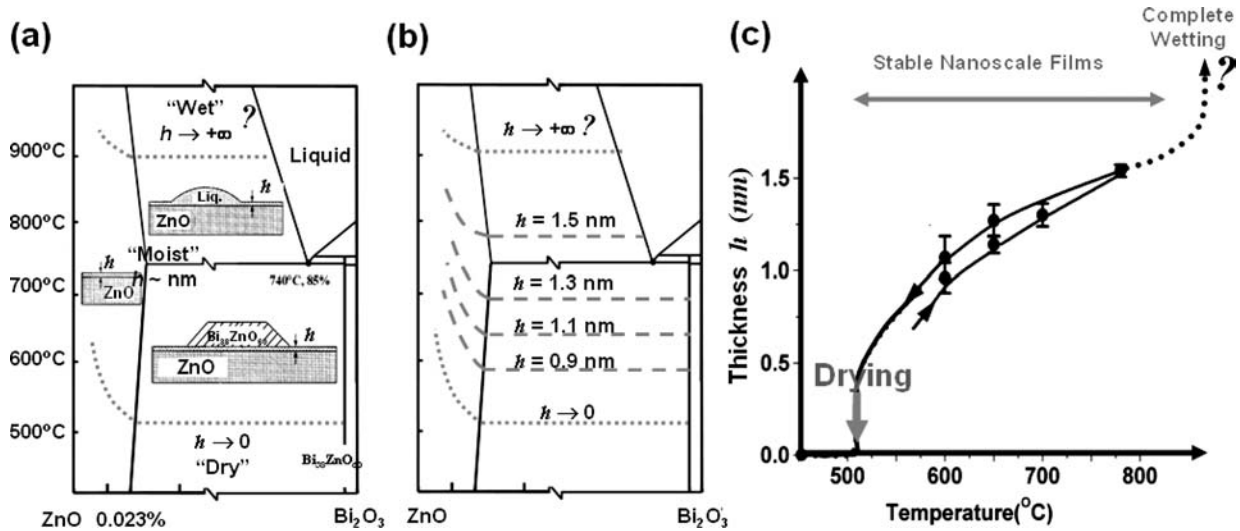
FIG. 12. (a) Schematic illustration of observed Bi_2O_3-enriched SAFs on ZnO $\{11\bar{2}0\}$ surfaces in the phase regions of the binary ZnO-Bi_2O_3 bulk phase diagram. (b) Lines of constant film thickness are plotted in the same phase diagram. (c) Reversible dependence of average thicknesses on temperature for Bi_2O_3-saturated samples. A complete wetting transition is expected from the simple prewetting model but has not been observed yet. Adapted from Ref. 9 with permission from Elsevier.

solid–liquid coexistence regime, nanometer-thick SAFs are in equilibrium with partial-wetting (non-wetting) liquid drops. A second class of thicker SAFs co-existing with nano-droplets was also observed and explained (Figure 6b).[10]

These surficial films have a nearly constant thickness at a fixed temperature and chemical potential. Once an equilibrium state has been reached, variations in additional annealing time and the amount of excess bulk secondary phase have no discernible influence on the average film thickness. It was therefore concluded that these SAFs have equilibrium thicknesses.[7,8] The equilibrium thickness exhibits a reversible dependence on temperature.[8,10] The film thickness, corresponding to the Gibbsian excess of solute, decreases monotonically with decreasing temperature in the subeutectic regime and vanishes at a lower drying temperature (Figure 12b). The surficial films are thinner in unsaturated specimens containing lower concentrations of Bi_2O_3 below the bulk solid-solubility limit.

A complete wetting transition is expected to occur at a higher temperature from a simple coupled surface prewetting and premelting model.[9] However, recent measurements of contact angle versus temperature show that complete wetting may be restrained by the presence of an attractive dispersion force of significant strength.[180] The measured contact angle decreases linearly with increasing temperature from 740 to 880°C but levels at about 5 degrees above ~880°C, although a complete wetting would be expected at ~970°C from an extrapolation of the linear regime. The formation of ridges at triple lines[181–183] have been revealed and may be another reason that spreading stops.

Like IGFs in the same system,[17] the nanoscale SAFs are markedly enriched in ZnO, as compared with the equilibrium liquid compositions (Figure 10b). The average measured composition of the film formed at 780°C is ~18 mole % Bi_2O_3, whereas the near-eutectic equilibrium bulk liquid contains ~83 mole% Bi_2O_3 at the same temperature.[8]

3.3.2 Systems with Repulsive Dispersion Forces

In the original theory for IGF stability,[3,4] the existence of attractive London dispersion interactions[184] was considered essential for the interfacial films to have an equilibrium thickness. However, other attractive interfacial interactions may exist; in particular, attractive pressures resulting from a volumetric free-energy term (§4.4.1) can become significant at subeutectic and undersaturation conditions.[8] It is therefore hypothesized that thin interfacial films may exhibit an equilibrium thickness without an attractive dispersion force. Unlike IGFs of symmetrical configurations where the London dispersion interaction is always attractive, dispersion interaction can be either attractive or repulsive for surficial films, providing a possibility to critically test this hypothesis.

Nanometer-thick SAFs have been observed in several oxide systems with negative Hamaker constants, including Bi_2O_3 on Fe_2O_3 ($A_{123} \approx -29$ zJ) and WO_3 on TiO_2($A_{123} \approx -105$ zJ), where the London dispersion forces/pressures are repulsive and act to thicken the films. SAFs in these two systems have been found to form at subeutectic conditions[8]: ~0.9 nm thick SAFs formed in Bi_2O_3-saturated Fe_2O_3 at 800°C ($T_{\text{eutectic}} = 960$ °C for the Bi_2O_3-Fe_2O_3binary system) and ~0.66 nm thick SAFs formed in WO_3-saturated TiO_2 at 1100°C ($T_{\text{eutectic}} = 1233$°C for the WO_3-TiO_2binary system). Representative HRTEM images are shown in Figures 13a and 13b. Additionally, the dispersion forces are also likely to be repulsive for the IGFs that have
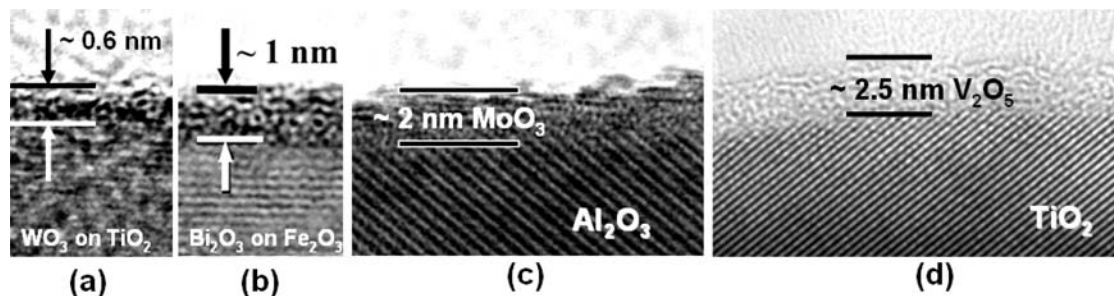
FIG. 13. HRTEM images of SAFs in several binary oxide systems. (a) and (b) are subeutectic SAFs in systems with repulsive London dispersion forces.[8] (c) and (d) are supported oxide catalyst systems.[10,147] Images (a)–(c) were adapted from Refs. 8, 10 with permission from Elsevier and the American Chemical Society.

been observed at heterophase interfaces in Si_3N_4-Yb_2SiO_5,[85] ZnO-Bi_2O_3,[16] TiO_2-SiO_2,[14] Al_2O_3-TiN,[137] and BN-SiC,[138] although quantification of Hamaker constants is difficult for these systems.

3.3.3 Other Systems

The formation of nanoscale surficial films has been observed in two important supported oxide catalyst systems: MoO_3 on Al_2O_3 (Figure 13c)[10] and V_2O_5 on TiO_2 (Figure 13d).[147,185–187] They are generally known as "monolayer catalysts" because the classical theories assumed the formation of monolayer adsorption of catalytic species (MoO_3 or V_2O_5) on support surfaces.[188] However, there is evidence showing that disordered, nanometer-thick (multilayer) adsorbates form under certain conditions. Further investigation using HRTEM is in progress.[147]

Stable, nanoscale, amorphous SiO_x films have also been observed to form on Si under controlled ultra-low oxygen partial pressures.[146] Amorphous films of $\sim$1 nm thick have also been found to form on the surfaces of various nanoparticles or nanowires grown from vapor phases or aqueous solutions.[189–193] These SAFs likely form at non-equilibrium conditions. Unfortunately, no systematic investigation has been conducted to reveal their formation mechanism and thermodynamic stability.

3.4 Disordered Interfacial Films in Multicomponent Metals

3.4.1 Grain Boundary Premelting/Prewetting Transitions in Cu-Bi and Fe-Si-Zn

Although nanometer-thick disordered GB films in metals (i.e., metallic IGFs) have not been widely found by direct HRTEM studies, GB structural transitions were indicated by measured discontinuities or abnormalities in macroscopic properties such as GB diffusivities[194,195] and GB energies[196] and Auger electron spectroscopy (AES) analysis of fractured GBs.[59,197] To date, the most systematic experiments have been conducted for Cu-Bi and Fe-Si-Zn systems.

The Cu-Bi binary system has been studied extensively,[59,194,197–202] and the key findings are summarized here. A complete GB wetting transition has been observed in the solid–liquid co-existence region, and the specific wetting transition temperature depends on boundary crystallography. The maximum and minimum complete wetting tie-lines are labeled in Figure 14a,[194] but a lower wetting transition temperature was suggested by another study.[203] Temperature- and chemical potential-dependent GB segregation has been carefully measured in the single-phase region. A prewetting transition occurs, giving rise to the formation of $\sim$2 monolayer-thick Bi films at GBs (estimated from AES), and the formation of these GB films results in two orders of magnitude increase in GB diffusivity.[200] Abrupt changes in GB segregation across a "GB solidus line" (i.e., prewetting line) have been observed. Furthermore, measurements of GB thermal grooving profile indicate that the abrupt change of segregation coincides with the discontinuity of the first derivative in the GB energy versus temperature.[196] These results clearly suggest the occurrence of first-order prewetting transitions. GB prewetting transition lines have been incorporated into the binary bulk phase diagram (Figure 14a), where the specific prewetting lines depend on boundary crystallography. The formation of GB quasi-liquid layers leads to increased brittleness and to measurable changes in electrical conductivity.

Premelting/prewetting transitions have also been revealed in the Fe-Si-Zn system by measuring Zn GB diffusivity along tilt GBs in bi-crystals in three Fe-Si alloys with 5, 10, and 12 at. % of Si. [194,204–207] Two distinct regions have been found in the penetration profiles of Zn along GBs: one abnormal region with high Zn concentrations and a low slope (high diffusivity) versus an ordinary region with low Zn concentrations and a high slope (low diffusivity). The diffusivity in the first (abnormal) region is about two orders of magnitude higher than that in the second (ordinary) region. The abnormal region with high Zn concentration and diffusivity was assumed to be the region where quasi-liquid IGFs develop. Additionally, the transition between the two regions occurs at a definite Zn concentration (denoted as C_{Bt} in the authors' original papers), which appears to be an equilibrium characteristic parameter of GBs. Furthermore, C_{Bt} was found to depend on the temperature and applied pressure. Because the
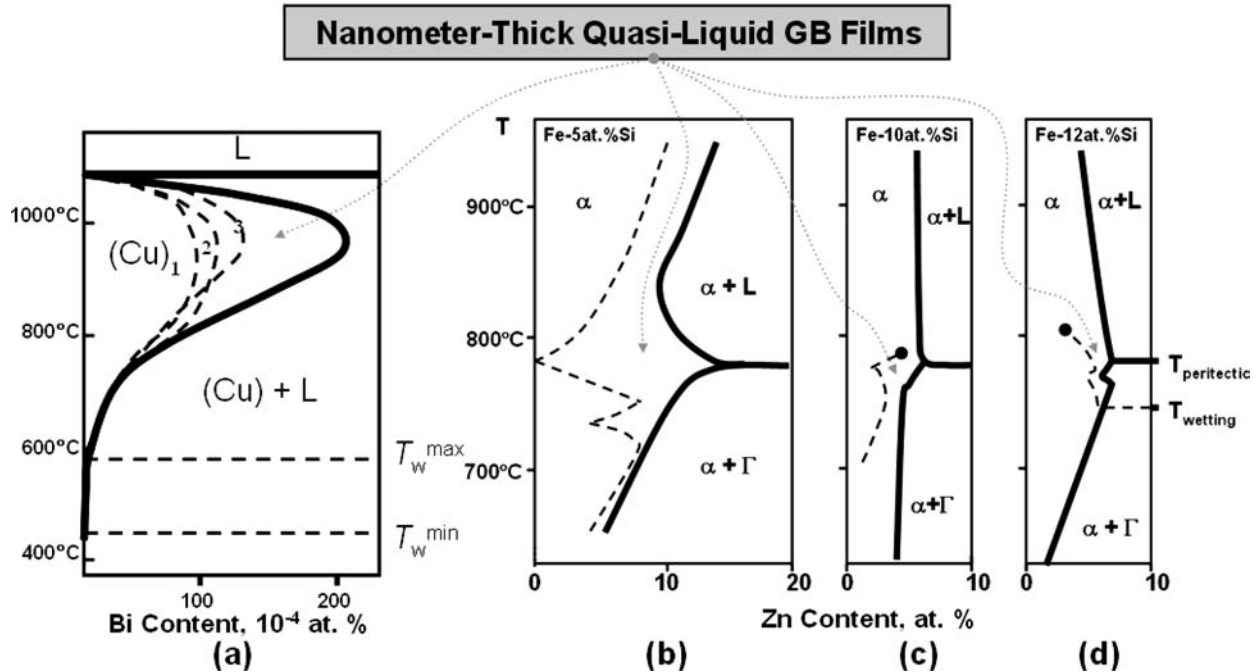
FIG. 14. (a) The GB prewetting/premelting phase diagram for Cu-Bi. Dashed lines 1–3 are prewetting lines for different GBs, and T_{wmax} and T_{wmin} are the maximum and minimum complete wetting temperatures (due to variation in crystallography among individual GBs). (b)–(d) are bulk and GB phase diagrams of Fe-Si-Zn ternary systems. Dashed lines represent first-order GB premelting/prewetting transitions in the single-phase region or complete wetting transition in the two-phase region. In (c) and (d), premelting/prewetting transition lines terminate at GB critical points. Reprinted from Ref. 194 and Ref. 204 with permission from Springer and Elsevier.

concentrations were measured by an electron microprobe with a relatively low spatial resolution, C_{Bt} represents the concentration of the bulk phase in equilibrium with two types of GBs (instead of the concentration at the GB). In other words, C_{Bt} represents the bulk concentration at which the high and low GB adsorption structures coexist, that is, the bulk concentration that gives a first-order GB premelting/prewetting transition. Consequently, GB phase diagrams have been constructed (Figures 14b–14d).

Furthermore, GB critical points have been observed for two cases (Figures 14c and 14d), where C_{Bt} can no longer be clearly defined because the penetration profiles of Zn become diffuse. Above the critical point, the prewetting/premelting transition should be continuous (second-order). Singularities in the premelting/prewetting transition lines below the peritectic temperatures were explained from superlattice ordering and ferromagnetic transitions in the bulk phases. At the peritectic temperature, the solubility of Zn in the Fe-Si alloy increases, but the premelting/prewetting concentration decreases (Figures 14b and 14c), which are rather surprising observations. Complete GB wetting has been observed in the two-phase regions above and below the bulk peritectic temperatures, and a complete wetting transition has also been reported for one case (Figure 14d). It is somewhat unclear whether GBs were wetted by the solid Γ phase or a metastable liquid phase below the bulk peritectic temperatures.

3.4.2 Direct Observation of Disordered Intergranular Films in W-Ni

A recent study[12,13,208] chose Ni-doped W as the model metallic system to obtain direct HRTEM evidence for the existence of nanometer-thick disordered IGFs in metals. Figure 15 shows HRTEM images of a representative GB in a W + 1 at. % Ni specimen sintered at 95°C below the bulk eutectic temperature. W lattice fringes are not contiguous at the GB and an ∼0.6 nm-thick intergranular film is identified. Despite indications of some local order existing within the film, the IGF is not fully crystallized. Furthermore, these IGFs cannot be the crystalline Ni phase, because complete solid-state GB wetting does not occur in W-Ni at 1400°C; the dihedral angle was found to be as great as 70° where the Ni-rich secondary phase meets a GB (at four-grain junctions).[13,208] AES analysis on fractured GBs with Ar sputtering has confirmed that these nanoscale IGFs are Ni-enriched.

These Ni-enriched IGFs likely have become more ordered during cooling. The fact that these IGFs appear to be largely disordered in cooled specimens implies that GB cores must be even more disordered and perhaps wider at firing temperatures. These disordered, Ni-enriched, IGFs exist in a true solid-state equilibrium. Only two stable bulk phases (solid (Ni) and W) are present between 1060°C and 1455°C (inset in Figure 15a), excluding the possibility of
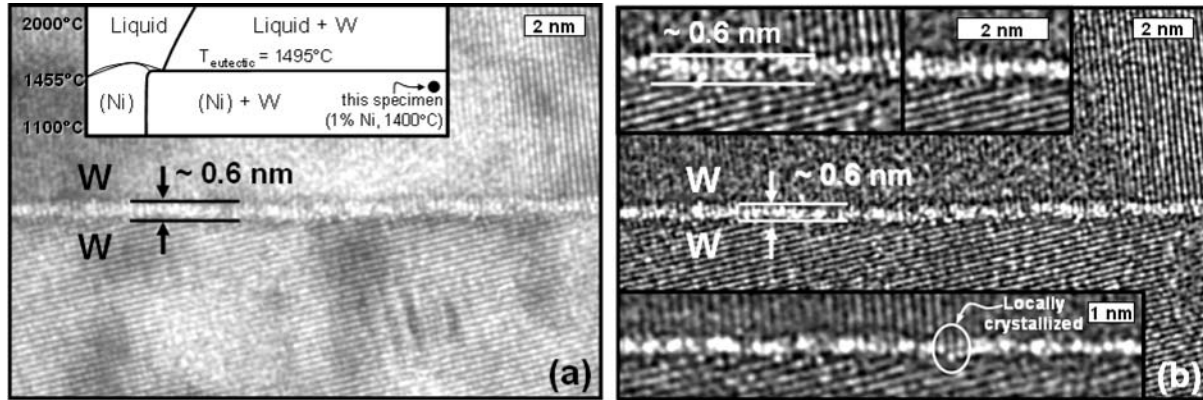
FIG. 15. (a) Original and (b) digitally enhanced HRTEM images of a disordered IGF in a W + 1 at. % Ni specimen annealed at 1400°C. The inset in (a) is the W-Ni phase diagram, in which the specimen conditions are indicated. Reprinted from Ref. 12 with permission from American Institute of Physics.

solid-state amorphization[209] or the formation of a transient liquid.

A rough estimation showed that stabilization of this quasi-liquid IGF is energetically-favored at an undercooling of 95°C if $-\Delta\gamma$ is greater than ~10% of the tungsten GB energy.[12] This observation was alternatively explained from a coupled GB premelting and prewetting transition in binary metals or as metallic counterparts of IGFs in ceramics.[12,13,208]

3.4.3 Other Systems and Related Phenomena

Nanometer-thick interfacial films have also been observed in a few other cases where definite explanations or conclusions are not available. For example, an ~2-nm-thick ordered (δ-NiMo compound) film has been observed at the GBs of activated sintered Ni-doped Mo[210] by HRTEM. It is unknown whether these films were disordered at firing temperatures but have crystallized during cooling. Because δ-NiMo is an equilibrium bulk phase at the firing temperature, it is unclear whether these δ-NiMo layers are complete wetting films (with supply-controlled thickness) or equilibrium-thickness IGFs. In another case, nanometer-thick IGFs have been found to be present at ~1/3 of GBs in liquid-phase sintered WC-Co composites (which are partially metallic).[211] In this study, the bulk Co liquid phase is present during sintering, but the intergranular Co layers, which are presumably quasi-liquid, remain at ~1 nm thick instead of becoming macroscopically thick wetting films.

Recently, the formation of nanometer-thick IGFs has been found to be important for the liquid metal embrittlement process. At both Ni and Cu GBs, intergranular penetration of Bi has been observed to occur in the form of nanometer-thick IGFs of constant thickness, which formed between the regions of the micrometer-thick liquid films and submonolayer GB adsorption.[203,212,213] Furthermore, without external stress, nanometer-thick Bi IGFs form, in spite of apparent non-zero dihedral angles at the emerging GBs with thick liquid films.[203] This

dynamic wetting configuration is closely analogous to the case of equilibrium-thickness IGFs coexisting with partial-wetting liquid pockets in ploycrystals. If the final equilibrium configuration is complete wetting, these nanometer-thick IGFs of constant thickness (formed during a dynamic penetration process) should represent metastable GB configurations; this process is analogous to the formation of precursor films during surface spreading.[64–66] The configuration used in these experiments is similar to that used in the studies of Fe-Si-Zn (§3.4.1), except that an applied or residual stress is sometimes (but not always) present. Al-Ga is another model system for liquid metal embrittlement studies in which the formation of nanometer-thick IGFs is also considered critical.[214] Prewetting transition was also suggested for Al-Ga within the Al single-phase region, because the GB mobility increases by a factor of 10 after the addition of 50 wt. ppm Ga (in contrast to the classical solute-drag model).[194,215]

Yet another related interfacial phenomenon is the formation of nanoscale (instead of macroscopic) interfacial amorphous films as a result of a special type of solid-state amorphization driven by excess interfacial energies. Solid-state amorphization refers to the phenomenon wherein a (bulk) amorphous phase forms via interfacial reaction in the solid state when intermediate compounds cannot nucleate.[209] This phenomenon, as originally defined, is a kinetically limited process, which is not directly related to the quasi-liquid interfacial films discussed here. However, solid-state amorphization can occur in $(A/B)_n$ multilayer structures where the free energy for mixing A and B is positive, driven by the excess interfacial energies stored in such multilayer structures.[216] Furthermore, a thermodynamic model[217] has been proposed for solid-state amorphization of nanometer-thick interfacial layers (occurring at hetero-interfaces or GBs) in binary systems with positive mixing free energies, which are driven by the reduction in the interfacial energies upon replacing a high-energy crystal-to-crystal interface with two low-energy crystal-to-glass interfaces; herein the underlying principles are identical to those for stabilization of premelting/prewetting layers. For

example, a recent study suggested that amorphous Si can "wet" the Al GBs and the intergranular Si layer can maintain its amorphous state up to a thickness of ~1.0 nm.[218] Another related observation is the formation of an amorphous layer up to 4-nm-thick at the tetragonal-Ta/Cu hetero-interfaces during a thermal annealing at 400°C and 600°C (Figure 7).[219] In this case, extensive intermixing has been observed in the Ta-Cu amorphous film while bulk Ta and Cu liquids are almost completely immiscible. After long annealing, the metastable tetragonal-Ta transformed to the stable body-centered cubic phase, and this amorphous layer disappeared at the same time.

Furthermore, the existence of GB prewetting layers in two-component metals is suggested by grand-canonical Monte Carlo simulations with embedded-atom potentials, which revealed that the Ag segregation at Cu high-angle GBs leads to the formation of thin quasi-liquid films.[220] Additionally, Monte Carlo simulations showed that layers of the disordered γ-phase develop at anti-phase boundaries in the Ni-Al system.[220] In both cases, prewetting transitions have been observed.

In conclusion, analogous disordered interfacial structures to IGFs in ceramics likely exist in metals and can become important under certain conditions. IGFs in non-glass-forming metals may exist in narrow undercooling and undersaturation ranges and are more likely to dry/crystallize during cooling than their ceramic counterparts. These are possible reasons that such nanoscale disordered interfacial films have not been widely found in metals.

3.5 Ice-Water-Impurity Systems

Recent studies using the DLVO theory indicated that the presence of minor ionic impurities, for example, NaCl, can stabilize and significantly thicken the premelting layers in ice.[46,148] Such impurity-based disordered films can form at ice surfaces, GBs, and hetero-interfaces with chemically inert walls. These are yet another class of impurity-based, quasi-liquid, interfacial films in multicomponent materials (molecular substances), wherein long-range dispersion and electrostatic forces dominate. More details of this phenomenon can be found in several recent articles[46,148] and a review.[21]

Another interesting analogous situation is the nanometer-thick confined water layers in swelling clays, which always contain some ionic impurities.[221–224] Such interfacial films can exhibit self-selecting "stable" thickness. Furthermore, these quasi-water films can form when the water vapor pressure is below the saturation (analogous to prewetting) or when the temperature is below the freezing point (analogous to premelting). Recently, such systems have been used as an ideal environment for studying confined 2-D liquids.[223]

4. THERMODYNAMIC STABILITY OF NANOSCALE INTERFACIAL FILMS

4.1 Assessment: Basic Physical Principles

A generalized picture is envisioned from summarizing and assessing the experimental observations discussed in §3 and crit-

ically comparing them with the existing theories for simpler systems discussed in §2. For example, Figure 16 schematically illustrates a possible sequence of interfacial adsorption and wetting events with increasing temperature for binary systems with eutectic reactions (e.g., ZnO-Bi$_2$O$_3$ or W-Ni) in the solid–solid and solid–liquid two-phase regions (where primary phases are saturated with dopants). Similarly, a sequence of three regions, namely submonolayer/monolayer adsorption, nanoscale interfacial films/multilayer adsorption, and complete wetting, can occur with increasing dopant activity. Additional complexity comes from the possible occurrence/appearance of layering or roughening transitions, incomplete or frustrated-complete melting/wetting, first-order or continuous adsorption/wetting transitions, and interfacial critical points, resulting in diversifying interfacial behaviors. A critical assessment of the experimental observations and existing theories was used to formulate the following basic physical principles and concepts for understanding the stabilization of these nanoscale interfacial films in multicomponent inorganic materials:

- These nanometer-thick interfacial films can be alternatively understood to be:
  - quasi-liquid layers that adopt an "equilibrium thickness" in response to a balance among several attractive and repulsive interfacial forces/pressures,[1–5,7–10,119] or
  - multilayer adsorbates with film compositions and interfacial excesses set by the bulk chemical potentials.[2,5,9,10,165,225]

- Stable nanoscale interfacial films represent a "prewetting regime" of multilayer adsorption behavior at GBs or surfaces[2,5,9,165–167] intermediate to that of "complete wetting" and "submonolayer/monolayer adsorption" (Figure 16; see §4.5.4 for further discussion regarding the definition of "prewetting regime").
  - As proposed by Cannon[2,5] and supported by Kikuchi and Cahn's prior lattice-gas model,[226] this interfacial prewetting/premelting regime is characterized by increasing interfacial excesses with increasing temperature, because adsorption promotes interfacial disordering and creates new adsorption sites (especially for GBs).

- The stabilization of quasi-liquid interfacial films at subsolidus (e.g., undersaturation, subeutectic, subperitectic) conditions wherein bulk liquid is no longer stable[7,8,12,14–18] can be conceived as if the reduction in interfacial energies over compensates for the positive volumetric free energies for amorphization (Figure 4):
  - An analogy to the theory of premelting in unary systems can be made.
  - In principle, nanoscale disordered interfacial films can be stabilized in multicomponent
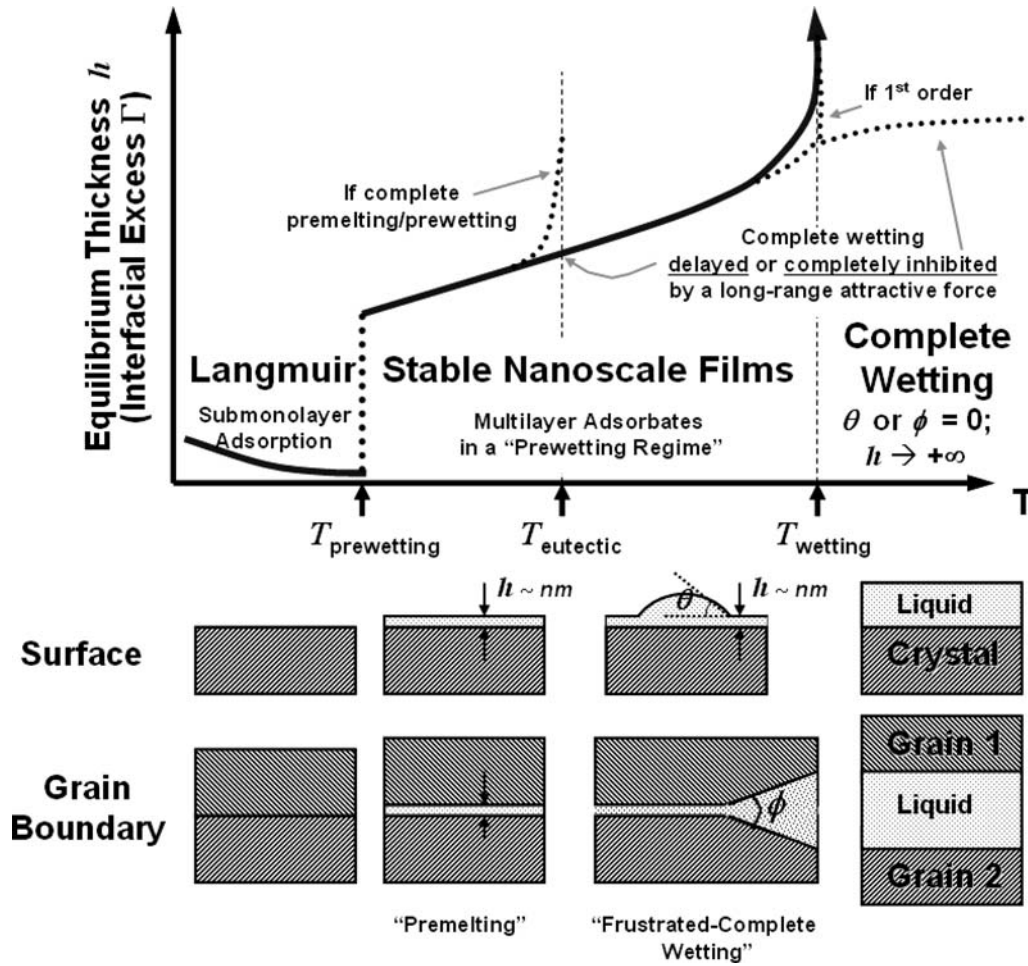
FIG. 16. Schematic illustration of a sequence of adsorption and wetting events with increasing temperature in a two-component material in the solid-solid and solid-liquid two-phase regions. Stable nanoscale interfacial films (multilayer adsorbates) form in a "prewetting regime," bounded by a drying/prewetting transition ($h \to \sim 0$) and a complete wetting transition ($h \to +\infty$ and θ or $\phi \to 0$). The stabilization of quasi-liquid interfacial films below the bulk eutectic temperature is analogous to the theory of premelting. The coexistence of a nanoscale interfacial film and a partial-wetting liquid drop in the solid-liquid two-phase region is analogous to the phenomenon of frustrate-complete wetting.

systems over wider ranges of undercooling (or undersaturation) than the simple premelting in unary materials, because interfacial disordering can be enhanced by concurrent segregation/adsorption (especially for GBs and other internal interfaces).

- These quasi-liquid interfacial films can be understood from coupled GB[167] or surface[9] premelting and prewetting transitions; the presence of additional interfacial forces, for example, long-range London dispersion forces, electrical double-layer interactions (if ionic species are involved), magnetic forces (e.g., in Fe-Si-Zn), and strain energies, alters the film stability regime and thickness.

- If an additional attractive interfacial force (e.g., a dispersion force of significant strength) is present to restrain the film from unlimited thickening at and above the bulk eutectic temperature (or the bulk solidus line), stable nanoscale interfacial films can persist into the solid-liquid coexisting regime (Figures 12 and 16).

  - Coexistence of a nanometer-thickness interfacial film with a partial-wetting bulk liquid is analogous to the phenomenon of frustrated-complete wetting (§2.5; Figure 6).

- These nanometer-thickness interfacial films can also be considered as confined liquids whose thermodynamic and physical properties are significantly modified by abutting crystals.

- The films adopt an average composition that minimizes their excess free energy, which differs (markedly) from that of the associated bulk liquid or glass phase, even if these quasi-liquid films are in equilibrium with the bulk liquid or glass phase.
- The abutting crystals impose some partial order into the films.
- Through-thickness structural and compositional gradients exist.
- These equilibrium-thickness interfacial films can represent either a true thermodynamic equilibrium or various types of metastable equilibrations.

The following sections review and discuss the diffuse-interface and force-balance models that utilize the above-mentioned physical principles and concepts to model the thermodynamic stability of these nanoscale interfacial films in a unifying theoretical framework.

4.2 Diffuse-Interface Theories

Surficial films in binary systems can be used as an example to illustrate why diffuse interfaces form.[10] The equilibrium film composition for a nanoscale surficial film should derive from a compromise: to minimize the volumetric free-energy penalty, the composition is coerced towards the bulk liquid; to minimize the interfacial transition energy, it approaches that of the bulk substrate; to minimize the short-range excess energy associated with a terminating surface, it approaches that of the surface of the bulk liquid. Obviously, this can be better achieved by including through-thickness compositional gradients in the film, but then further energy penalties arise. Likewise, structural gradients exist. These volumetric and gradient free-energy terms of structural and chemical origins are coupled and can be explicitly described in the context of diffuse-interface theories.

In a seminal paper, Cahn[25] analyzed prewetting and critical point wetting in a binary liquid system exhibiting a miscibility gap using a diffuse-interface model by finding the spatially-varying concentration function $c(x)$ that minimizes the excess free energy per unit area of a flat surface:

$$\sigma^x = \Phi(c_s) + \int_0^\infty [\Delta f(c(x)) + \kappa_c \cdot |\nabla c(x)|^2] dx. \qquad [13]$$

x is the spatial parameter, perpendicular to the surface located at $x = 0$. $\Phi(c_s)$ is the excess short-range energy term associated with the terminating surface, where c_s is the concentration at the terminating surface. $\Delta f(c)$ is the homogenous free-energy density referred to equilibrium bulk phases. κ_c is a gradient energy coefficient. Minimization of Eq. 13 (as well as Eqs. 14–18 and Eq. 21) is a standard problem in calculus of variations; $c(x)$ (and other the spatially varying fields) is a solution of the corresponding Euler equation with specific boundary conditions. Description of the minimization procedure and Euler equations can

be found in any textbook of calculus of variations. A schematic phase diagram of the system studied by Cahn is depicted in Figure 3c. The basic predications and experimental verifications of Cahn's critical point wetting model have been discussed in §2.3.

A diffuse-interface model can also be proposed for surface premelting for one-component material systems with short-range interactions (e.g., metals). In the simplest form, the spatially varying crystallinity function, $\eta(x)$, ($\eta = 0$ for liquid and $\eta = 1$ for perfect crystal) near the surface can be found by minimizing the following excess free-energy functional:

$$\sigma^x = \Phi(\eta_s) + \int_0^\infty [\Delta f(\eta(x)) + \kappa_\eta |\nabla \eta(x)|^2] dx. \qquad [14]$$

$\Phi(\eta_s)$, $\Delta f(\eta)$ and κ_η have similar definitions as $\Phi(\eta_c)$, $\Delta f(c)$ and κ_c, except that they are associated with the crystallinity parameter (η). Eq. 14 is isomorphic to Eq. 13 by substituting crystallinity $\eta(x)$ for concentration $c(x)$. (The corresponding kinetic equations are different since the concentration field is conservative, but the crystallinity field is non-conservative.) More sophisticated and realistic surface premelting models have been developed and systemically analyzed by Lipowsky in a continuum approach.[227–231]

GB premelting is more complex than surface premelting where the field of an orientation parameter, $\theta(x)$, should also be considered. Based on the Kobayashi-Warren-Carter (KWC) model,[232] GB premelting was analyzed, where the excess GB free energy functional is written as

$$\sigma^x = \int_{-\infty}^{+\infty} [\Delta f(\eta(x)) + \kappa_\eta |\nabla \eta(x)|^2 + s \cdot g(\eta) \cdot |\nabla \theta(x)|$$
$$+ \frac{\beta^2}{2} \cdot |\nabla \theta(x)|^2] dx. \qquad [15]$$

The GB is located at $x = 0$. β, s, and $g(\eta)$ are additional gradient energy coefficients. The crystallinity $\eta(x)$ and orientation $\theta(x)$ fields can be found by minimizing Eq. 15 with boundary conditions of $\theta(\pm\infty) = \pm\theta_0$; $\eta(\pm\infty) = 1$, where $\Delta\theta = 2\theta_0$ represents the misorientation. The above model has been analyzed numerically[43] and analytically.[44,45] The existence of continuous and first-order premelting transitions has been demonstrated.

Stability of nanoscale quasi-liquid interfacial films in multicomponent systems can be understood from coupled interfacial prewetting and premelting transitions.[9,167] Before discussing the specific diffuse-interface equations, some general concepts and thoughts are illustrated in Figure 17. In binary systems, the formation of nanoscale quasi-liquid interfacial films can be understood as a result of combined interfacial disordering and adsorption. A generic coupled prewetting and premelting interfacial phase diagram for a two-component solid–liquid system is shown in Figure 17a. The same interfacial phase diagram can be alternatively represented in the T-($\mu_B - \mu_B^{(\alpha/L)}$) space (Figure 17b) where $\mu_B^{(\alpha/L)}$ is the chemical potential of the end
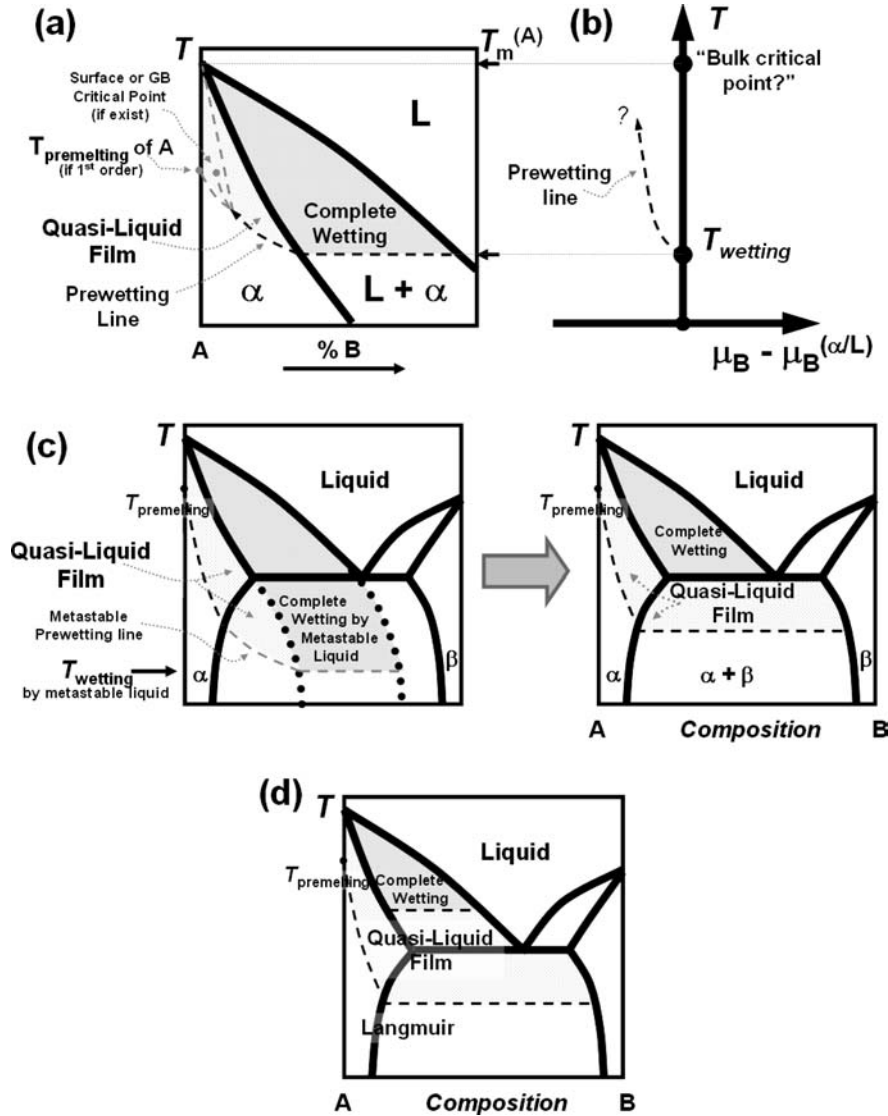
FIG. 17. (a) The first generic prewetting/premelting interfacial phase diagram for a two-component solid-liquid system. The tie-line for complete wetting transition in the solid-liquid coexistence region extends into the single-phase region as a prewetting transition line. Cu-Bi likely belongs to this group. (b) Representation of the same interfacial phase diagram in the T-$(\mu_B - \mu_B^{(\alpha/L)})$ space. (c) The second generic interfacial phase diagram where the complete wetting transition temperature (for a metastable liquid) is lower than the bulk eutectic temperature. W-Ni and Fe-Si-Zn likely belong to this group. (d) The third generic interfacial phase diagram where the complete wetting is delayed by additional attractive interfacial forces. Most IGFs in ceramics may belong to this group. In all figures, dashed lines represent first-order wetting or prewetting/premelting transitions.

member B on the solidus/liquidus line. If the end member A premelts completely (thus the melting transition becomes continuous), the bulk melting point of A may be treated a "critical point" for this solid-liquid system, where the difference between the solid and liquid phases vanishes continuously. Thus, this situation is in an analogy to the generic prewetting phase diagram shown in Figure 3d. If a first-order complete wetting transition occurs in the solid-liquid coexistence region, the tie-line of the complete wetting transition will extend into the single-phase

region as a first-order prewetting transition line (Figures 17a and 17b). However, it is still unknown whether this prewetting line ends at a surface/GB critical point or at the premelting or bulk melting point of the end member A (Figure 17a). Cu-Bi likely belongs to this group. Figure 17c shows a second generic interfacial phase diagram if the complete wetting temperature (for a metastable liquid) is lower than the bulk eutectic (or peritectic) temperature. In this case, nanoscale quasi-liquid interfacial films are also stable in the subeutectic solid-solid two-phase

region, bounded by a first-order prewetting transition at lower temperature and a (continuous) complete wetting transition at the eutectic temperature. W-Ni and Fe-Si-Zn likely belong to this group. Finally, if an additional attractive interfacial force of significant strength is present, the complete wetting transition is delayed or even completely inhibited (Figures 16 and 17d). Most IGFs in ceramics may belong to this group.

A rigorous analysis of coupled GB prewetting and premelting transitions in a binary alloy with an eutectic reaction was originally given by Tang, Carter, and Cannon[167] using a diffuse-interface model based on the KWC theory.[232] In their model, the excess (film) energy functional for a 2-component GB is

$$\sigma^x = \int_{-\infty}^{+\infty} [\Delta f(\eta(x), c(x)) + \kappa_\eta |\nabla \eta(x)|^2 + s \cdot g(\eta) \cdot |\nabla \theta(x)|$$
$$+ \frac{\beta^2}{2} \cdot |\nabla \theta(x)|^2 + \kappa_c \cdot |\nabla c(x)|^2] dx. \tag{16}$$

The concentration $c(x)$, crystallinity $\eta(x)$, and orientation $\theta(x)$ fields should be found by minimizing Eq. 16 with boundary conditions of $\theta(\pm\infty) = \pm\theta_0$; $\eta(\pm\infty) = 1$; $c(\pm\infty) = c_{\text{bulk}}$. Tang, Carter, and Cannon initially analyzed this model using a graphical method and constructed a GB phase diagram that is similar to Figure 17c. They concluded that first-order coupled GB prewetting and premelting transitions can occur in subeutectic and undersaturation regions, the prewetting/premelting line terminates at a GB critical point in the single-phase region, and the specific GB behavior depend on the misorientation.[167] This model, which does not consider the long-range forces, predicts that the thickness of GB quasi-liquid film is divergent at the bulk eutectic temperature, where a (continuous) complete wetting transition occurs.

This simple coupled GB premelting and prewetting model may apply (reasonably well) to metals where the short-range interactions dominate (although dispersion forces still exist[233,234]). For IGFs in ceramics, long-range London dispersion forces of a significant strength and electrostatic interactions should be added separately. Bishop, Carter, and Cannon[165,166] recently proposed and numerically analyzed a sophisticated diffuse-interface model for IGFs in Si3N4-SiO2, which included the effects of defects and electrostatic interactions; the dispersion interaction still needs to be added separately.

A coupled surface prewetting and premelting diffuse-interface model has also been proposed as a basis for understanding SAFs in ceramics,[9,10] where the excess film energy functional is expressed as

$$\sigma^x = \Phi(c_s, \eta_s, \theta_s) + \int_0^\infty [\Delta f(\eta(x), c(x)) + \kappa_\eta \cdot |\nabla \eta(x)|^2$$
$$+ \kappa_c \cdot |\nabla c(x)|^2 + s \cdot g(\eta) \cdot |\nabla \theta(x)| + \frac{\beta^2}{2} \cdot |\nabla \theta(x)|] dx. \tag{17}$$

Here, $\Phi(c_s, \eta_s, \theta_s)$ is a short-range energy term associated with the terminating surface similar to that in Cahn's critical

point wetting model (Eq. 13). It depends on the values of all three parameters at the terminating surface (c_s, η_s, θ_s), but one parameter, for example, the concentration at the terminating surface (c_s), can dominate. The integral is the same as that in Eq. 16 for IGFs. However, the gradient in orientation ($\nabla\theta$) is less important for SAFs than that in IGFs, where a "forced" $\Delta\theta$ is imposed by two boundary conditions, and thus may be neglected. Then, for a fixed surface orientation, θ_0, Eq. 17 can be simplified to:

$$\sigma^x = \Phi(c_s, \eta_s, \theta_0) + \int_0^\infty [\Delta f(\eta(x), c(x)) + \kappa_\eta \cdot |\nabla \eta(x)|^2$$
$$+ \kappa_c \cdot |\nabla c(x)|^2] dx. \tag{18}$$

The concentration $c(x)$ and crystallinity $\eta(x)$ fields should be found by minimizing Eq. 18 with appropriate boundary conditions and a specific surface term $\Phi(c_s, \eta_s, \theta_0)$. A recent publication utilized this diffuse-interface model to analyze the surficial film stability for a binary system exhibiting an eutectic reaction, where surface phase diagrams similar to Figures 17c and17d have been deduced.[9] The predicted surface phase diagrams are qualitatively consistent with experimental observations shown in Figure 12 for Bi2O3-enriched SAFs on ZnO. Like IGFs, further refinements of this model for SAFs in ceramic materials should include the effects of dispersion forces, electrostatic interactions, and perhaps strain energies.

The film-crystal interfaces in HRTEM images (e.g., Figures 7 and13) are nearly atomically abrupt, appearing to contradict the "diffuse interface" hypothesis. A recent work[9] used the diffuse-interface theory to qualitatively explain the different sharpnesses at the substrate(primary phase)-adsorbates interfaces that are associated with two types of bulk phase diagrams: a binary liquid with a miscibility gap (the system studied in Cahn's critical point wetting model) versus a binary liquid-solid system with a deep eutectic reaction (e.g., ZnO-Bi2O3 and W-Ni). From Eq. 7 in Cahn's original paper on the critical point wetting theory,[25] the compositional gradient at the transition between the matrix phase and adsorbates is

$$\left| \frac{dc}{dx} \right|_{\text{trans}} = \sqrt{\frac{\Delta E}{\kappa_c}}, \tag{19}$$

where ΔE is the height of the potential barrier between the minimum energy states for the two immiscible liquids in the free energy versus concentration. Because prewetting occurs at temperatures close to the bulk critical point, ΔE is moderate and results in rather diffuse interfaces between the adsorbates and the matrix phase (Figure 18a). An extension of Eq . 19 for binary solid-liquid systems has been deduced[9]:

$$\sqrt{\kappa_\eta \cdot \left| \frac{d\eta}{dx} \right|_{\text{trans}}^2 + \kappa_c \cdot \left| \frac{dc}{dx} \right|_{\text{trans}}^2} = \sqrt{\Delta E}. \tag{20}$$

In the case of binary systems with deep eutectic reactions (e.g., ZnO-Bi2O3 or W-Ni), the free energy barrier ΔE for the structural transition is high and results in abrupt film-crystal
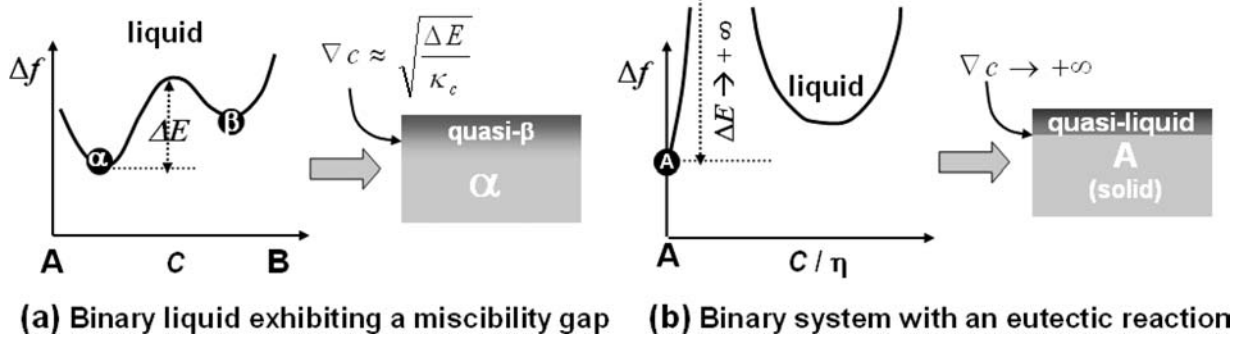
FIG. 18. The diffuse versus abrupt substrate (primary phase)—adsorbate interfaces can be understood through different volumetric free-energy functions associated with the bulk phase diagrams. Adapted from Ref. 9 with permission from Elsevier.

transition (Figure 18b), consistent with the experimental observations (e.g., Figure 13).

Because the crystal-film interfaces are sharp, alternative models for IGFs can be devised by applying diffuse-interface theories with pre-selected boundary conditions at the abrupt crystal-film interfaces. Clarke's original model[3] for the steric force belongs to this group, where excess film energy due the partial ordering and structural gradients are:

$$\sigma_{steric}^{x} = \int_{-h/2}^{h/2} [\Delta f(\eta(x)) + \kappa_\eta \cdot |\nabla \eta(x)|^2] dx. \qquad [21]$$

The steric free-energy term ($E_{steric}(h)$) was found by minimizing Eq. 21 with the boundary conditions of: $\eta(x = +h/2) = +\eta_0$ and $\eta(x = -h/2) = -\eta_0$. The corresponding steric pressure was found to be:

$$\Pi_{steric}(h) = \frac{dE_{steric}(h)}{dh} \approx -4a\eta_0^2 \cdot \exp(-h/\xi), \qquad [22]$$

where a is a coefficient in the Landau expansion of $\Delta f(\Delta f(\eta) = a \cdot \eta^2 + \cdots)$ and $\xi \equiv \sqrt{\kappa_\eta/a}$ is a coherent length. This model has also been examined for different boundary conditions at the film/crystal interface[14,121] and extended to surficial films.[7] Further refinements that include additional concentration and orientation fields in the KWC theory can be envisioned. This approach may realistically represent IGFs and SAFs in many instances, for example, representing strong steric effects in IGFs made of polymeric oxides (silicates) that may be related to metastable boundary conditions at crystal–film interfaces. Selection of realistic boundary conditions is a challenge (and somewhat subjective).

The existence of abrupt film–crystal interfaces also supports contemplation of the simplified treatment of the film free energy in force-balance models discussed in §4.3 and §4.4 where through-thickness gradients are neglected except for approximations concerning short-range forces related to the gradient terms.

4.3 Force-Balance Models

The stability of nanoscale interfacial films can be conveniently analyzed in force-balance models. In these models, an "equilibrium thickness" represents a balance among several attractive and repulsive interfacial pressures/forces. Equivalently, the equilibrium thickness corresponds to a global or local minimum in excess film free energy versus film thickness. Such methods and concepts have been used extensively in colloidal theory to explain the equilibrium separation among particles. These force-balance models are in fact "pressure-balance models," because "forces per unit area" are typically considered.

The basic concepts of the force-balance models can be demonstrated using a phenomenological premelting theory,[20,21] where the excess free energy of an undercooled surficial liquid layer with thickness h is given by

$$G(h) = \mu_{\text{liquid}} \cdot \rho \cdot h + (\gamma_{cl} + \gamma_{lv}) + E_{int}(h), \qquad [23]$$

where ρ and μ_{liquid} are the molecular/atomic density and chemical potential, respectively, of the bulk liquid phase. $(\gamma_{cl} + \gamma_{lv})$ represents the sum of crystal–liquid and liquid–vapor interfacial energies, and these two excess interfacial energies are well defined when the film is sufficiently thick. When the film is thin, an extra interfacial energy term $E_{int}(h) \equiv \Delta\gamma \cdot (f(h) - 1)$ arises (from the interaction between the two interfaces), representing the total contributions of all interfacial forces. Here, $\Delta\gamma = \gamma_{lv} + \gamma_{cl} - \gamma_{cl}^{(0)}$ is defined in Eq. 5 for free surfaces. $f(h)$ is defined as the interfacial coefficient, ranging from 0 to 1 as thickness h increases from 0 to ∞. Correspondingly, the total excess interfacial energy $[(\gamma_{cl} + \gamma_{lv}) + E_{int}(h)]$ changes from $\gamma_{cl}^{(0)}$ to $(\gamma_{cl} + \gamma_{lv})$. To be consistent, the interfacial interaction term $E_{int}(h) \equiv \Delta\gamma \cdot (f(h) - 1)$ (as well as all other individual interfacial energy terms discussed later) is defined so that it vanishes as $h \to +\infty$ in this article. (Alternatively, interfacial interaction term can be defined as $E_{int}^*(h) \equiv E_{int}(h) + \Delta\gamma = \Delta\gamma \cdot f(h)$, which vanishes at $h = 0$. The total excess interfacial energy: $(\gamma_{cl} + \gamma_{lv}) + E_{int}(h) = \gamma_{cv}^{(0)} + E_{int}^*(h)$.) A similar equation can be proposed for GBs.

The dependence of $E_{int}(h)$ or $f(h)$ on thickness reflects the type of basic interaction in the material. The $f(h)$ attenuates quadratically with thickness for molecular substances with long-range, non-retarded, dispersion forces (e.g., ice), or decays exponentially for metals where the short-range interactions dominate. Correspondingly, the interfacial energy term $E_{int}(h)$ represents a dispersion interaction ($E_{int}(h) = E_{dispersion}(h) = -\Delta\gamma_d \cdot \delta^2/(\delta^2 + h^2)$) for molecular substances (§4.4.3 and Eq. 39) and a short-range interaction ($E_{int}(h) = E_{short-range}(h) = -\Delta\gamma_{short-range} \cdot \exp(-h/\xi)$) for metals (§4.4.2), respectively.

If the difference in densities of solid and liquid phases can be ignored (otherwise, a correction factor should be included in Eq. 24), the following approximation can be used to estimate the volumetric free-energy term:

$$\Delta G_{vol} = (\mu_{liquid} - \mu_{solid}) \cdot \rho \approx \Delta S_{vol}^{fusion} \cdot (T_{melting} - T). \quad [24]$$

Here ΔS_{vol}^{fusion} is the fusion entropy per unit volume and $T_{melting}$ is the melting temperature. Thus, the excess film free energy as a function of film thickness, referred to the equilibrium bulk solid phase and the state of $h = 0$, is given by:

$$\Delta\sigma(h) \equiv [G(h) - G(0)] - \mu_{solid} \cdot \rho \cdot h = \Delta\gamma$$
$$+ \Delta S_{fusion} \cdot (T_{melting} - T) \cdot h + E_{int}(h). \quad [25]$$

Equation 24 or the second term in Eq. 25 represents the positive volumetric free energy for forming a metastable liquid layer.

A premelted film of thickness h, for which $\Delta\sigma(h) < 0$, is thermodynamically stable. The equilibrium thickness is obtained by minimizing the excess free energy $\Delta\sigma(h)$. The spatial derivatives of the interactions in Eq. 25 are equivalent to attractive or repulsive pressures/forces acting across the film. Thus, the equilibrium thickness is alternatively represented by a pressure/force balance:

$$\left. \frac{d\Delta\sigma(h)}{dh} \right|_{h=h_{eq.}} = 0, \quad [26]$$

which implies:

$$\Delta S_{vol}^{fusion} \cdot (T_{melting} - T) = -\frac{dE_{int}(h)}{dh}. \quad [27]$$

The left-hand side of Eq. 27 is a (constant) attractive pressure due the volumetric free energy for forming the metastable stable liquid phase, which scales with the undercooling, $(T_{melting} - T)$. The right-hand side of Eq. 27 represents a repulsive interfacial force. By inserting the specific function of interfacial interaction $E_{int}(h)$, the thickness of the premelting layer versus temperature can be calculated. In general, $h_{eq} \propto t^{-1/3}$ for materials controlled by long-range dispersion forces (e.g., ice), and $h_{eq} \propto |\ln(t)|$ for materials controlled by the short-range forces (e.g., metals), where $t \equiv (T_{melt\,inf} - T)/T_{melting}$ is the reduced temperature.

Force-balance models can also be used for assessing the thickness of prewetting layers (Figure 3) using the following

equation, which is similar to Eq. 25:

$$\Delta\sigma(h) = \Delta\gamma + \Delta G_{vol} \cdot h + E_{int}(h), \quad [28]$$

where ΔG_{vol} represents volumetric free energy for forming the metastable β phase (Figure 3) and the interfacial interaction term $E_{int}(h)$ scales with $\Delta\gamma \equiv \gamma_\beta + \gamma_{\alpha\beta} - \gamma_\alpha^{(0)}$. Although this model is intrinsically inaccurate for prewetting films in binary de-mixed liquid systems with significant compositional gradients, it can predict the stabilization of the prewetting layers and the basic trends in thickness versus concentration or temperature.

Clarke[3] initially proposed that the thickness of the IGFs represents an equilibrium separation between grains in a force-balance model. In a simple form of this model, the equilibrium thickness is determined by a balance among a long-range dispersion pressure, a short-range steric interaction, and capillary and applied pressures:

$$\Pi_{dispersion}(h) + \Pi_{steric}(h) + (P_{capillary}) + (P_{applied}) = 0. \quad [29]$$

If capillary and applied pressures are not present, Eq. 29 can be alternatively expressed in the form of excess film free energy versus thickness:

$$\Delta\sigma(h) = \Delta\gamma + E_{dispersion}(h) + E_{steric}^{(h)}. \quad [30]$$

The excess film free energy exhibits a minimum at the equilibrium thickness, representing a balance between the attractive long-range dispersion force and the repulsive short-range steric force.

Attempts to refine the force-balance model have led to introduction of an electrical double-layer interaction,[4] new diffuse-interface models for short-range interactions of structural and chemical origins,[14,121,170] and improved treatments of Hamaker constants.[184,235] A refined continuum model has also been proposed for IGFs in Si_3N_4 ceramics.[236] For quasi-liquid interfacial films forming at subsolidus conditions (e.g., IGFs at GBs in ZnO-Bi_2O_3,[16–18] Al_2O_3-(Y_2O_3+ SiO_2),[15] W-Ni,[12] and Cu-Bi[194]; IGFs at heterophase interfaces in SiO_2-TiO_2[14] and ZnO-Bi_2O_3[16]; and SAFs for Bi_2O_3 on ZnO,[7,8,10] Bi_2O_3 on Fe_2O_3,[8] and WO_3 on TiO_2[8]), a volumetric free energy term $\Delta G_{vol} \cdot h$ (§4.4.1) should be added. Eq. 30 is then generalized to:

$$\Delta\sigma(h) = \Delta\gamma + E_{dispersion}(h) + E_{short-range}(h) + E_{elec}(h)$$
$$+ (\Delta G_{vol} \cdot h) + \cdots. \quad [31]$$

The term $E_{short-range}(h)$ is the (coupled) short-range interaction of structural and chemical origins (§4.4.2), and $E_{elec}(h)$ is the electrostatic interaction (§4.4.4). For consistence, the author assumes that all the interfacial free energy terms (except for $\Delta G_{vol} \cdot h$) vanish as $h \to +\infty$. The four thickness-dependent free-energy terms in Eq. 31 are discussed further in §4.4.1-4.4.4. The Clarke force-balance model can be regarded as a high-temperature colloid theory.[5]

Force/pressure-balance models have also been developed for SAFs.[6–11] The excess free energy as a function of film thickness h for an SAF has the same generic form as Eq. 31, but
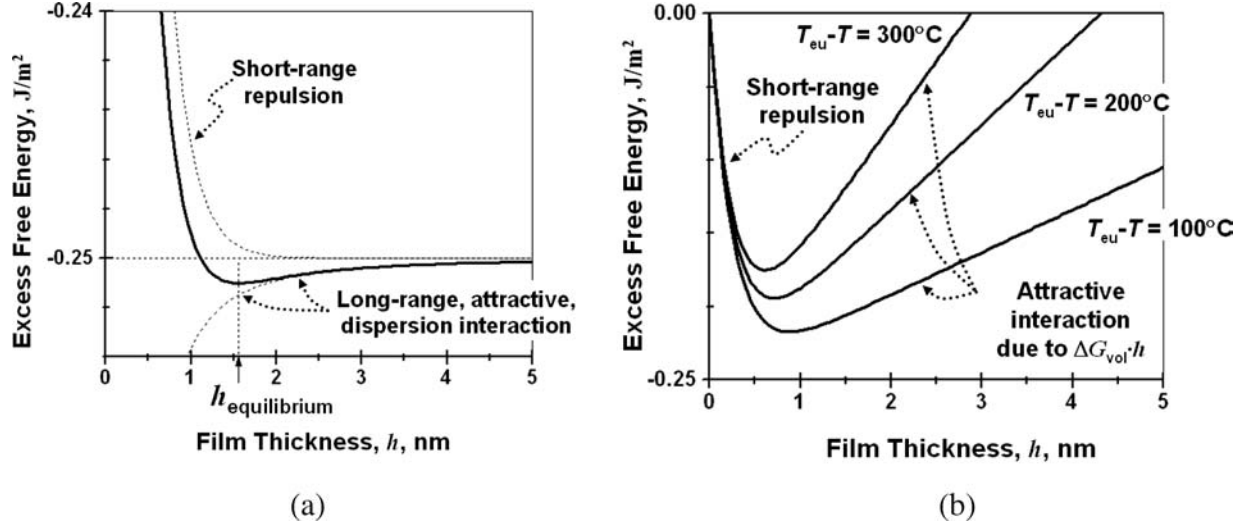
FIG. 19. Computed excess film free energy versus film thickness for Bi_2O_3-enriched SAFs on ZnO.[9] (a) Above the bulk eutectic temperature, the equilibrium thickness corresponds to a balance between an attractive long-range dispersion interaction and a short-range repulsion. (b) Below the bulk eutectic temperature, the attractive interaction due to the volumetric free energy for amorphization limits the film thickness.

the specific interfacial forces/interactions are often different for the configuration of surficial films. Figure 19 illustrates computed excess film free energy versus thickness using estimated parameters for Bi_2O_3-enriched SAFs on ZnO.[9] Above the bulk eutectic temperature, the equilibrium thickness corresponds to a balance between attractive long-range dispersion interaction and a generic, exponentially decaying, short-range repulsion. Below the bulk eutectic temperature, the attractive pressure due to the volumetric free energy for amorphizing the film ($\Delta G_{vol} \cdot h$) is the dominant interaction that limits the film thickness. Furthermore, this force-balance model with the volumetric free energy being the dominant temperature-dependent interaction has been used to compute film thickness versus undercooling for Bi_2O_3-enriched SAFs on ZnO[9]. This quantitative model predicts thicknesses versus temperature for subeutectic SAFs consistent with experimental results (Figure 12). It is therefore concluded that the film becomes thinner with increasing undercooling due to the increasing volumetric free energy for amorphization, wherein an analogy to the premelting theory exists.

Several specific interfacial forces and their roles in determining the stability and thickness of surficial and intergranular films are discussed further in the next section (§4.4). The limitations of the force-balance model are discussed in §4.5.1.

4.4 Interfacial Forces and Their Roles in Film Stability

4.4.1 Volumetric Free-Energy Term

The $\Delta G_{vol} \cdot h$ term is often the dominant attractive interaction in the subeutectic and undersaturation regions that limits the film thickness and controls the thickness dependence on temperature or chemical potential. ΔG_{vol} is defined as the volumetric Gibbs free energy for forming a hypothesized uniform

liquid film from a mixture of the bulk (crystal or liquid) phases. The value of ΔG_{vol} depends on temperature, the composition of the hypothesized uniform liquid film, and the selection of bulk phases from which the film forms. The ΔG_{vol} term can be zero, positive, or negative. It is negative for the case of solid-state amorphization,[209] where spontaneous amorphization occurs from mixing two crystalline phases (which are not in equilibrium with each other) below the bulk solidus temperature when the intermediate compounds cannot nucleate.

If a thermodynamic equilibrium is achieved in a multicomponent system, the interfacial films form from equilibrium bulk phases. In this case, ΔG_{vol} is positive and can be significant when the liquid phase is not a stable bulk phase, for example, in subeutectic or undersaturation regions. It is important to note that in most Si_3N_4-based ceramics, the secondary silicate phase exists as a glassy phase (instead of the equilibrium crystalline phase(s)). In this case, $\Delta G_{vol} \cdot h$ should be calculated with respect to crystalline Si_3N_4 and the metastable glassy silicate phase.

The $\Delta G_{vol} \cdot h$ term is included in diffuse-interface models as part of the integral of the volumetric term in Eqs. 16–18. By definition,

$$\Delta G_{vol} \equiv \Delta f(\eta = 0, c_0), \qquad [32]$$

where c_0 is the solute concentration of the hypothesized uniform film. Thus, if the $\Delta G_{vol} \cdot h$ term is included separately, it should to be subtracted from these equations or any other diffuse-interface equation that is used to calculate the short-range interaction (§4.4.2).

The adoption of the $\Delta G_{vol} \cdot h$ term is conceptually useful for understanding the film stability, but caution should be used in defining this term, because doing so is sometimes subjective.

Because there are through-thickness compositional gradients in the interfacial films, calculation of the ΔG_{vol} term depends on the (somewhat subjective) choice of c_0. Here the author proposes two approaches. First, c_0 can be selected to be the average concentration of the actual films.[9,10] In this approach, ΔG_{vol} can be positive even in the bulk liquid–solid two-phase region, if the film has an average composition distinct from that of the equilibrium bulk liquid. In reality, the film adopts an average composition that minimizes the excess film energy, which is not known *a priori*. Additionally, the average film composition varies with increasing film thickness (approaching that of the bulk liquid as $h \rightarrow +\infty$ in the solid-liquid two-phase region). Thus, ΔG_{vol} is a function of film thickness and it cannot be easily computed. In the second approach, c_0 can be selected to be the concentration that minimizes ΔG_{vol}. Then, the $\Delta G_{vol} \cdot h$ term represents the minimum additional free energy required to form a uniform liquid film of any composition. The rest of the excess volumetric free energy should be considered in the short-range interactions (§4.4.2). In this case, ΔG_{vol} is zero in the solid–liquid coexistence region and positive at subeutectic or undersaturation conditions, and it is independent of the film thickness (h).

For a two-component system, ΔG_{vol} can be computed from the fusion free energy of both end members as well as the enthalpy and entropy of mixing. With known film composition or using the second definition, ΔG_{vol} can be accurately calculated from the standard methods and databases used in CALPHAD. Using the second definition, the $\Delta G_{vol} \cdot h$ term represents a constant attractive pressure in the subsolidus region.

4.4.2 Short-Range Forces of Structural and Chemical Origins

Short-range forces of structural and chemical origins are often the key repulsive forces that stabilize the interfacial films to finite thicknesses (against vanishing) in metals and ceramics. They are related to the non-uniform composition and structure of the nanoscale interfacial film. These short-range forces are alternatively referred as "medium-range" interactions in several articles[9,10] to differentiate them from the Φ's used in Eqs. 13, 14, 17, and 18, which are associated with shorter-range interactions related to terminating surfaces. Because short-range interactions include both gradient terms and volumetric thermodynamic terms in the diffuse-interface theories, they must be defined and computed consistently with the specific definition of $\Delta G_{vol} \cdot h$. With diffuse-interface theories, the author proposes to define the short-range forces as

$$E_{short-range}(h) \equiv \sigma^x - \Delta G_{vol} \cdot h - [\sigma^x - \Delta G_{vol} \cdot h]_{h \rightarrow +\infty}, \quad [33]$$

where σ^x is defined in Eq. 13–18 or 21, or any other apporpriate diffuse-interface intergral. The $-[\sigma^x - \Delta G_{vol} \cdot h]_{h \rightarrow +\infty}$ term, which is a constant of finite value, insures that the short-range energy term vanishes as $h \rightarrow +\infty$.

Clarke derived a steric force in a diffuse-interface theory using only one order parameter and an anti-phase type bound-

ary condition at abrupt film-grain interfaces (Eqs . 21 and 22)[3], which have been further extended to consider compositional gradients[170] or the order parameter at the film/crystal interfaces.[14,121] In the original model for polymeric silicate based IGFs, this steric force represents a structural disjoining force due to the "interference" between the different imposed partial orders at the two crystal-film interfaces during a forced approach of two grains (relating to the distortion of SiO_4^{4-} tetrahedra). A similar simplified diffuse-interface model for repulsive short-range forces in surficial films has also been proposed.[7] These steric type forces can but do not always correspond to the true thermodynamic equilibration, because the boundary conditions at the abrupt film/crystal interfaces may represent metastable situations (particularly for silicate-based IGFs).

In general, short-range forces of structural and chemical origins are perhaps the least understood term. Nonetheless, useful approximation for these short-range forces reduces to

$$E_{short-range}(h) = K_s \cdot e^{-h/\xi}, \quad [34]$$

where ξ is a correlation length that scales with a characteristic molecular bond or chain length. In a "normal" case,

$$K_s = E_{short-range}(0) - E_{short-range}(+\infty) \equiv -\Delta \gamma_{short-range}, \quad [35]$$

where $\Delta \gamma_{short-range}$ is the contribution of the short-range intercation to the $\Delta \gamma$. However, Eq. 35 is not true in some instances (e.g., the steric force) when the exponential approximation is valid only for $h > \xi$. In general, the short-range force can exhibit complex dependence on the film thickness,[121] and it is more complicated in ceramics.

4.4.3 Long-Range Dispersion Forces

Long-range dispersion forces, arising from the electromagnetic interaction of fluctuating dipoles, are assumed to be the major attractive interaction that prevents IGFs from complete wetting in the bulk solid-liquid (or solid-glass) coexistence region in ceramics. Dispersion forces also dominate the interfacial behaviors in ice and other molecular substances, and they appear to have some significance in metals (e.g., in surface and GB premelting of metals[233,234]). Within the continuum and non-retarded limits, the dispersion interaction for a thin film between two dissimilar materials is:

$$E_{dispersion}(h) = \frac{-A_{123}}{12\pi h^2}, \quad [36]$$

where A_{123} is the Hamaker constant for the system "material (1)/film (2)/material (3)," scaling the strength of the dispersion interaction. If material (3) is vapor or air, the configuration represents a surficial film. The dispersion forces for surficial films can be either attractive or repulsive. In-depth discussions of dispersion forces can also be found in books by Israelachvili[63] and Parsegian.[237] For an IGF of a symmetric

flat geometry, the dispersion interaction is then

$$E_{dispersion}(h) = \frac{-A_{121}}{12\pi h^2}, \qquad [37]$$

which is always attractive ($A_{121} > 0$). A_{123} and A_{121} can be computed from the dielectric/optical functions of the associated materials.[63,184] A full spectral method has been developed to accurately compute Hamaker constants.[235] A comprehensive review of London dispersion forces has been written by French.[184] Dispersion forces in IGFs at metal-ceramic interfaces have also been quantified.[139] Recent progresses have also been made to use theoretically computed optical spectra to estimate Hamaker constants and to do layer-by-layer evaluation of dispersion forces for graded films.[184,238]

Several issues need precautions. First, retarded dispersion interactions should be used for large separation:

$$E_{dispersion}^{(retarded)}(h) = \frac{-B_{123}}{3h^3} \qquad (h > \lambda/2\pi), \qquad [38]$$

where λ roughly relates to a characteristic ultraviolet adsorption wavelength. Because the thickness of interfacial films discussed in this article is generally on the order of 1 nm, retardation effects seem unimportant. However, retardation effects can be more complex than suggested by Eq. 38. For example, with complex retardation effects, dispersion forces can produce equilibrium-thickness surficial films without other interfacial forces. This is the reason for incomplete surface premelting of ice (i.e., the formation of equilibrium-thickness surficial water layer on ice at the triple point).[21] French demonstrated that a similar effect can, in principle, produce equilibrium-thickness surficial films in ceramics.[184]

Second, the dispersion energy is divergent at $h = 0$ in Eqs. 36–37, which is a meaningless consequence of the continuum description. This singularity can be eliminated from the model that considers finite atomic separation. For example, Eq. 36 can be modified as

$$E_{dispersion}(h) = \frac{-A_{123}}{12\pi(h^2 + \delta^2)} = -\Delta\gamma_d \cdot \frac{\delta^2}{h^2 + \delta^2}, \qquad [39]$$

where δ is the distance between two atomic planes. $\Delta\gamma_d \equiv A_{123}/(12\pi\delta^2)$ is the contribution of dispersion interaction to $\Delta\gamma$.

Finally, the film compositions (and the associated optical properties) need to be known *a priori* to calculate Hamaker constants. Furthermore, it is assumed in Eqs. 36–39 that the interfacial film is homogenous. Practically, researchers typically use the properties of the bulk phases to compute Hamaker constants. However, the nanoscale interfacial films often exhibit an average composition and structure that markedly differ from the bulk glass or liquid phase, as well as significant through-thickness compositional and structural gradients. Refinements of Eq. 36 and Eq. 37 have been made for graded films.[184,238] Furthermore, a method has been developed to determine *in situ*

the dispersion interactions in IGFs from measurements of local optical properties using spatially-resolved valence electron energy loss spectrum imaging.[239,240]

4.4.4 Electrostatic Interactions

If ionic species are involved, electrostatic interactions can exist and affect the stability of nanoscale interfacial films. If ionic species are present in a quasi-liquid film, some ions will be preferentially adsorbed onto the crystal faces and a counter-ion cloud will form in the film, leading to the formation of an electrical double layer. For IGFs, a screened Coulombic (entropic) interaction arises. For surficial films, the double layer is repelled by an electrostatic image. If a weak overlap approximation ($h > \kappa^{-1}$) holds, the electrical double-layer interaction is given by

$$E_{elec.}(h) = K_e \cdot e^{-\kappa \cdot h} \qquad [40]$$

for IGFs ($h \to 2h$ for image forces in SAFs). κ^{-1} is the Debye length. K_e is a function of the surface potential (ψ_s) or surface charge density (q_s) as well as other parameters [$K_e \approx 2q_s^2/(\kappa\varepsilon\varepsilon_o)$ if $\psi_s < kT/e = 25\ mV$]. The actual electrical double-layer interaction can be more complex than Eq. 40, for example, in the cases when the interfacial films are thin in comparison to the Debye length (κ^{-1}) or if there are multiple ionic species. Rigorous analysis of the general electrical double-layer interactions under different conditions can be found elsewhere.[63]

Possible electrical double-layer contribution to the equilibrium thickness of IGFs in ceramics has been examined by Clarke *et al.*[4] Recently, electrostatic and entropic interactions for glassy IGFs in three configurations, namely ceramic-film-ceramic, ceramic-film-metal, and metal-film-metal, have been investigated.[241] The roles of electrical double-layer interactions in ice premelting with ionic impurities (at surfaces, GBs, and interfaces with inert walls),[21,46,148] prewetting in ionic solutions,[56] and disjoining pressures in thin wetting films[67,242] have also been analyzed, showing ubiquitous importance of these electrostatic forces.

Several issues need to be noted. Steric effects may become important if the ion size is comparable to film thickness.[243] For IGFs and SAFs formed in ionic crystals, in principle counter ions or charged defects can form in both quasi-liquid films and adjacent ionic crystals, leading to more complex electrostatic space charges and interactions.

4.4.5 Other Interfacial Forces

Other interfacial interactions also exist and can be important. Cannon *et al.*[2,5] listed three possible forces at very short range for IGFs in ceramics: namely the residual Coulombic attraction, Born type (orbital overlap) repulsion, and, most importantly, an "adsorption interaction" (i.e., an interaction term relating to "how much of the atomic species from the liquid would remain during a forced approach of two grains,"[2] which is related to

the Π_{ADS} term, or "interactions resulting from solute adsorption on the two grain surfaces," in Clarke's original paper[3]). Cannon also proposed that a strain effect can be important, for example, in delaying the complete wetting of IGFs and SAFs in ceramics.[225] In principle, complex interfacial forces akin to those proposed in colloidal theory,[63] for example, some oscillating forces, can also be present in high-temperature ceramic systems.[2,5] Ferromagnetic interactions[205] and superlattice ordering interactions[206] have also been investigated for the premelting/prewetting IGFs in Fe-Si-Zn.

4.5 Further Discussion

4.5.1 Limitations of Force-Balance Models

Assessing the stability of nanoscale interfacial films via force-balance models is convenient and provides useful physical insight. However, there are limitations. First, the force-balance models are largely based on the assumption of uniform films (except that the effects of gradient energy terms are considered in the approximations for short-range forces or interfacial coefficients), while it is known that significant through-thickness compositional and structural gradients exist in these interfacial films. Second, computing interfacial forces requires knowledge of the film composition and structure, which are typically not known *a priori*. Practically, researchers often use the properties of bulk glass or liquid phases, which differ significantly from those of quasi-liquid interfacial films, to estimate these interfacial forces. This approach often results in errors. On the other hand, force-balance models provide little or no information on how to determine the distinct film composition, structure, and their gradients, which are important for understanding the stability and properties of these films. Finally, interfacial forces are not (completely) independent. In some cases, they can be strongly coupled.

Some of these issues can be addressed in diffuse-interface models, which also need further refinements for yielding quantitative predictions. Some of limitations of force-balance (and diffuse-interface) models discussed above can also be addressed by first-principle or molecular dynamics simulations. The possibility and great potential of conducting realistic first-principle and atomistic simulations for complex interfacial configurations in multicomponent materials have been demonstrated by modeling special GBs in yttrium-doped alumina[244–246] as well as several modeling studies of IGFs discussed in §4.6.

4.5.2 Metastable Equilibration

It is important to recognize that nanoscale interfacial films can form at various types of metastable equilibria. In general, interfacial films in ceramics are more likely to form at metastable equilibria than their counterparts in metals and molecular substances. Within ceramics, silicate-based IGFs are more likely to exhibit metastable equilibria than IGFs that are not based on viscous, polymeric oxides. Additionally, true thermodynamic
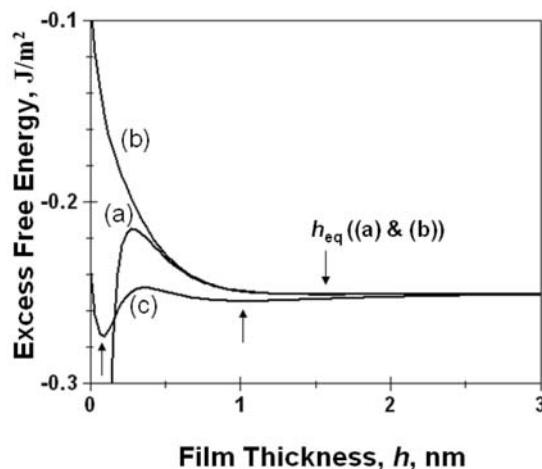

FIG. 20. Excess film energy versus thickness in a force-balance model where the dispersion force is computed based on (a) Eq. 36 and (b) Eq. 39. In this case, the primary minimum in (a) is an artifact due to the singularity associated with the continuum limit. The parameters used for computing plots (a) and (b) represent the SAFs in Bi_2O_3-doped ZnO, where the equilibrium thicknesses correspond to shallow minima (with an expanded view in Figure 19a). (c) Using Eq. 39 where the singularity has been removed, two (primary and metastable) minima can exist but only with a hypothesized strong dispersion force ($A_{123} = 360\ zJ$).

equilibria are more likely to be achieved for SAFs than IGFs that are confined between two crystals.

In colloidal literature, it is often considered that a primary minimum exists at (virtually) zero separation irrespective of the existence of a finite, equilibrium separation. IGFs in ceramics, particularly silicate-based IGFs, may also exhibit both primary and metastable minima. On the other hand, a "primary minimum" always exists in force-balance models if Eq. 36 or Eq. 37 are used, which is a meaningless consequence of the singularity due to the continuum description of dispersion forces. This can be corrected by using Eq. 39 instead of Eq. 36 (Figure 20a versus 20b). Using Eq. 39 where the singularity has been removed, a primary minimum can exist only if the strength of the attractive dispersion force is significant compared with the short-range repulsion (Figure 20c).

A key difference between the current case and that in colloidal systems is that the short-range forces are typically much stronger. Thus, the equilibrium thicknesses of IGFs and SAFs in the solid-liquid coexistence regime typically correspond to rather shallow minima in excess film energy versus thickness (Figures 19a and 20), and the existence of both primary and metastable minima may not be ubiquitous. However, the short-range forces can be more complex than the simple exponentially decaying form, and it can, in principle, produce two minima by itself.[1,121] A more critical assessment is not warranted at this time because these interfacial forces, particularly interactions at

the very short range, are still poorly understood. Although the existence of both primary and metastable minima is possible and has been demonstrated at least for one system (TiO$_2$-SiO$_2$, which exhibits rather high A_{121}),[121] it is likely that the singularity issue associated with the continuum description of dispersion forces, as well as the (perhaps incorrect) analogy to the colloid theory, contributes to a perception of the ubiquitous existence of this primary minimum for IGFs in ceramics. On the other hand, it has been demonstrated that the equilibrium thickness of IGFs in ZnO-Bi$_2$O$_3$ represents a global minimum in excess film energy versus thickness.[16] Additionally, IGFs at the heterointerface in SiO$_2$-TiO$_2$[14] and GBs in Pb$_2$Ru$_2$O$_7$-based thick-film resistors[2,120] also likely represent true thermodynamic equilibria. The extent to which IGFs and SAFs in ceramics (as well as their counterparts in metals and molecular substances) exhibit both primary and metastable minima is still unknown.

In previous discussions, it is largely assumed that a thermodynamic equilibrium has been achieved for bulk phases. This is a not always true. As discussed in §4.4.1, IGFs in Si$_3$N$_4$-SiO$_2$-based ceramics are often in equilibrium with a metastable glassy silicate phase. If a thermodynamic equilibrium has not been achieved for the bulk phases, the volumetric free energy term $\Delta G_{vol} \cdot h$ and the diffuse-interface equations should be adjusted to represent the actual (non-equilibrium) referencing bulk phases.

Finally, an assumption of the force-balance and diffuse-interface models is that the kinetics is fast enough to allow the films to reach equilibrium (or metastable) states, which can often be violated. Both force-balance and diffuse-interface models can be used to assess metastable equilibria (with cautions).

4.5.3 Uniqueness of Silicate-Based Intergranular Films

It should be recognized that silicate-based IGFs are rather unique. SiO$_2$ has the lowest fusion entropy ($<0.2k$ per cation, k being the Boltzmann constant) among all one-component oxides, high viscosity, and a polymeric structure. Silica and silicate are easy to amorphize and difficult to crystallize. Furthermore, silicate-based IGFs are more likely to retain their amorphous structure upon cooling. These properties are consistent with the fact that silicate-based IGFs are the most widely observed nanoscale disordered interfacial films in inorganic materials. It is also possible that the formation mechanism and stability of silicate-based IGFs are unique to some extent. For example, silicate-based films are more likely to form at metastable equilibration and exhibit more significant (if not unique) steric forces. However, the extent to which silicate-based IGFs are unique is still an open question. On the other hand, silicate-based IGFs and disordered interfacial films observed in other inorganic materials have many similarities.

4.5.4 Terminologies: Prewetting and Premelting

In binary systems with deep eutectic reactions, models and experiments illustrated the formation of nanometer-thick, quasi-liquid, intergranular and surficial films, bounded by two different transitions: a drying (i.e., prewetting) transition at a lower temperature and a complete wetting transition at a higher temperature, with the latter occurring either at or above the bulk eutectic temperature. In a broad definition, it is conceptually useful to consider these nanoscale quasi-liquid interfacial films formed before the occurrence of a complete wetting transition as "prewetting films," as originally suggested by Cannon.[2] Somewhat more rigorously, one may argue that only the formation of quasi-liquid films in the regions where bulk liquid is thermodynamically unstable can be considered in the "prewetting region." In the wetting literature, prewetting transitions refer to the wetting transitions when the phase that does the wetting is not yet stable. To the best of the author's knowledge, only "prewetting transitions" have been rigorously defined, and the terms "prewetting regions" or "prewetting films" have been used somewhat vaguely. In the present case, the complete wetting transition can be delayed well above the bulk eutectic temperature (or even completely inhibited) and the properties of the SAFs and IGFs in the solid-liquid coexistence region are not distinctly different from those formed at subsolidus conditions. Thus, an open question is whether the IGFs and SAFs that are in equilibrium with a partial-wetting liquid can be called "prewetting films," which is a somewhat subjective issue of terminology definition.

Premelting is originally defined for pure materials or compounds that melt congruently. If both interfacial adsorption and disordering occur, one can consider that the resultant interfacial films form from coupled interfacial prewetting and premelting transitions. Again, one may argue that only the disordered interfacial films formed below the bulk eutectic or solidus temperatures can be regarded as "premelting" or "premelting/prewetting" films, although the character of nanometer-thick SAFs and IGFs in the solid-liquid coexistence region may not be distinctly different. In principle, prewetting transitions can also occur in binary crystalline systems without interfacial disordering (premelting).

4.5.5 Related Interfacial Phenomena: Roughening and Faceting

Surface and interfaces (including GBs) can also undergo roughening (defaceting) transitions,[247,248] which represent another important class of interfacial transitions. Roughening and premelting are related but different interfacial phenomena. Interplay of roughening, faceting, and disordering can be important in determining the surface behaviors in unary systems[23] as well as the stability of nanoscale interfacial films in multicomponent materials. There is also a "roughening" transition associated with multilayer gas adsorption, below which layering occurs.[57]

4.6 Atomistic and First-Principle Modeling

Other theoretical and simulation approaches, including molecular dynamics,[40,41,160–164,249–251] classical density functional theory, grand-canonical Monte Carlo simulations,[252] and first-principle/ab initio methods,[83,250,253–255] have been used to

study IGFs. A brief overview of these methods can be found in Ref. 1. Molecular dynamics and density functional theory have also been used to study surface premelting. (See reviews by Tartaglino *et al.*[23,24] and references therein.) GB disordering in one-component systems (Si and metals) has been studied extensively using molecular dynamics.[37−42,256,257] Recently, grand-canonical Monte Carlo simulations have been conducted for studying prewetting in binary metallic alloys.[220]

In principle, atomistic and first-principle simulations can advance the understanding of IGFs, SAFs, and related interfacial phenomena at a more fundamental level. Simulations of complex interfacial structures in multicomponent systems are becoming more realistically with rapid advancements in computation power and modeling techniques. Many progresses have been made in modeling GBs and IGFs in the last a few years and there is no doubt that atomistic and first-principle simulations will become increasingly more important in future. An in-depth discussion of atomistic and first-principle simulations is beyond the scope of this review.

5. IMPORTANCE OF DISORDERED INTERFACIAL FILMS IN MATERIALS PROCESSING AND PROPERTIES

5.1 Broad Technological Implications

The existence of disordered interfacial films is technologically important. A rich variety of processing,[13,15,18] electronic,[16,17,120,123] mechanical,[73,76,77,92,98−100,108,109,111,113,122,132,134,150] and catalytic[10,147,185−187] properties of materials have been found to depend on the existence of such thin interfacial films. Selected applications and the technological importance of such films are listed in Table 2 and discussed as follows.

First, the existence, stability, structure, and chemistry of IGFs have significant technological implications for several

TABLE 2

Selected technologically important roles of impurity-based, nanoscale, quasi-liquid, interfacial films. A rough assessment of the level of existing experimental evidence and belief are given in parentheses

High-Temperature Material Properties	• High T strength, fracture behaviors, creep resistance, and oxidation of Si_3N_4- and SiC-based structural ceramics (confirmed)[76,77,91,92,104,105,111,113,150]
	• Superplasticity of ZrO_2-based ceramics (spot evidence)[122]
	• WC-Co composites (spot evidence)[211]
	• Tungsten and other refractory metal alloys (anticipated)[12,13]
Mechanical Properties and Chemical Stability	• Toughness, strength, fatigue, and wear resistance of Si_3N_4-, SiC-, and Al_2O_3-based structural ceramics (confirmed)[73,99,100,108,109,132,134]
	• Liquid metal embrittlement for Ni-Bi, Cu-Bi, and Al-Ga (confirmed)[203,212−214]
	• Corrosion of synroc (spot evidence)[124]
	• GB embrittlement of W-Ni, Cu-Bi, and other systems (anticipated)
Solid-State Activated Sintering	• ZnO-Bi_2O_3(confirmed)[18]
	• W-Ni (confirmed)[12,13,208]
	• CeO_2-CoO (some evidence)[264,280]
	• Other ceramics and refractory metals (anticipated)
	• Ice-impurities (predicted)[20,21]
Rapid GB Migration (Abnormal Grain Growth)	• Al_2O_3-(Y_2O_3+SiO_2) (confirmed)[15]
	• Al-Ga, W-Ni, and ZnO-Bi_2O_3 (some evidence)[260−263]
Electronic and Physical Properties	• Ruthenate-based thick-film resistors (confirmed)[120]
	• ZnO-Bi_2O_3 based varistors (confirmed)[16−18]
	• (Ba, Sr)TiO_3-based sensors and actuators (some evidence)[126−130,259]
	• Thermal conductivity in AlN (spot evidence)[106,107]
	• High-T_c superconductors (spot evidence)[123]
Applications of Nanoscale SAFs of Self-Selecting Thickness and Composition	• Support oxide catalysts (some evidence)[10,147,185−187]
	• Stability of ultra-thin dielectric oxide films (suggested)
	• Shape and growth kinetics of nanoparticles and nanowires (spot evidence)[189−192,265]
	• Low-friction coatings for MEMS and NEMS; bio-active coatings, etc. (suggested)

advanced ceramics. They play critical roles in fracture tough-ness, strength, fatigue, wear and creep resistance, and oxi-dation of Si_3N_4- and SiC-based high-temperature structural ceramics,[73,76,77,91,92,103−105,108,109,111,113,150,251,258] mechanical properties and erosive wear behaviors of Al_2O_3,[132,134] super-plasticity of Y_2O_3-stabilized ZrO_2,[122] tunable conductivities for ruthenate-based thick-film resistors,[120] nonlinear I-V charac-teristics for ZnO-Bi_2O_3-based varistors,[16,17] and functions of (Sr, Ba)TiO_3-based perovskite sensors and actuators.[126−130,259] For example, recent studies have demonstrated that control of IGFs is critical for achieving low-temperature toughness and yet optimizing high-temperature creep resistance for Si_3N_4-based ceramics.[73,99,100] Furthermore, there is spot evidence showing that such IGFs can exist in a host of other ma-terials, from synroc[124] and AlN substrates[106,107] to high T_c superconductors,[123] with attendant detrimental implications on corrosion resistance and thermal or electrical conductivity.

Second, controlling the formation of disordered IGFs is im-portant for improving the properties of certain metallic alloys. The existence of quasi-liquid GB films has been observed or suggested in several metallic alloys that exhibit significant GB embrittlement, such as Cu-Bi and solid-state activated sintered W-Ni alloys. It is highly likely that GB embrittlement in these systems relates to such disordered IGFs and can be improved by optimal fabrication plus heat treatment with predictive knowl-edge of IGF stability. The formation of stable or metastable, nanometer-thick IGFs is important in the process of liquid metal embrittlement for Cu-Bi, Ni-Bi, Al-Ga, and perhaps other systems.[203,212−214] The presence of quasi-liquid GB films in doped tungsten and other refractory alloys should also critically impact their high-temperature mechanical and chemical prop-erties (e.g., creep, oxidation, and corrosion resistance). There is also evidence showing that nanoscale IGFs can form and af-fect the properties of liquid-phase sintered WC-Co metal-matrix composites.[211]

Third, disordered IGFs in ceramics and metals have impor-tant technological roles in materials fabrication because of their unique implications in GB diffusion and migration kinetics. For example, the presence of nanoscale quasi-liquid films at GBs can promote very rapid GB migration and abnormal grain growth. This mechanism has been confirmed for $(Y_2O_3+SiO_2)$-doped Al_2O_3[15] and suggested for Bi_2O_3-doped ZnO,[260] Ni-doped W,[261] and Ga-doped Al.[262] These predictions differ from the predictions of the classical solute-drag model, which is widely accepted, at least for metals.[262] This new mechanism of rapid GB migration associated with the formation of quasi-liquid films will compete with, and sometimes overwhelm, the solute-drag effect (which is undesirable for processing nanocrystalline or fine-grained materials). The competition between prewetting and the solute-drag effects on GB mobility has been quanti-tatively assessed for Ga-doped Al.[263] In another example, the long-sought mechanism for solid-state activated sintering has recently been attributed to rapid diffusion in subeutectic amor-

phous interfacial films,[13,18,264] which is discussed in detail in §5.2.

Finally, understanding and control of SAFs of self-selecting thickness and composition are technologically important, for example, in engineering support oxide catalysts[10,147,185−187] and controlling the stability of ultra-thin dielectric films (e.g., gate oxides). The formation of nanometer-thick SAFs can also play a critical role in determining the form/shape and growth kinetics of nanoparticles and nanowires.[189−192,265]

5.2 An Example: Activated Sintering of Ceramics, Refectory Metals, and Ice

Solid-state activated sintering refers to the phenomenon whereby sintering rates are improved because of solid-state ad-ditives. A well-known example is the accelerated sintering of tungsten that results from the addition of less than 0.5 weight percent of transition metals (e.g., Ni, Pd, Co, Fe, and Pt), which can initiate below 60% of the corresponding bulk solidus or eutectic temperatures.[210,266−279] In general, densification of re-fractory metals is strongly enhanced with the minor addition of a transition metal, typically at a level of about a 1-nm coat-ing on original powder, and further addition beyond the opti-mal level does not generate additional benefits. Enhancement of solid-state GB diffusion must relate to some degree of GB adsorption and disorder, but exactly what controls this behavior is not obvious.

In a classic review article in 1978, Coble and Cannon[272] noted that "in authors' view, the most significant change which have been taken place in recent years regards the finding with respect to densification below the eutectics in numerical systems, no-tably tungsten-carbide:cobalt, tungsten:nickel, . . . " The exact mechanism for enhanced sintering below the eutectic tempera-tures remained a mystery for decades. Recent studies indicated that short-circuit diffusion in nanoscale disordered interfacial films that form at subeutectic conditions is responsible for solid-state activated sintering for ceramics[18,264,280] and refractory metals.[12,13,208]

A study[18] using Bi_2O_3-doped ZnO as a model ceramic sys-tem found that ∼1-nm-thick amorphous films form at GBs and on some free surfaces well below the bulk eutectic temperature, concurrently with the onset of accelerated sintering (Figure 21). Consequently, solid-state activated sintering in this system was attributed to accelerated mass transport through these subeutec-tic, disordered, interfacial films. Recently, a similar activated sintering mechanism due to disordered GBs has been inferred for another ceramic system.[264,280]

W-Ni has been widely used as the model refractory metal system for studying solid-state activated sintering. In a classical model, it is assumed that the secondary crystalline Ni phase com-pletely wets and penetrates along GBs to be an effective sold-state activator.[266] A recent study[12,13,208] showed that although activated sintering starts more than 400°C below the bulk eu-tectic temperature, the nickel-rich crystalline secondary phase
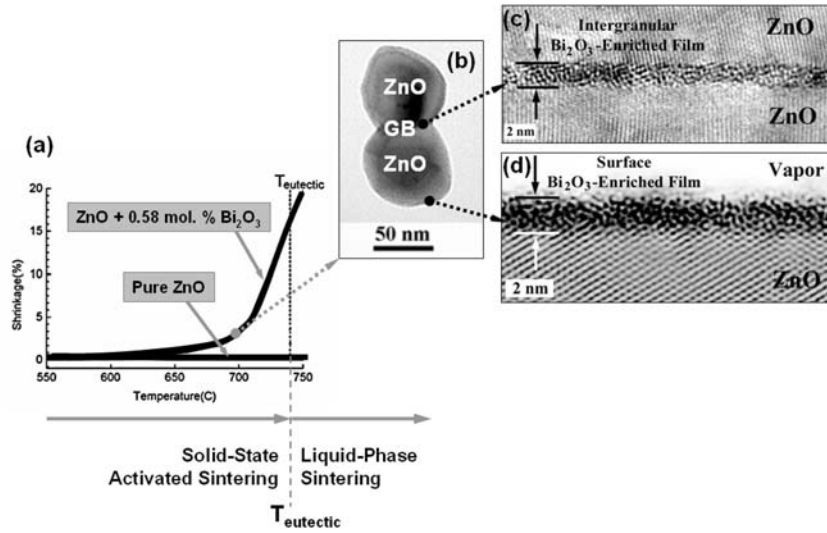
FIG. 21. The solid-state activated sintering of Bi_2O_3-doped ZnO is attributed to enhanced diffusion in subeutectic IGFs. (a) Shrinkage versus temperature for Bi_2O_3-doped ZnO and pure ZnO. (b)–(d) The stabilization of Bi_2O_3-enriched IGFs and SAFs below the bulk eutectic temperature, $T_{eutectic}$, occurring concurrently with the onset of accelerated densification. Adapted from Ref. 18 and Ref. 10 with permission from The American Ceramic Society and American Chemical Society.

does not wet the tungsten GBs in the solid state (Figure 22). Instead, nanometer-thick, nickel-enriched, disordered films formed at GBs well below the bulk eutectic temperature during solid-state sintering (Figure 22). It is therefore concluded that enhanced diffusion in prewetting, instead of wetting, thin intergranular films is responsible for solid-state activated sintering in this model refractory metal system.

FIG. 22. The solid-state activated sintering of Ni-doped W is attributed to enhanced diffusion in disordered, Ni-enriched, IGFs.[12,13,208] (a) Sintered density versus Ni content for specimens sintered at 95°C below the bulk eutectic temperature for 2 h. (b) Scanning electron micrograph shows that the Ni-rich, secondary, crystalline phase does not completely wet GBs. (c) HRTEM images of a subeutectic disordered IGF.

It is interesting to note that ice exhibits similar activated sintering behaviors, presumably due to the enhanced diffusion in the interfacial premelting layers.[20,21] Both formation of premelting layers and densification rates can be significantly enhanced by the presence of minor impurities. This shows the analogous behaviors among ceramics, metals, and molecular substances, although the underlying interfacial forces that control the behaviors are not exactly the same.
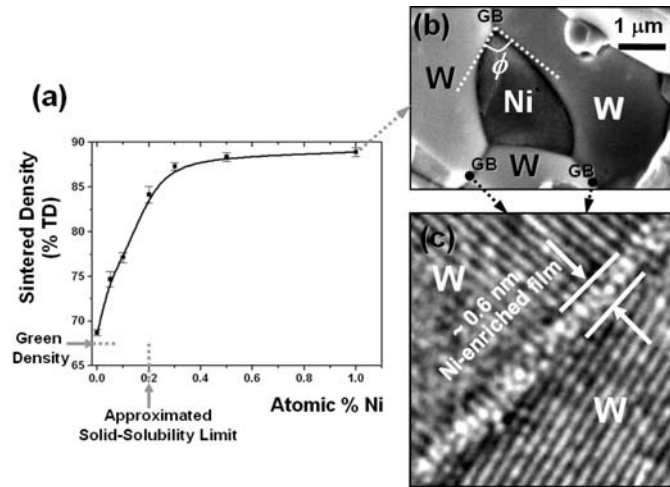
6. SUMMARY, FURTHER ASSESSMENT, AND OUTLOOK

Diffuse-interface and force-balance models have demonstrated the stabilization of nanoscale interfacial films at subeutectic and undersaturation conditions as well as in the solid–liquid coexistence region in multicomponent materials. Both models have their own advantages and shortcomings. Diffuse-interface theories (in the simple form discussed here) do not include long-range dispersion and electrostatic forces, which should be added separately. In general, diffuse-interface models are perhaps not good for systems where long-range forces dominate (or are significant). On the other hand, diffuse-interface models can represent the important through-thickness compositional and structural gradients, which are largely ignored in force-balance models. Force-balance models' merits lie in their simplicity and extendability, as well as the clear physical pictures that they present. The limitations of force-balance models have been discussed in §4.5.1. Most recently, atomistic and first-principle simulations of complex interfacial structures become more realistic, which can be used complementarily to overcome some limitations of force-balance and diffuse-interface models.

Diffuse-interface and force-balance models can illustrate some general trends for the thickness and stability of IGFs in ceramics. However, quantitative and predictive models are still not available. In surface chemistry, it is common to measure the interfacial excess as a function of temperature and chemical potential to critically validate thermodynamic models. Despite wide observations of IGFs in ceramics, experiments that used samples with well-controlled impurities to systematically map film thickness and stability as functions of temperature and bulk composition have rarely been conducted. This is due in part to the difficulty in preparing TEM specimens efficiently. Lack of systematic data and the complex nature of ceramics contribute to the lack of predictive models. Perhaps the best existing data on chemistry dependence of IGF thickness are those measured for the high-purity $\underline{Si}_3\underline{N}_4$-SiO$_2$ with controlled CaO doping (Figure 8a) [75,78,88] and $\underline{Si}_3\underline{N}_4$-SiO$_2$-Al$_2O_3$ with controlled rare-earth oxide doping (Figure 8b),[79] where the observed trends can be qualitatively explained from the force-balance models plus analyses of adsorption of Ca or rare-earth elements on the grain surfaces.[2,5,69,78,79,236] Cannon *et al.*[2,5] assessed the trends of IGF formation and stability in a variety of ceramics based on the strengths of dispersion forces with some limited success, pointed out many discrepancies, and concluded that "these (force-balance models) rationalize some trends, but have little predictive power especially regarding specific impurity effects or films not based on silicates, and lack generality."[2]

Rather systematic data have been collected for Bi$_2$O$_3$-enriched SAFs on ZnO (Figure 12), where the measurements of temperature- and composition-dependent film thickness and stability enable the test of a general thermodynamic model. A quantitative force-balance model[9] with the volumetric free energy for amorphization being the dominating attractive interaction predicted a thickness versus temperature that agrees with experimental measurements in the subeutectic regime, suggesting a clear parallel between the stabilization of subeutectic quasi-liquid SAFs in binary systems and the phenomenon of premelting in unary systems. The importance of the volumetric free-energy term at subeutectic conditions is further illustrated by the observations of nanoscale SAFs in systems with repulsive dispersion forces (§3.3.2). A diffuse-interface model[9] can qualitatively predict all observed trends plus prewetting/drying and wetting transitions, but such a model is yet unable to yield quantitative predictions. For this system, the predicted drying transition has been observed at a lower temperature, but a complete wetting transition, which is expected from the simple coupled surface prewetting and premelting model,[9] is significantly delayed (if not completely inhibited), which is likely a result of the presence of an attractive dispersion force of significant strength. Thus, these critical comparisons between models and experiments suggest the formation of SAFs can be understood from coupled surface prewetting and premelting transitions, while the existence of additional interfacial forces significantly alter the film stability region and affect the film thickness.

Although similar general trends on thickness versus temperature (Figure 16) are expected for IGFs in ceramics, systematic experimental data on any model binary system are yet to be obtained to yield similar critical assessment as those that have been done for SAFs. On the other hand, surficial and intergranular films can be different in some other aspects. In particular, the confinement of IGFs between two crystalline planes results in forced gradients in orientation, which can induce further structural frustration and the increased possibility of forming metastable equilibrium configurations. Consequently, perhaps SAFs are in general more ordered and more easily achieve thermodynamic equilibria. On the other hand, IGF stability and structure could significantly depend on the misorientation. It is relatively easy to conduct critical hot-stage *in situ* experiments on SAFs.

Recently proposed diffuse-interface models of coupled interfacial prewetting and premelting transitions[44,45,167] may provide a framework for understanding IGFs and SAFs in ceramics, but they are not developed specifically to represent the interactions in ceramics. Using $\underline{Si}_3\underline{N}_4$-SiO$_2$ as a model system, effort has been made to include defects and electrostatic interactions that pertain to ceramics in diffuse-interface models,[165,166] but further developments are still needed to yield quantitative agreements. On the other hand, the disordered interfacial films in binary or ternary metals, which have now been directly observed or indirectly suggested for at least three systems ($\underline{Wi}$-Ni, $\underline{Cu}$-Bi, and $\underline{Fe}$-Si-Zn, §3.4), can offer a test bed to critically validate diffuse-interface models, from which additional interfacial interactions can be further added to develop more complex models for SAFs and IGFs in ceramics. To date, $\underline{Cu}$-Bi is the only system for which a complete spectrum of wetting and adsorption events with increasing dopant activity, that is, submonolayer adsorption, multilayer adsorption/prewetting, and complete wetting, has been documented. The basic observations in $\underline{Cu}$-Bi can be explained from a simple prewetting model (Figure 17a). Future research is needed in two areas: (1) systemic characterization of film structure, stability, and thickness as functions of temperature and chemical potentials in several representative model metallic systems with well-controlled experimental conditions; and (2) quantification of the models with thermodynamic data of specific systems. Experimental effort needs to be focused on high-angle, random GBs. Hot-stage HRTEM and other *in situ* experiments will be particularly useful for obtaining reliable data (especially for metals).

If dispersion forces are attractive and the "longest" range interaction in the system, in principle a complete wetting can never occur.[234] The observations of apparently complete GB wetting (wherein the dispersion forces are always attractive for the symmetrical configuration of IGFs) in both ceramics[2,5] and metals[194] indicated that either the dispersion forces are too weak to be significant (against thermal fluctuation or kinetic limitations to equilibration) or there is another unaccounted for long-range interaction. For $\underline{ZnO}$-Bi$_2$O$_3$, the dispersion force is significantly stronger in SAFs than that in IGFs, which appears to be

consistent with the fact that penetration of GBs by a Bi_2O_3-rich liquid has been observed at $\sim 950°C$,[152] but complete wetting on the surface appears to be inhibited (with a residual contact angle of $\sim 5°$).[180] If dispersion forces are indeed the major reason for delaying or inhibiting complete wetting, complete wetting should occur for SAFs in systems with repulsive dispersion forces at or above the bulk eutectic temperature; a future critical experiment to clarify this point is needed.

Although the focus of this assessment article is on the general trends in the stability of nanoscale interfacial films and thermodynamic/phenomenological models, it is important to note that recent significant advancements in molecular dynamics, grand-canonical Monte Carlo simulations, and first-principle calculations, in conjunction with parallel advancements in HAADF-STEM and other advanced experimental techniques, offer alternative and complementary routes to understand the detailed, atomic-level interfacial structures, and to relate them with materials processing or properties. Most efforts in this regard are for specific systems (instead of predicting general trends). Rapid and significant progresses in these areas are anticipated.

The observations of nanoscale interfacial films in a variety of materials and configurations are summarized in Table 1. In general, these interface-stabilized disordered films exhibit the following distinct characteristics: (1) self-selecting (equilibrium) thicknesses on the order of one nanometer; (2) structures and compositions that markedly differ from the associated bulk liquid or glass phases (which are not stable as bulk phases in many instances, for example, with compositions sitting in a bulk miscibility gap); and (3) unique kinetic/processing, mechanical, and physical properties. Thus, the existence and stability of such disordered interfacial films have important technological implications; some have been revealed (§5, Table 2) and many more need to be explored.

A related long-term scientific goal is to develop interfacial phase diagrams to quantitatively represent the unique structure-composition stability regimes for surfaces, GBs, and heterophase interfaces. This is an essential component for achieving the predicable fabrication of materials by design, which involves the following concepts: guided by quantitative interfacial phase diagrams, composition and processing recipes can be designed to utilize the most appropriate GB or surface structures to achieve optimal microstructures; furthermore, heat treatment recipes can be devised to optimize GB or surface structures for the desired material properties. Such concepts are especially important for designing and fabricating nanostructured materials. The need for the development of such interfacial phase diagrams is demonstrated by recent observations in a model ceramic system, ZnO-Bi_2O_3, and a model metallic system, W-Ni, as well as the parallel phenomena in the ice-impurity system, wherein nanoscale quasi-liquid interfacial films were found to form at thermodynamic equilibria well below the bulk eutectic or solidus temperatures and play significant roles in sintering, creep, and other material properties.

7. CONCLUSIONS

The observations of equilibrium-thickness intergranular films in ceramic materials, their free surface counterparts, that is, surficial amorphous films, and their metallic counterparts are reviewed, together with several classes of related wetting and adsorption phenomena in simpler systems. These interfacial films have a self-selecting (equilibrium) thickness on the order of one nanometer, which can be altered by changing the equilibrated temperature and bulk chemical potentials, and they exhibit distinct composition, structure, and properties. Quasi-liquid surficial and intergranular films can be stabilized at subeutectic or undersaturation conditions, where an analogy to the theory of premelting or prewetting can be made. These quasi-liquid films can also persist into the solid–liquid two-phase regime, in equilibrium with a partial-wetting bulk liquid, where phenomenological similarities to frustrated-complete wetting exist.

These IGFs and SAFs can alternatively be understood to be quasi-liquid layers that adopt equilibrium thicknesses in response to a balance among several attractive and repulsive interfacial forces or disordered multilayer adsorbates with compositions and interfacial excesses set by the bulk chemical potentials. Correspondingly, a unifying thermodynamic framework has been developed to treat these interface-stabilized films with force-balance and diffuse-interface models. The formation and stabilization of these intergranular and surficial films in ceramics, metals, and other materials can be understood from coupled interfacial premelting and prewetting transitions in models that are extended from the Cahn critical point wetting theory. Furthermore, other interfacial interactions that are not considered in diffuse-interface theories, for example, dispersion and electrostatic forces, can significantly alter the film stability region and modify the film thickness and composition.

Quantitative thermodynamic models that can be used to predict the general trends in film stability are needed to be developed. Recent progresses in atomistic and first-principle simulations, together with parallel advancements in HAADF-STEM and other advanced experimental techniques, provide a complementary research direction to investigate the detailed interfacial structures for specific materials. Major effort is also needed to further explore the technological importance of these disordered interfacial films.

REFERENCES

1. A. Subramaniam, C. T. Koch, R. M. Cannon, and M. Rühle, Intergranular glassy films: An overview, *Materials Science and Engineering A* **422**, 3 (2006).

2. R. M. Cannon, M. Rühle, M. J. Hoffmann, R. H. French, H. Gu, A. P. Tomsia, and E. Saiz, Adsorption and wetting mechanisms at ceramic grain boundaries, Ceramic Transactions, Vol. 118, *Grain Boundary Engineering in Ceramics*, T. Sakuma and Y. Ikuhara, Eds., 427 (2000).

3. D. R. Clarke, On the equilibrium thickness of intergranular glass phases in ceramic materials, *Journal of the American Ceramic Society* **70**, 15 (1987).

4. D. R. Clarke, T. M. Shaw, A. P. Philipse, and R. G. Horn, Possible electrical double-layer contribution to the equilibrium thickness of intergranular glass films in polycrystalline ceramics, *Journal of the American Ceramic Society* **76**, 1201 (1993).

5. Cannon, R. M. and L. Esposito, High temperature colloidal behavior: Particles in liquid silicates, *Zeitschrift Fur Metallkunde* **90**, 1002 (1999).

6. J. Luo, Existence and stability of nanometer-thick disordered films on oxide surfaces, Ph.D. thesis, M.I.T., Cambridge, MA (2001).

7. J. Luo and Y.-M. Chiang, Equilibrium-thickness amorphous films on {11-20} surfaces of Bi$_2$O$_3$-doped ZnO, *Journal of the European Ceramic Society* **19**, 697 (1999).

8. J. Luo and Y.-M. Chiang, Existence and stability of nanometer-thick disordered films on oxide surfaces, *Acta Materialia* **48**, 4501 (2000).

9. J. Luo, M. Tang, R. M. Cannon, W. C. Carter, and Y.-M. Chiang, Pressure-balance and diffuse-interface models for surficial amorphous films, *Materials Science and Engineering A* **422**, 19 (2006).

10. J. Luo, Y.-M. Chiang, and R. M. Cannon, Nanometer-thick surficial films in oxides as a case of prewetting, *Langmuir* **21**, 7358 (2005).

11. J. Luo, Y.-M. Chiang, and R. M. Cannon, Inorganic nanoscale surficial films of self-selecting thickness, in *Bottom-up nanofabrication: Superamolecules, self-assemblies and organized films*, H. S. Nalwa and K. Ariga, Eds., American Scientific Publishers, Valencia, California, in press.

12. J. Luo, V. K. Gupta, D. H. Yoon, and H. M. Meyer, Segregation-induced grain boundary premelting in nickel-doped tungsten, *Applied Physics Letters* **87**, 231902 (2005).

13. V. K. Gupta, D. H. Yoon, Meyer H. M. III, and J. Luo, Thin intergranular films and solid-state activated sintering in nickel-doped tungsten, *Acta Materialia*, **55**, 3131–3142 (2007).

14. H. D. Ackler and Y.-M. Chiang, Model experiment on thermodynamic stability of retained intergranular amorphous films, *Journal of the American Ceramic Society* **80**, 1893 (1997).

15. I. MacLaren, R. M. Cannon, M. A. Gülgün, R. Voytovych, N. P. Pogrion, C. Scheu, U. Täffner, and M. Rühle, Abnormal grain growth in alumina: Synergistic effects of yttria and silica, *Journal of the American Ceramic Society* **86**, 650 (2003).

16. H. Wang and Y.-M. Chiang, Thermodynamic stability of intergranular amorphous films in bismuth-doped zinc oxide, *Journal of the American Ceramic Society* **81**, 89 (1998).

17. Y.-M. Chiang, H. Wang, and J.-R. Lee, HREM and STEM of intergranular films at zinc oxide varistor grain boundaries, *Journal of Microscopy* **191**, 275 (1998).

18. J. Luo, H. Wang, and Y.-M. Chiang, Origin of solid state activated sintering in Bi2O3-doped ZnO, *Journal of the American Ceramic Society* **82**, 916 (1999).

19. J. F. van der Veen, B. Pluis, and A. W. Denier, Surface melting, in *Chemistry and Physics of Solid Surfaces*, Vol. 7, R. Vanselow and R. F. Howe, Eds., Berlin Springer, 1988 (455).

20. J. G. Dash, H. Fu, and J. S. Wettlaufer, The premelting of ice and its environmental consequences, *Reports on Progress in Physics* **58**, 115 (1995).

21. J. G. Dash, A. M. Rempel, and J. S. Wettlaufer, The physics of premelted ice and its geophysical consequences, *Reviews of Modern Physics* **78**, 695 (2006).

22. J. G. Dash, Surface melting, *Contemporary Physics* **30**, 89 (1989).

23. U. Tartagglino, Zykova-Timan, T., F. Ercolessi, and E. Tosatti, Melting and nonmelting of solid surface and nanosystems, *Physics Reports* **411**, 291 (2005).

24. U. Tartagglino, T. Zykova-Timan, F. Ercolessi, and E. Tosatti, Material surfaces and nanosystems close to the melting temperature, *Journal of Materials Science* **40**, 2141 (2005).

25. J. W. Cahn, Critical point wetting, *Journal of Chemical Physics* **66**, 3667 (1977).

26. H. Nakanishi and M. E. Fisher, Multicriticality of wetting, prewetting, and surface transitions, *Physical Review Letters* **49**, 1565 (1982).

27. C. Ebner and W. F. Saam, New phase-transition phenomena in thin argon films, *Physical Review Letters* **38**, 1486 (1977).

28. P. G. de Gennes, Wetting: Statics and dynamics, *Reviews of Modern Physics* **57**, 827 (1985).

29. D. Bonn and D. Ross, Wetting transitions, *Reports on Progress in Physics* **64**, 1085 (2001).

30. Frenken, J. W. M., P. M. Maree, and J. F. van der Veen, Observation of surface initiated melting, *Physical Review B* **34**, 7506, 1986.

31. J. W. M. Frenken and J. F. van der Veen, Observation of surface melting, *Physical Review Letters* **54**, 134 (1985).

32. D.-M. Zhu and J. G. Dash, Surface melting of neon and argon films: Profile of the crystal-melt interface, *Physical Review Letters* **60**, 432 (1988).

33. R. Rosenberg, Why is ice slippery? *Physics Today*, 58(12), 50 (2005).

34. B. Pluis, D. A. W. van der Gon, J. W. M. Frenken, and J. F. van der Veen, Crystal-face dependence of surface melting, *Physical Review Letters* **59**, 2678 (1987).

35. B. Pluis, A. W. D. van der Gon, J. F. van der Veen, and A. J. Riemersma, Surface-induced melting and freezing. I.

Medium-energy ion scattering investigation of the melting of Pb(hkl) crystal faces, *Surface Science* **239**, 265 (1990).

36. O. G. Shpyrko, R. Streitel, Balagurusamy, V. S. K., A. Y. Grigoriev, M. Deutsch, B. M. Ocko, M. Meron, B. Lin, and P. S. Pershan, Surface crystallization in a liquid AuSi alloy *Science* **313**, 77 (2006).

37. P. Keblinski, D. Wolf, S. R. Phillpot, and H. Gleiter, Self diffusion in high-angle fcc metal grain boundaries by molecular dynamics simulation, *Philosophical Magazine A* **79**, 2735 (1999).

38. D. Wolf, High-temperature structure and properties of grain boundaries: Long-range vs. short-range structural effects, *Current Opinion in Solid State and Material Sciences* **5**, 435 (2001).

39. A. Suzuki and Y. Mishin, Atomic mechanisms of grain boundary diffusion: Low versus high temperatures, *Journal of Materials Science* **40**, 3155 (2005).

40. P. Keblinski, S. R. Phillpot, and D. Wolf, Thermodynamic criterion for the stability of amorphous intergranular films in covalent materials, *Physical Review Letters* **77**, 2965 (1996).

41. P. Keblinski, S. R. Phillpot, D. Wolf, and H. Gleiter, On the thermodynamic stability of amorphous intergranular films in covalent materials, *Journal of the American Ceramic Society*, 80 717 (1997).

42. P. Keblinski, S. R. Phillpot, D. Wolf, and H. Gleiter, Thermodynamically stable amorphous intergranular films in nanocrystalline silicon, *Physics Letters A* **226**, 205 (1997).

43. Lobkovsky, A. E. and J. A. Warren, Phase field model of premelting of grain boundaries, *Physica D* **164**, 202 (2002).

44. M. Tang, W. C. Carter, and R. M. Cannon, Diffuse interface model for structural transitions of grain boundaries, *Physical Review B* **73**, 024102 (2006).

45. M. Tang, W. C. Carter, and R. M. Cannon, Grain boundary order-disorder transitions, *Journal of Materials Science* **41**, 7691 (2006).

46. L. Benatov and J. S. Wettlaufer, Abrupt grain boundary melting in ice, *Physical Review E* **70**, 061606 (2004).

47. T. E. Hsieh and R. W. Balluffi, Experimental study of grain boundary melting in aluminum, *Acta Metallurgica* **37**, 1637 (1989).

48. A. M. Alsayed, M. F. Islam, J. Zhang, P. J. Collings, and A. G. Yodh, Premelting at defects within bulk colloidal crystals, *Science* **309**, 1207 (2005).

49. S. Engemann, H. Reichert, H. Dosch, J. Bilgram, V. Honkimaki, and A. Snigirev, Interfacial melting of ice in contact with SiO2, *Physical Review Letters* **92**, 205701 (2004).

50. U. Dahmen, S. Hagege, F. Faudot, T. Radetic, and E. Johnson, Observations of interface premelting at grain-boundary precipitates of Pb in Al, *Philosophical Magazine* **84**, 2651, 2004.

51. H. Kellay, D. Bonn, and J. Meunier, Prewetting in a binary liquid mixture, *Physical Review Letters* **71**, 2607 (1993).

52. J. W. Schmidt and M. R. Moldover, A search for the prewetting line, *The Journal of Chemical Physics* **84**, 4563 (1986).

53. D. Chatain and P. Wynblatt, Experimental evidence for a wetting transition in liquid Ga-Pb alloys, *Surface Science* **345**, 85 (1996).

54. P. Wynblatt and D. Chatain, Wetting and prewetting transitions in Ga-Pb alloys, *Berichte Der Bunsen-Gesellschaft-Physical Chemistry Chemical Physics* **102**, 1142 (1998).

55. C. Ebner and W. F. Saam, New reentrant wetting phenomena and critical behavior near bulk critical points, *Physical Review Letters* **58**, 588 (1987).

56. N. A. Denesyuk and J. P. Hansen, Wetting transitions of ionic solutions, *The Journal of Chemical Physics* **121**, 3613 (2004).

57. R. Pandit, M. Schick, and M. Wortis, Systematics of multilayer adsorption phenomena on attractive substrates, *Physical Review B* **26**, 5112 (1982).

58. Y.-M. Chiang, A. F. Henriksen, W. D. Kingery, and D. Finello, Characterization of grain boundary segregation in MgO, *Journal of the American Ceramic Society* **64**, 383 (1981).

59. L. S. Chang, E. Rabkin, B. B. Straumal, B. Baretzky, and W. Gust, Thermodynamic aspects of the grain boundary segregation in Cu(Bi) alloys *Acta Materialia* **47**, 4041 (1999).

60. P. Lejcek and S. Hofmann, Thermodynamics and structural aspects of grain boundary segregation, *Critical Reviews in Solid State and Material Sciences* **20**, 1 (1995).

61. E. Bertrand, H. Dobbs, D. Broseta, J. Indekeu, D. Bonn, and J. Meunier, First-order and critical wetting of alkanes on water, *Physical Review Letters* **85**, 1282 (2000).

62. F. Brochard-Wyart, di Meglio, J.-M., Quéré, D., and de P. G. Gennes, Spreading of nonvolatile liquids in a continuum picture, *Langmuir* **7**, 335 (1991).

63. J. N. Israelachvili, *Intermolecular and Surface Forces*, 4th ed., Academic Press Limited, London (1994).

64. J. Moon, S. Garoff, P. Wynblatt, and R. Suter, Pseudopartial wetting and precursor film growth in immiscible metal systems, *Langmuir* **20**, 402 (2004).

65. J. Moon, J. Lowekamp, P. Wynblatt, G. Stephen, and R. M. Suter, Effects of concentration dependent diffusivity on the growth of precursing films of Pb on Cu(1 1 1), *Surface Science* **488**, 73 (2001).

66. J. Moon, J. Yoon, P. Wynblatt, S. Garoff, and R. M. Suter, Simulation of spreading of precursing ag films on Ni(1 0 0), *Computational Materials Science* **25**, 503 (2002).

67. N. V. Churaev, Surface forces in wetting films, *Advances in Colloid and Interface Science* **103**, 197 (2003).

68. L. K. L. Falk, Imaging and microanalysis of liquid phase sintered silicon-based ceramic microstructures, *Journal of Materials Science* **39**, 6655 (2004).

69. H. Gu, R. M. Cannon, I. Tanaka, and M. Rühle, Calcia partition in phase-separated intergranular glass and interfaces in doped silicon nitride produced by hot isostatic pressing, *Materials Science and Engineering A* **422**, 51 (2006).

70. A. Ziegler, C. Kisielowski, M. J. Hoffmann, and R. O. Ritchie, Atomic resolution transmission electron microscopy of the intergranular structure of a Y203-containing silicon nitride ceramic, *Journal of the American Ceramic Society* **86**, 1777 (2003).

71. H.-J. Kleebe, Structure and chemistry of interfaces in Si_3N_4 materials studied by transmission electron microscopy, *Journal of the Ceramic Society of Japan* **105**, 453 (1997).

72. H.-J. Kleebe, M. K. Cinibulk, R. M. Cannon, and M. Rühle, Statistical analysis of the intergranular film thickness in silicon nitride ceramics, *Journal of the American Ceramic Society* **76**, 1969 (1993).

73. P. F. Becher, G. S. Painter, E. Y. Sun, C. H. Hsueh, and M. J. Lance, The importance of amorphous intergranular films in self-reinforced Si3N4 ceramics, *Acta Materialia* **48**, 4493 (2000).

74. H. Gu, R. M. Cannon, and M. Rühle, Composition and chemical width of ultra-thin amorphous films at grain boundaries in silicon nitride, *Journal of Materials Research* **13**, 476 (1998).

75. H. Gu, X. Pan, R. M. Cannon, and M. Rühle, Dopant distribution in grain-boundary films in calcia-doped silicon nitride ceramics, *Journal of the American Ceramic Society* **81**, 3125 (1998).

76. Q. Jin, D. S. Wilkinson, and G. C. Weatherly, High-resolution electron microscopy investigation of viscous flow creep in a high-purity silicon nitride, *Journal of the American Ceramic Society* **82**, 1492 (1999).

77. I. Tanaka, K. Igashira, T. Okamoto, K. Niihara, and R. M. Cannon, High-temperature fracture mechanism of low-Ca doped silicon nitride, *Journal of the American Ceramic Society* **78**, 673 (1995).

78. I. Tanaka, Kleebe, H.-J., M. K. Cinibulk, J. Bruley, D. R. Clarke, and M. Rühle, Calcium concentration dependence of the intergranular film thickness in silicon nitride, *Journal of the American Ceramic Society* **77**, 911 (1994).

79. C.-M. Wang, X. Pan, M. J. Hoffmann, R. M. Cannon, and M. Rühle, Grain boundary films in rare-earth-glass-based silicon nitride, *Journal of the American Ceramic Society* **79**, 788 (1996).

80. G. B. Winkelman, C. Dwyer, T. S. Hudson, D. Nguyen-Manh, M. Döblinger, R. L. Satet, M. J. Hoffmann, and Cockayne, D. J. H., Arrangement of rare-earth elements at prismatic grain boundaries in silicon nitride, *Philosophical Magazine Letters* **84**, 755 (2004).

81. G. B. Winkelman, C. Dwyer, T. S. Hudson, D. Nguyen-Manh, M. Döblinger, R. L. Satet, M. J. Hoffmann, and D. J. H. Cockayne, Three-dimensional organization of rare-earth atoms at grain boundaries in silicon nitride, *Applied Physics Letters* **87**, 061911 (2005).

82. M. Yoshiya, H. Adachi, and I. Tanaka, Interpretation of Si-l2,3 edge electron energy loss near edge structures (ELNES) from intergranular glassy film of Si3N4 ceramics, *Journal of the American Ceramic Society* **82**, 3231 (1999).

83. N. Shibata, S. J. Pennycook, T. R. Gosnell, G. S. Painter, W. A. Shelton, and P. F. Becher, Observation of rare-earth segregation in silicon nitride ceramics at subnanometre dimensions, *Nature* **428**, 730 (2004).

84. A. Ziegler, J. C. Idrobo, M. K. Cinibulk, C. Kisielowski, N. D. Browning, and R. O. Ritchie, Interface structure and atomic bonding characteristics in silicon nitride ceramics, *Science* **306**, 1768 (2004).

85. H.-J. Kleebe, M. J. Hoffman, and M. Rühle, Influence of secondary phase chemistry on grain boundary film thickness in silicon nitride, *Zeitschrift Fur Metallkunde* **83**, 610 (1992).

86. M. K. Cinibulk and H.-J. Kleebe, Grain-boundary films in silicon nitride ceramic at high temperature, in *Ceramic Microstructure: Control at the Atomic Level,* A. P. Tomsia and A. Glaeser, Eds., Plenum, New York, 1998 (123).

87. M. K. Cinibulk, H.-J. Kleebe, and M. Rühle, Quantitative comparison of TEM techniques for determining amorphous intergranular film thickness, *Journal of the American Ceramic Society* **76**, 426 (1993).

88. X. Pan, H. Gu, R. van Weeren, S. C. Danforth, R. M. Cannon, and M. Rühle, Grain-boundary microstructure and chemistry of a hot isostatically pressed high-purity silicon nitride, *Journal of the American Ceramic Society* **79**, 2313 (1996).

89. D. R. Clarke and G. Thomas, Grain boundary phases in a hot-pressed MgO fluxed silicon nitride, *Journal of the American Ceramic Society* **60**, 491 (1977).

90. M. K. Cinibulk, H.-J. Kleebe, G. A. Schneider, and M. Rühle, Amorphous intergranular films in silicon nitride ceram-

ics quenched from high temperatures, *Journal of the American Ceramic Society* **76**, 2801 (1993).

91. M. K. Cinibulk and H.-J. Kleebe, Effects of oxidation on intergranular phases in silicon nitride ceramics, *Journal of Materials Science* **28**, 5775 (1993).

92. G. Pezzotti, T. Wakasugi, T. Nishida, R. Ota, Kleebe, H.-J., and K. Ota, Chemistry and inherent viscosity of glasses segregated at grain boundaries of silicon nitride and silicon carbide ceramics, *Journal of Non-Crystalline Solids* **271**, 79 (2000).

93. J. S. Vetrano, Kleebe, H.-J., E. Hampp, M. J. Hoffmann, M. Rühle, and R. M. Cannon, Yb2O3-fluxed sintered silicon nitride, *Journal of Materials Science* **28**, 3529 (1993).

94. H.-J. Kleebe, J. Bruley, and M. Rühle, HREM and AEM studies of Yb2O3-fluxed silicon nitride ceramics with and without CaO addition, *Journal of the European Ceramic Society* **14**, 1 (1994).

95. H.-J. Kleebe, High-resolution electron microscopy studies on Si3N4 ceramics, *Key Engineering Materials*, 89–91, 339 (1994).

96. H.-J. Kleebe, G. Pezzotti, and T. Nishida, Transmission electron microscopy characterization of a fluorine-doped Si3N4, *Journal of Materials Science Letters* **14**, 1668 (1995).

97. H.-J. Kleebe, G. Pezzotti, and T. Nishida, Interface structure of a chlorine-doped Si3N4 studied by high-resolution transmission electron microscopy, *Journal of Materials Science Letters* **16**, 453 (1997).

98. P. F. Becher and M. K. Ferber, Temperature-dependent viscosity of SiREAl-based glasses as a function of N:O and re:Al ratios (re = La, Gd, Y, and Lu), *Journal of the American Ceramic Society* **87**, 1274 (2004).

99. P. F. Becher, G. S. Painter, M. J. Lance, S. Li, and Y. Ikuhara, Direct observations of debonding of reinforcing grains in silicon nitride ceramics sintered with yttria plus alumina additives, *Journal of the American Ceramic Society* **88**, 1222 (2005).

100. P. F. Becher, E. Y. Sun, C. H. Hsueh, G. S. Painter, and K. L. More, Role of intergranular films in toughened ceramics, *Key Engineering Materials*, **175–176**, 97 (2000).

101. S. Bhattacharyya, A. Subramaniam, C. T. Koch, R. M. Cannon, and M. Rühle, The evolution of amorphous grain boundaries during in-situ heating experiments in Lu-mg doped Si3N4, *Materials Science and Engineering A* **422**, 92 (2006).

102. S. Bhattacharyya, A. Subramaniam, C. T. Koch, and M. Rühle, Aspects regarding measurement of thickness of intergranular glassy films, *Journal of Microscopy-Oxford* **221**, 46 (2006).

103. M. Doblinger, G. B. Winkelman, C. Dwyer, C. Marsh, A. I. Kirkland, Cockayne, D. J. H., and M. J. Hoffmann, Structural and compositional comparison of Si3N4 ceramics with different fracture modes, *Acta Materialia* **54**, 1949 (2006).

104. S. Guo, N. Hirosaki, Y. Yamamoto, T. Nishimura, Y. Kitami, and M. Mitomo, Microstructural characterization and high-temperature strength of hot-pressed silicon nitride ceramics with Lu2O3 additives, *Philosophical Magazine Letters* **83**, 357, 2003.

105. S. Stemmer, G. Roebben, and van der O. Biest, Evolution of grain boundary films in liquid phase sintered silicon nitride during high-temperature testing, *Acta Materialia* **46**, 5599 (1998).

106. H. Nakano, K. Watari, and K. Urabe, Grain boundary phase in AlN ceramics fired under reducing n2atmosphere with carbon, *Journal of the European Ceramic Society* **23**, 1761, 2003.

107. D. L. Callahan and G. Thomas, Impurity distribution in polycrystalline aluminum nitride ceramics *Journal of the American Ceramic Society* **73**, 2167 (1990).

108. H.-J. Kleebe, SiC and Si3N4 materials with improved fracture resistance, *Journal of the European Ceramic Society* **10**, 151 (1992).

109. D. Chen, X.-F. Zhang, and R. O. Ritchie, Effects of grain-boundary structure on the strength, toughness, and cyclic-fatigue properties of a monolithic silicon carbide, *Journal of the American Ceramic Society* **83**, 2079 (2000).

110. E. Volz, A. Roosen, S.-C. Wang, and W.-C. J. Wei, Formation of intergranular amorphous films during the microstructural development of liquid phase sintered silicon carbide ceramics, *Journal of Materials Science* **39**, 4095 (2004).

111. D. Chen, M. E. Sixta, Zhang, X.-F., L. C. DeJonghe, and R. O. Ritchie, Role of the grain boundary phase on the elevated-temperature strength, toughness, fatigue and creep resistance of silicon carbide sintered with Al, b, and c, *Acta Materialia* **48**, 4599 (2000).

112. F. Siegelin, Kleebe, H.-J., and L. S. Sigl, Interface characteristics affecting electrical properties of Y-doped SiC, *Journal of Materials Research* **18**, 2608 (2003).

113. G. Pezzotti, Kleebe, H.-J., and K. Ota, Grain-boundary viscosity of polycrystalline silicon carbides, *Journal of the American Ceramic Society* **81**, 3293 (1998).

114. L. K. L. Falk, Microstructural development during liquid phase sintering of silicon carbide ceramics, *Journal of the European Ceramic Society* **17**, 983 (1997).

115. X. F. Zhang and L. C. De Jonghe, Thermal modification of microstructures and grain boundaries in silicon carbide, *Journal of Materials Research* **18**, 2807 (2003).

116. X. F. Zhang and R. M. Wang, Short-range order in nanoscale amorphous intergranular films in liquid-phase sintered silicon carbide, *Applied Physics Letters* **89**, 211902 (2006).

117. X. F. Zhang and L. C. De Jonghe, Aluminum-containing intergranular phases in hot-pressed silicon carbide, *Journal of Materials Research* **19**, 2510 (2004).

118. R. Brydson, S.-C. Chen, F. L. Riley, S. J. Milne, X. Pan, and M. Rühle, Microstructure and chemistry of intergranular glassy films in liquid-phase-sintered alumina, *Journal of the American Ceramic Society* **81**, 369 (1998).

119. T. M. Shaw and P. R. Duncombe, Forces between aluminum oxide grains in a silicate melt and their effect on grain boundary wetting, *Journal of the American Ceramic Society* **74**, 2495 (1991).

120. Y.-M. Chiang, L. A. Silverman, R. H. French, and R. M. Cannon, Thin glass film between ultrafine conductor particles in thick-film resistors, *Journal of the American Ceramic Society* **77**, 143 (1994).

121. H. D. Ackler and Y.-M. Chiang, Effect of initial microstructure on final intergranular phase distribution in liquid phase sintered ceramics, *Journal of the American Ceramic Society* **82**, 183 (1999).

122. S. Primdahl, A. Tholen, and T. G. Langdon, Microstructural examination of a superplastic yttria-stabilized zirconia: Implications for the superplasticity mechanism, *Acta Metallurgica et Materialia* **43**, 1211 (1995).

123. R. Ramesh, S. M. Green, and G. Thomas, Microstructure property relations in the Bi(Pb)-Sr-Ca-Cu-O ceramic superconductors, in *Studies of High Temperature Superconductors: Advances in Research and Applications*, Vol. 5, A. Narlikar, Ed., Nova Science Publ., Commack, NY, 1990 (363).

124. J. A. Cooper, D. R. Cousens, S. Myhra, and R. S. C. Smart, Intergranular films and pore surfaces in synroc c: Structure, composition, dissolution characteristics, *Journal of the American Ceramic Society* **69**, 347 (1986).

125. S. Kanzaki, T. Kumazawa, J. Asaumi, O. Abe, and H. Tabata, Dependency of mechanical property of sintered mullite on chemical composition, *Journal of the Ceramic Society of Japan* **93**, 407 (1985).

126. S.-Y. Choi, D.-Y. Yoon, and S.-J. L. Kang, Kinetic formation and thickening of intergranular amorphous films at grain boundaries in barium titanate, *Acta Materialia* **52**, 3721 (2004).

127. S.-Y. Choi and S.-J. L. Kang, Sintering kinetics by structural transition at grain boundaries in barium titanate, *Acta Materialia* **52**, 2937 (2004).

128. F. Ernst, O. Kienzle, and M. Rühle, Structure and composition of grain boundaries in ceramics, *Journal of the European Ceramic Society* **19**, 665 (1999).

129. S.-Y. Chung and S.-J. L. Kang, Intergranular amorphous films and dislocations-promoted grain growth in SrTiO3, *Acta Materialia* **51**, 2345 (2003).

130. J.-H. Lee, J.-J. Kim, H. Wang, and S.-H. Cho, Observation of intergranular films in bab2o4-added BaTiO3 ceramics, *Journal of Materials Research* **15**, 1600 (2000).

131. M. Chi, H. Gu, P. Qian, X. Wang, and P. Wang, Effect of TiO2-SiO2 distribution on bimodal microstructure of TiO2-doped alpha-Al2O3 ceramics *Zeitschrift Fur Metallkunde* **96**, 486 (2005).

132. P. Svancarek, D. Galusek, C. Calvert, F. Loughran, A. Brown, R. Brydson, and F. Riley, A comparison of the microstructure and mechanical properties of two liquid phase sintered aluminas containing different molar ratios of calcia-silica sintering additives, *Journal of the European Ceramic Society* **24**, 3453, 2004.

133. P. Svancarek, D. Galusek, F. Loughran, A. Brown, R. Brydson, A. Atkinson, and F. Riley, Microstructure-stress relationships in liquid-phase sintered alumina modified by the addition of 5 wt.% of calcia-silica additives, *Acta Materialia* **54**, 4853 (2006).

134. R. Brydson, P. C. Twigg, F. Loughran, and F. L. Riley, Influence of CaO-SiO2 ratio on the chemistry of intergranular films in liquid-phase sintered alumina and implications for rate of erosive wear, *Journal of Materials Research* **16**, 652 (2001).

135. L. Gremillard, T. Epicier, J. Chevalier, and G. Fantozzi, Effect of cooling rate on the location and chemistry of glassy phases in silica-doped 3y-TZP ceramics, *Journal of the European Ceramic Society* **25**, 875 (2005).

136. W. Onreabroy, N. Sirikulrat, A. P. Brown, C. Hammond, and S. J. Milne, Properties and intergranular phase analysis of a ZnO-CoO-Bi2O3 varistor, *Solid State Ionics* **177**, 411 (2006).

137. H. K. Schmid, Identification of intergranular phases in ceramic nanocomposites, *Journal of Microscopy-Oxford* **194**, 192 (1999).

138. Knowles, K. M. and S. Turan, Boron nitride-silicon carbide interphase boundaries in silicon nitride-silicon carbide particulate composites, *Journal of the European Ceramic Society* **22**, 1587 (2002).

139. A. Avishai and W. D. Kaplan, Intergranular films at metal-ceramic interfaces part ii – calculation of Hamaker coefficient, *Acta Materialia* **53**, 1571 2005.

140. A. Avishai, C. Scheu, and W. D. Kaplan, Intergranular films at metal-ceramic interfaces part I—interface structure and chemistry, *Acta Materialia* **53**, 1559 2005.

141. C. Scheu, G. Dehm, and W. D. Kaplan, Equilibrium amorphous silicon-calcium-oxygen films at interfaces in copper-alumina composite prepared by melt infiltration, *Journal of the American Ceramic Society* **84**, 623 (2000).

142. A. Avishai and W. D. Kaplan, Intergranular films in metal-ceramic composites and the promotion of metal particle occlusion, *Zeitschrift Fur Metallkunde* **95**, 266 (2004).

143. A. Avishai, C. Scheu, and W. D. Kaplan, Amorphous films at metal/ceramic interfaces, *Zeitschrift Fur Metallkunde* **94**, 272 (2003).

144. M. Baram and W. D. Kaplan, Intergranular films at au-sapphire interfaces, *Journal of Materials Science* **41**, 7775 (2006).

145. H. G. Jeong, K. Hiraga, M. Mabuchi, and K. Higashi, Interface structure of Si3N4-whisker-reinforced Al-mg-Si alloy (Al alloy 6061) composites studied by high resolution electron microscopy, *Philosophical Magazine Letters* **74**, 73 (1996).

146. Y.-M. Chiang, A. Ramos, and M. Tang, Unpublished results (2004).

147. H. Qian and J. Luo, Unpublished results (2006).

148. J. S. Wettlaufer, Impurity effects in the premelting of ice, *Physical Review Letters* **82**, 2516 (1999).

149. H.-J. Kleebe and G. Pezzotti, Grain-boundary wetting-dewetting in z = 1 SiAlON ceramic, *Journal of the American Ceramic Society* **85**, 3049 (2002).

150. G. Pezzotti, Kleebe, H.-J., K. Okamoto, and K. Ota, Structure and viscosity of grain boundary in high-purity SiAlON ceramics, *Journal of the American Ceramic Society* **83**, 2549 (2000).

151. H. Gu, Variation of width and composition of grain-boundary film in a high-purity silicon nitride with minimal silica, *Journal of the American Ceramic Society* **85**, 33 (2002).

152. J. R. Lee and Y.-M. Chiang, Unpublished results (1995).

153. J. P. Gambino, Effect of heat treatments on the wetting behavior of bismuth-rich intergranular phases in ZnO:Bi:Co varistors, *Journal of the American Ceramic Society* **72**, 642, 1989.

154. M. Fujimoto and W. D. Kingery, Microstructures of SrTiO3 internal boundary layer capacitors during and after processing and resultant electrical properties., *Journal of the American Ceramic Society* **68**, 169 (1985).

155. X.-F. Zhang, M. E. Sixta, and L. C. DeJonghe, Grain boundary evolution in hot-pressed ABC-SiC, *Journal of the American Ceramic Society* **83**, 2813 (2000).

156. Y. Ikuhara, P. Thavorniti, and T. Takuma, Solute segregation at grain boundaries in superplastic SiO2-doped TZP, *Acta Materialia* **45**, 5275 (1997).

157. P. Thavorniti, Y. Ikuhara, and T. Takuma, Microstructural characterization of superplastic SiO2-doped TZP with a small amount of oxide addition, *Journal of the American Ceramic Society* **81**, 2927 (1998).

158. J. A. S. Ikeda, Y.-M. Chiang, Garratt-A. J. Reed, and J. B. V. Sande, Space charge segregation at grain boundaries in titanium dioxide: Part ii, model experiments, *Journal of the American Ceramic Society* **76**, 2447 (1993).

159. H. Gu, R. M. Cannon, H. J. Seifert, and M. J. Hoffmann, Solubility of Si_3N_4 in liquid SiO_2, *Journal of the American Ceramic Society* **85**, 25 (2002).

160. X. Su and S. H. Garofalini, Atomistic structure of calcium silicate intergranular films between prism and basal planes in silicon nitride: A molecular dynamics study, *Journal of Materials Research* **19**, 752 (2004).

161. S. Blonski and S. H. Garofalini, Atomistic structure of calcium silicate intergranular films in alumina studied by molecular dynamics simulations, *Journal of the American Ceramic Society*, 80 1997 (1997).

162. S. Garofalini and W. Luo, Molecular dynamics simulations of calcium silicate intergranular films between silicon nitride crystals, *Journal of the American Ceramic Society* **86**, 1741 (2003).

163. X. T. Su and S. H. Garofalini, Effect of interphase mixing on the structure of calcium silicate intergranular film/silicon nitride crystal interfaces, *Journal of Applied Physics* **97**, 113526 (2005).

164. S. H. Zhang and S. H. Garofalini, Molecular dynamics computer simulations of the interface structure of calcium-alumino-silicate intergranular films between combined basal and prism planes of alpha-Al2O3, *Journal of the American Ceramic Society* **88**, 202 (2005).

165. C. M. Bishop, M. Tang, R. M. Cannon, and W. C. Carter, Continuum modelling and representations of interfaces and their transitions in materials, *Materials Science and Engineering A* **422**, 102 (2006).

166. C. M. Bishop, R. M. Cannon, and W. C. Carter, A diffuse interface model of interfaces: Grain boundaries in silicon nitride, *Acta Materialia* **53**, 4755 (2005).

167. M. Tang, W. C. Carter, and R. M. Cannon, Grain boundary transitions in binary alloys, *Physical Review Letters* **97**, 075502 (2006).

168. W. D. Kaplan and Y. Kauffmann, Structural order in liquids induced by interfaces with crystals, *Annual Review of Materials Research* **36**, 1 (2006).

169. C. Dwyer, A. Ziegler, N. Shibata, G. B. Winkelman, R. L. Satet, M. J. Hoffmann, M. K. Cinibulk, P. F. Becher, G. S. Painter, N. D. Browning, Cockayne, D. J. H., R. O. Ritchie, and S. J. Pennycook, Interfacial structure in silicon nitride sintered with lanthanide oxide *Journal of Materials Science* **41**, 4405, 2006.

170. M. Bobeth, D. R. Clarke, and W. Pompe, Diffuse interface description of intergranular films in polycrystalline ceramics, *Journal of the American Ceramic Society* **82**, 1537 (1999).

171. N. Shibata, G. S. Painter, P. F. Becher, and S. J. Pennycook, Atomic ordering at an amorphous/crystal interface, *Applied Physics Letters* **89**, 051908 (2006).

172. P. F. Becher and G. S. Painter, Private communication (2007).

173. S. Bhattacharyya, C. T. Koch, and M. Rühle, Projected potential profiles across intergranular glassy films, *Journal of the Ceramic Society of Japan* **114**, 1005 (2006).

174. C. T. Koch, Examination of structural properties of interfaces by electron diffraction, *Materials Science and Engineering a-Structural Materials Properties Microstructure and Processing* **422**, 41 (2006).

175. C. T. Koch, S. Bhattacharyya, M. Rühle, R. L. Satet, and M. J. Hoffmann, Measuring electrostatic potential profiles across amorphous intergranular films by electron diffraction, *Microscopy and Microanalysis* **12**, 160 (2006).

176. C. T. Koch and S. H. Garofalini, Determining the radial pair-distribution function within intergranular amorphous films by numerical nanodiffraction, *Ultramicroscopy* **106**, 383 (2006).

177. I. Tanaka, T. Mizoguchi, and T. Yamamoto, XANES and ELNES in ceramic science, *Journal of the American Ceramic Society* **88**, 2013 (2005).

178. M. F. Chi and H. Gu, Comparison of segregation behaviors for special and general boundaries in polycrystalline Al2O3 with SiO2-TiO2 impurities, *Interface Science* **12**, 335 (2004).

179. H. Gu, Private communication (2006).

180. H. Qian, Y.-M. Chiang, R. M. Cannon, and J. Luo, Wetting and spreading of Bi2O3-rich liquid on ZnO single crystal surfaces, Vol. 2, *Materials Science & Technology 2006: Fundamentals and Characterization*, L. P. Cook and W. D. Kaplan, Eds. (251).

181. E. Saiz, R. M. Cannon, and A. P. Tomsia, Reactive spreading: Adsorption, ridging and compound formation, *Acta Materialia* **48**, 4449 (2000).

182. E. Saiz, A. P. Tomsia, and R. M. Cannon, Ridging effects on wetting and spreading of liquids on solids *Acta Materialia* **46**, 2349 (1998).

183. E. Saiz, A. P. Tomsia, and R. M. Cannon, Triple line ridging and attachment in high-temperature wetting, *Scripta Materialia* **44**, 159 (2001).

184. R. H. French, Origin and applications of London dispersion forces and Hamaker constants in ceramics, *Journal of the American Ceramic Society* **83**, 2117 (2000).

185. G. Centi, Nature of active layer in vanadium oxide supported on titanium oxide and control of its reactivity in the selective oxidation and ammoxidation of alkylaromatics, *Applied Catalysis A: General* **147**, 267 (1996).

186. G. N. Kryukova, G. A. Zenkovets, G. Mestl, and R. Schlogl, Structural study of titanium doped vanadia and vanadium doped titania catalysts, *Reaction Kinetics and Catalysis Letters*, V80, 161 (2003).

187. M. Sanati, R. L. Wallenberg, A. Andersson, S. Jansen, and Y. To, Vanadia catalysts on anatase, rutile, and TiO2(b) for the ammoxidation of toluene: An ESR and high-resolution electron microscopy characterization, *Journal of Catalysis* **132**, 128 (1991).

188. Y.-C. Xie and Tang, Y.-Q., Spontaneous monolayer dispersion of oxides and salts onto surfaces of supports: Applications to heterogeneous catalysis, *Advances in Catalysis* **31**, 1, 1990.

189. B. Gates, Y. Wu, Y. Yin, P. Yang, and Y. Xia., Single-crystalline nanowires of ag2se can be synthesized by templating against nanowires of trigonal se *Journal of the American Chemical Society* **123**, 11150 2001.

190. X. Y. Kong, Y. Ding, and Z. L. Wang, Metal-semiconductor Zn-ZnO core-shell nanobelts and nanotubes, *Journal of Physical Chemistry B* **108**, 570 (2004).

191. T. Kuykendall, P. Pauzauskie, S. Lee, Y. Zhang, J. Goldberger, and P. Yang, Metalorganic chemical vapor deposition route to GaN nanowires with triangular cross sections, *Nano Letters* **3**, 1063 2003.

192. T. T. Xu, Zheng, J.-G., A. W. Nicholls, S. Stankovich, R. D. Piner, and R. S. Ruoff, Single-crystal calcium hexaboride nanowires: Synthesis and characterization, *Nano Letters* **4**, 2051 2004.

193. X. Feng, D. S. Sayle, Z. L. Wang, M. S. Paras, B. Santora, A. C. Sutorik, T. X. T. Sayle, Y. Yang, Y. Ding, X. Wang, and Y.-S. Her, Converting ceria polyhedral nanoparticles into single-crystal nanospheres, *Science* **312**, 1504 (2004).

194. B. B. Straumal and B. Baretzky, Grain boundary phase transitions and their influence on properties of ploycrystals, *Interface Science* **12**, 147 (2004).

195. B. B. Straumal, Grain boundary phase transitions. Influence on diffusion, plasticity and charge transfer, *Archives of Metallurgy and Materials* **49**, 323 (2004).

196. J. Scholhammer, B. Baretzky, W. Gust, E. Mittemeijer, and B. Straumal, Grain boundary grooving as an indicator of grain boundary phase transformations, *Interface Science* **9**, 43 (2001).

197. L.-S. Chang, E. I. Rabkin, B. Straumal, P. Lejcek, S. Hofmann, and W. Gust, Temperature dependence of the grain boundary segregation of Bi in Cu polycrystals, *Scripta Metallurgica Et Materialia* **37**, 729 (1997).

198. B. B. Straumal, P. Zieba, and W. Gust, Grain boundary phase transitions and phase diagrams, *International Journal of Inorganic Materials* **3**, 1113 (2001).

199. S. Divinski, M. Lohmann, and C. Herzig, Grain boundary diffusion and segregation of Bi in Cu: Radiotracer measurements in b and c regimes, *Acta Materialia* **52**, 3973 (2004).

200. S. Divinski, M. Lohmann, C. Herzig, B. Straumal, B. Baretzky, and W. Gust, Grain boundary melting phase transition in the Cu-Bi system, *Physical Review B* **71**, 104104 (2005).

201. B. B. Straumal, S. I. Prokofjev, L. S. Chang, N. E. Sluchanko, B. Barezky, W. Gust, and E. J. Mittemeijer, Grain boundary phase transitions in the Cu-Bi system, in *Diffusions in materials: Dimat2000, pts 1 & 2*, **194-1**, 1343 (2001).

202. B. B. Straumal, N. E. Sluchanko, and W. Gust, Influence of grain boundary phase transitions on the properties of Cu-Bi polycrystals, Defect and Diffusion Forum, Vol. 188-1, *Defects and Diffusion in Metals* (185).

203. K. Wolski, V. Laporte, N. Marie, and M. Biscondi, About the importance of nanometer-thick intergranular penetration in the analysis of liquid metal embrittlement, *Interface Science* **9**, 183 (2001).

204. B. B. Straumal, O. I. Noskovich, V. N. Semenov, L. S. Shvindlerman, W. Gust, and B. Predel, Premelting transition on 38<100> tilt grain boundaries in (Fe- 10 at. % Si)-Zn alloys, *Acta Metallurgica et Materialia* **40**, 795 (1992).

205. E. I. Rabkin, V. N. Semenov, L. S. Shvindlerman, and B. B. Straumal, Penetration of tin and zinc along tilt grain boundaries 43° [100] in Fe-5 at.% Si alloy: Premelting phase transition? *Acta Metallurgica et Materialia* **39**, 627 (1991).

206. O. I. Noskovich, E. I. Rabkin, V. N. Semenov, B. B. Straumal, and L. S. Shvindlerman, Wetting and premelting phase transitions in 38° [100] tilt grain boundary in (Fe-12 at.% Si)-Zn alloy in the vicinity of the A2-B2 bulk ordering in Fe-12 at.% Si alloy *Acta Metallurgica et Materialia* **39**, 3091 (1991).

207. B. B. Straumal, E. Rabkin, W. Lojkowski, W. Gust, and L. S. Shvindlerman, Pressure influence on the grain boundary wetting phase transition in Fe-Si alloys, *Acta Materialia* **45**, 1931, 1997.

208. V. K. Gupta, D. H. Yoon, J. Luo, and Meyer H. M. III, Preliminary results of activated sintering mechanism and grain boundary prewetting/ premelting in nickel-doped tungsten, Ceramic Transactions, Vol. 172, *Ceramic Nanomaterials and Nanotechnology IV*, M. Z. H. R. M. Lane, S. Lu, Ed., 2005 (159).

209. W. L. Johnson, Amorphization by interfacial reaction, in *Materials Interfaces*, Chapman and Hall, New York, 1993 (517).

210. K. S. Hwang and H. S. Huang, Identification of the segregation layer and its effects on the activated sintering and ductility of Ni-doped molybdenum, *Acta Materialia* **51**, 3915 (2003).

211. V. Jayaram and R. Sinclair, Detection of thin intergranular cobalt layers in wc-co composites by lattice imaging, *Journal of the American Ceramic Society* **66**, C137 (1983).

212. N. Marie, K. Wolski, and M. Biscondi, Intergranular penetration and embrittlement of solid nickel through bismuth vapour condensations at 700°C, *Journal of Nuclear Materials* **296**, 282 (2001).

213. N. Marie, K. Wolski, and M. Biscondi, Grain boundary penetration of nickel by liquid bismuth as a film of nanometeric thickness *Scripta Materialia* **43**, 943 (2000).

214. E. Pereiro-López, W. Ludwig, D. Bellet, P. Cloetens, and C. Lemaignan, Direct evidence of nanometric invationlike grain boundary penetration in the Al/Ga system, *Physical Review Letters* **95**, 215501 (2005).

215. D. A. Molodov, U. Czubayko, G. Gottstein, L. S. Shvindlerman, B. Straumal, and W. Gust, Acceleration of grain boundary motion in Al by small additions of Ga, *Philosophical Magazine Letters* **72**, 361 (1995).

216. B. X. Liu, W. S. Lai, and Z. J. Zhang, Solid-state crystal-to-amorphous transition in metal-metal multilayers and its thermodynamic and atomistic modelling, *Advances in Physics* **50**, 367 (2001).

217. R. Benedictus, A. Böttger, and E. J. Mittemijer, Thermodynamic model for solid-state amorphization in binary systems at interfaces and grain boundaries, *Physical Review B* **54**, 9109 (1996).

218. J. Y. Wang, D. He, Y. H. Zhao, and E. J. Mittemijer, Wetting and crystallization at grain boundaries: Origin of aluminum-induced crystallization of amorphous silicon *Applied Physics Letters* **88**, 061910 (2006).

219. K.-W. Kwon, Lee, H.-J., and R. Sinclair, Solid-state amorphization at tetragonal-Ta/Cu interfaces, *Applied Physics Letters* **75**, 935 (1999).

220. P. L. Williams and Y. Mishin, Phase transformation at interfaces in metals and compounds, in *2006 MRS Fall Meeting* Boston, MA, HH4.5 (2006).

221. D. A. Laird, Influence of layer charge on swelling of semetics, *Applied Clay Science* **34**, 74 (2006).

222. S. Karaborni, B. Smit, W. Heidug, J. Urai, and E. van Oort, The swelling of clays: Molecular simulations of the hydration of montmorillonite, *Science* **271**, 1102 (1996).

223. N. T. Skipper, P. A. Lock, J. O. Titiloye, J. Swenson, Z. A. Mirza, W. S. Howells, and Fernandez-F. Alonso, The structure and dynamics of 2-dimensional fluids in swelling clays *Chemical Geology* **230**, 182 (2006).

224. E. K. Frinak, C. D. Mashburn, M. A. Tilbert, and O. B. Toon, Infrared characterization of water uptake by low-temperature Na-montmorillonite: Implications for earth and mars, *Journal of Geophysical Research* **110**, D09308 (2005).

225. R. M. Cannon, Unpublished results (2006).

226. R. Kikuchi and J. W. Cahn, Grain boundaries with impurities in a two-dimensional lattice-gas model, *Physical Review B* **36**, 418 1987.

227. R. Lipowsky, Critical surface phenomena at first-order bulk transitions, *Physical Review Letters* **49**, 1575 (1982).

228. H. Löwen and R. Lipowsky, Surface melting away from equilibrium, *Physical Review B* **43**, 3507 (1991).

229. R. Lipowsky, Surface-induced order and disorder: Critical phenomena at first-order phase transitions *Journal of Applied Physics* **55**, 2486 (1983).

230. R. Lipowsky and W. Speth, Semi-infinite systems with first-order bulk transitions, *Physical Review B* **28**, 3983 (1983).

231. R. Lipowsky, U. Breuer, K. C. Prince, and H. P. Bonzel, Multicomponent order parameter for surface melting, *Physical Review Letters* **62**, 913 (1989).

232. R. Kobayashi, J. A. Warren, and W. C. Carter, Vector-valued phase field model for crystallization and grain boundary formation *Physica D* **119**, 415 (1998).

233. B. Pluis, T. N. Taylor, D. Frenkel, and J. F. van der Veen, Role of long-range interaction in melting of a metallic surface *Physical Review B* **40**, 1354 (1989).

234. R. Lipowsky, Melting at grain boundaries and surfaces, *Physical Review Letters* **57**, 2876 (1986).

235. R. H. French, R. M. Cannon, L. K. DeNover, and Y.-M. Chiang, Full spectral calculation of non-retarded Hamaker constants for ceramic systems from interband transition strengths, *Solid State Ionics* **75**, 13 (1995).

236. H.-J. Choi, G.-H. Kim, J.-G. Lee, and Y.-W. Kim, Refined continuum model on the behavior of intergranular films in silicon nitride ceramics, *Journal of the American Ceramic Society* **83**, 2821 (2000).

237. V. A. Parsegian, *Van der waals Forces: A Handbook for Biologists, Chemists, Engineers and Physicists*, Cambridge University Press (2006).

238. K. van Benthem, G. L. Tan, R. H. French, L. K. DeNoyer, R. Podgornik, and V. A. Parsegian, Graded interface models for more accurate determination of van der waals-London dispersion interactions across grain boundaries, *Physical Review B* **74**, 205110 (2006).

239. R. H. French, H. Müllejans, D. J. Jones, G. Duscher, R. M. Cannon, and M. Rühle, Dispersion forces and Hamaker constants for intergranular films in silicon nitride from spatially resolved-valence electron energy loss spectrum imaging, *Acta Materialia* **46**, 2271 (1998).

240. K. van Benthem, G. L. Tan, L. K. DeNoyer, R. H. French, and M. Ruhle, Local optical properties, electron densities, and London dispersion energies of atomically structured grain boundaries *Physical Review Letters* **93**, 227201 (2004).

241. K. Johnston and M. W. Finnis, Electrostatic and entropic intercations between parallel interfaces separated by a glassy film *Journal of the American Ceramic Society* **85**, 2562 (2002).

242. Karraker, K. A. and C. J. Radke, Disjoining pressures, zeta potentials and surface tensions of aqueous non-iionic surfactant/electrolyte solutions: Theory and comparison to experiment, *Advances in Colloid and Interface Science* **96**, 231, 2002.

243. I. Borukhov and D. Andelman, Steric effects in electrolytes: A modified Poisson-Boltzmann equation, *Physical Review Letters* **79**, 435 (1997).

244. J. Chen, L. Z. Ouyang, and W. Y. Ching, Molecular dynamics simulation of Y-doped sigma 37 grain boundary in alumina, *Acta Materialia* **53**, 4111 (2005).

245. P.-L. Chen and Chen, I.-W., Grain boundary mobility in Y_2O_3: Defect mechanism and dopant effects, *Journal of the American Ceramic Society* **79**, 1801 (1996).

246. J. P. Buban, K. Matsunaga, J. Chen, N. Shibata, W. Y. Ching, T. Yamamoto, and Y. Ikuhara, Grain boundary strengthening in alumina by rare earth impurities, *Science* **311**, 212 (2006).

247. J. Lapujoulade, Roughening of metal surfaces, *Surface Science Reports* **20**, 191 (1994).

248. I. Daruka and J. C. Hamilton, Atomistic and lattice model of a grain boundary defaceting phase transition, *Physical Review Letters* **92**, 246105 (2004).

249. A. Honda, K. Matsunaga, and H. Matsubara, Molecular dynamics simulation of an intergranular glass phase in alumina based ceramics, *Journal of the Japan Institute of Metals* **64**, 1113 (2000).

250. P. Rulis, J. Chen, L. Ouyang, W. Y. Ching, X. Su, and S. H. Garofalini, Electronic structure and bonding of intergranular glassy films in polycrystalline Si3N4: Ab initio studies and classical molecular dynamics simulations, *Physical Review B* **71**, 235317 (2005).

251. I. Szlufarska, A. Nakano, and P. Vashishta, A crossover in the mechanical response of nanocrystalline ceramics, *Science* **309**, 911 (2005).

252. T. S. Hudson, D. Nguyen-Manh, A. C. T. van Duin, and A. P. Sutton, Grand canonical Monte Carlo simulations of intergranular glassy films in beta silicon nitride, *Materials Science and Engineering A* **422**, 123 (2006).

253. J. Chen, L. Z. Ouyang, P. Rulis, A. Misra, and W. Y. Ching, Complex nonlinear deformation of nanometer intergranular glassy films in beta-Si3N4, *Physical Review Letters* **95**, 256103 (2005).

254. W. Y. Ching, J. Chen, P. Rulis, L. Ouyang, and A. Misra, Ab initio modeling of clean and Y-doped grain boundaries in alumina and intergranular glassy films (IGF) in beta-Si3N4, *Journal of Materials Science* **41**, 5061 (2006).

255. G. S. Painter, P. F. Becher, H. J. Kleebe, and G. Pezzotti, First-principles study of the effects of halogen dopants on the properties of intergranular films in silicon nitride ceramics, *Physical Review B* **65**, 064113 (2002).

256. S. R. Phillpot, J. Wang, D. Wolf, and H. Gleiter, Computer simulation of the structure and dynamical properties of grain boundaries in a nanocrystalline model material, *Journal of Engineering and Applied Science*, A204, 76 (1995).

257. von S. Alfthan, P. D. Haynes, K. Kaski, and A. P. Sutton, Are the structures of twist grain boundaries in silicon ordered at 0 k, *Physical Review Letters* **96**, 055505 (2006).

258. X. F. Zhang, G. Y. Lee, D. Chen, R. O. Ritchie, and De L. C. Jonghe, Abrasive wear behavior of heat-treated abc-silicon carbide, *Journal of the American Ceramic Society* **86**, 1370, 2003.

259. O. Kienzle, S. Hutt, F. Ernst, and M. Rühle, Grain boundaries in strontium titanate, *Ceramic Transaction* **118**, 215 (2000).

260. J. H. Choi, N.-M. Hwang, and D. Y. Kim, Pore-boundary separation behavior during sintering of pure and Bi_2O_3-doped ZnO ceramics, *Journal of the American Ceramic Society* **84**, 1398 (2001).

261. I.-H. Moon, K.-Y. Kim, S.-T. Oh, and M.-J. Suk, Nickel-enhanced grain growth in tungsten wire, *Journal of Alloys and Compounds* **201**, 129 (1993).

262. G. Gottstein and D. A. Molodov, Grain boundary migration in metals: Recent developments, *Interface Science* **6**, 7 (1998).

263. D. Weygand, Y. Breichet, E. Rabkin, B. Straumal, and W. Gust, Solute drag and wetting of a grain boundary *Philosophical Magazine Letters* **76**, 133 (1997).

264. E. Jud, Z. Zhang, W. Sigle, and L. J. Gauckler, Microstructure of cobalt oxide doped sintered ceria solid solutions, *Journal of Electroceramics* **16**, 191 (2006).

265. X. Feng, D. S. Sayle, Z. L. Wang, M. S. Paras, B. Santora, A. C. Sutorik, T. X. T. Sayle, Y. Yang, Y. Ding, X. Wang, and Y.-S. Her, Converting ceria polyhedral nanoparticles into single-crystal nanospheres, *Science* **312**, 1504 (312).

266. J. H. Brophy, L. A. Shepard, and J. Wulff, The nickel-activated sintering of tungsten, in *Powder metallurgy*, W. Leszynski, Ed., Interscience, 1961 (113).

267. H. W. Hayden and J. H. Brophy, Activated sintering of tungsten with group viii elements, *Journal of Electrochemcial Society* **110**, 805 (1963).

268. A. P. Prill, W. W. Hayden, and J. H. Brophy, The role of phase relations in activated sintering of tungsten, *Transaction of American Institute of Mining Engineers* **230**, 769 (1964).

269. I. J. Toth and N. A. Lockington, The kinetics of metallic activation sintering of tungsten, *Journal of Less-Common Metals* **12**, 353 (1967).

270. G. Flether, M. R. James, and J. R. Moon, The nickel activated sintering of tungsten, *Scripta Metallurgica* **5**, 105 1971.

271. R. M. German and Z. M. Munir, Enhanced low-temperature sintering of tungsten, *Metallurgical Transactions*, 7A, 1873 (1976).

272. R. L. Coble and R. M. Cannon, Current paradigms in powder processing, *Processing of Crystalline Ceramics*, H. Palmour III, Ed., 1978 (151).

273. D. N. Lee and S. H. Ahn, Nickel activated model sintering of tungsten, *Science of Sintering* **11**, 43 (1979).

274. R. M. German, Activated sintering of refractory metals by transition metal additions, *Reviews on Powder Metallurgy and Physical Ceramics* **2**, 9 (1982).

275. R. M. German, Diffusional activated sintering—densification, microstructure and mechanical properties, *Progress in Powder Metallurgy* **39**, 243 (1984).

276. H. Yoon, J.-S. Kim, and Y.-L. Kim, The effect of the doping method on the sinterability nickel-doped tungsten compacts, *Journal of Less-Common Metals* **102**, 219 (1984).

277. R. M. German, The identification of enhanced sintering systems through phase diagrams, *Modern Development in Powder Metallurgy* **15**, 253 (1985).

278. J. L. Johnson and R. M. German, Theoretical modeling of densification during activated solid-state sintering, *Metallurgical and Materials Transactions*, 27A, 441 (1996).

279. N. W. Hwang, Y. J. Park, Kim, D.-Y., and D. Y. Yoon, Activated sintering of nickel-doped tungsten: Approach by grain boundary structural transition, *Scripta Materialia* **42**, 421 (2000).

280. E. Jud, C. B. Huwiler, and L. J. Gauckler, Sintering analysis of undoped and cobalt oxide doped ceria solid solutions, *Journal of the American Ceramic Society* **88**, 3013 (2005).